Order Number 9502623

Bond of glass-fiber-reinforced-plastic reinforcing bars to concrete

Tao, Shicheng, Ph.D.

The University of Arizona, 1994

U·M·I
300 N. Zeeb Rd.
Ann Arbor, MI 48106

BOND OF GLASS-FIBER-REINFORCED-PLASTIC REINFORCING BARS TO CONCRETE

by

Shicheng Tao

A Dissertation Submitted to the Faculty of the

DEPARTMENT OF CIVIL ENGINEERING AND ENGINEERING MECHANICS

In Partial Fulfillment of the Requirements
For the Degree of

DOCTOR OF PHILOSOPHY
WITH A MAJOR IN CIVIL ENGINEERING

In the Graduate College

THE UNIVERSITY OF ARIZONA

1 9 9 4

THE UNIVERSITY OF ARIZONA
GRADUATE COLLEGE

As members of the Final Examination Committee, we certify that we have read the dissertation prepared by Shicheng Tao

entitled Bond of Glass-Fiber-Reinforced-Plastic Reinforcing Bars to Concrete

and recommend that it be accepted as fulfilling the dissertation requirement for the Degree of Doctor of Philosophy

M R Ehsani Dr. Mohammad R. Ehsani	5/12/94 Date
Hamid Saadatmanesh Dr. Hamid Saadatmanesh	5/12/94 Date
Tribikram Kundu Dr. Tribikram Kundu	5/12/94 Date
	Date
	Date

Final approval and acceptance of this dissertation is contingent upon the candidate's submission of the final copy of the dissertation to the Graduate College.

I hereby certify that I have read this dissertation prepared under my direction and recommend that it be accepted as fulfilling the dissertation requirement.

M R Ehsani Dissertation Director Dr. Mohammad R. Ehsani	5/12/94 Date

STATEMENT BY AUTHOR

This dissertation has been submitted in partial fulfillment of requirements for an advanced degree at The University of Arizona and is deposited in the University Library to be made available to borrowers under rules of the Library.

Brief quotations from this dissertation are allowable without special permission, provided that accurate acknowledgment of source is made. Requests for permission for extended quotation from or reproduction of this manuscript in whole or in part may be granted by the head of the major department or the Dean of the Graduate College when in his or her judgment the proposed use of the material is in the interests of scholarship. In all other instances, however, permission must be obtained from the author.

SIGNED: 

ACKNOWLEDGEMENTS

The author would like to express his sincere appreciation to Professor Mohammad R. Ehsani, academic advisor, for his invaluable guidance, encouragement, and support throughout this research project.

The author would like to thank Professors Hamid Saadatmanesh, Tribikram Kundu, Lorne G. Wilson, and Simon Ince for their kindly advice and time spent in servicing in the author's committee. The author also would like to thank Shop Technicians Peter Boyle and Carl Peters for their assistance in setting up the specimens during the testing. Thanks are also to a number of graduate and undergraduate students for their help in the experimental program of this research.

The author would like to express his special gratitude to his wife, Ying Zou, and his parents, Dayu Tao and Guilin Zhang, for their understanding and infinite moral support during the entire period of this study.

Finally, the author would like to thank the support of International Grating Inc., Houston, Texas, for donating the KODIAK™ GFRP rebars used in this research program.

TABLE OF CONTENTS

TABLE OF CONTENTS-*Continued*

LIST OF ILLUSTRATIONS

LIST OF ILLUSTRATIONS-*Continued*

LIST OF ILLUSTRATIONS-*Continued*

LIST OF ILLUSTRATIONS-*Continued*

LIST OF ILLUSTRATIONS-*Continued*

LIST OF ILLUSTRATIONS-*Continued*

LIST OF TABLES

NOTATION

A_b	nominal cross section area of rebars, in.^{2}
C_b	clear concrete cover, in.
d_b	rebar diameter, in.
E_i	initial stiffness, kips/in.
f_c'	concrete compressive strength for each specimen, psi
$f_{cavg.}'$	average of f_c' for all 4000- or 8000-psi (28- or 56-MPa) concrete, psi
f_h	tensile stress of hook, psi
f_s	tensile stress of rebars, ksi
f_s^*	adjusted maximum tensile stress of rebars, ksi
f_{sc}	critical tensile stress of rebars, psi
f_y	yield strength of steel rebars or tensile strength of GFRP rebars, psi
L	straight embedment length of the rebar, in.
L'	tail length, in.
l_d	embedment length, in.
l_{db}	basic development length of straight rebars, in.
L_{dh}	modified development length of hooked rebars, in.
$L_{eq.}$	development length calculated in Equation (21), in.
L_{hb}	basic development length of hooked rebars, in.
MOF	mode of failure

NOTATION-*Continued*

r	radius of bend, in.
S_{fmax}	ultimate slip at free end, in.
S_{lmax}	ultimate slip at loaded end, in.
T	applied tensile load, kips
T_c^*	defined as the smaller of T_{cf}^* and T_{cl}^*, kips
T_{cf}^*	adjusted applied tensile load at free end slip of 0.0025 in. (0.064 mm), kips
T_{cl}^*	adjusted applied tensile load at loaded end slip of 0.015 in. (0.38 mm), kips
T_m^*	adjusted ultimate applied tensile load, kips
T_u	ultimate tensile capacity of rebar, kips
U	bond stress, psi
U_c	critical bond stress, psi
U_m^*	adjusted ultimate bond stress, psi
U_m	measured bond stress, psi
δ_a	loaded end slip after correction for elastic elongation of rebar, in.
δ_e	elastic elongation of rebar, in.
δ_m	loaded end slip measured during testing, in.

ABSTRACT

The objective of this research project was to study the bond behavior of Glass-Fiber-Reinforced-Plastic (GFRP) reinforcing bars (rebars) to concrete. A total of 102 specimens were experimentally investigated and theoretically analyzed at The University of Arizona.

The static tensile load was applied to the rebars in a gradual increment of load level until splitting of concrete, rebar pull out failure, or rebar fracture occurred. The slip between the rebars and concrete was measured at the loaded and free ends at each load level. Variables included in the specimens were concrete compressive strength, embedment length, clear concrete cover, rebar diameter, concrete cast depth, radius of bend, tail length, and lead embedment length.

On the basis of the experimental results, the study showed that concrete compressive strength, embedment length, clear concrete cover, concrete cast depth, and radius of bend had significant effects on bond of GFRP rebars to concrete. New criteria for acceptable bond performance of GFRP rebars to concrete were established. Furthermore, the practical design guidelines for calculating the development lengths of straight and hooked GFRP rebars to concrete were determined. In addition, confinement factors were also derived to reflect the influence of concrete cover and casting position.

1. INTRODUCTION

1.1 Statement of the Problem

Concrete reinforced with steel rebars is widely used in a large number of construction projects, such as bridge decks, parking garages, tunnels, etc. However, corrosion of reinforcing steel is a severe problem in concrete structures located in corrosive and marine environment, especially where deicing chemicals are used. Intensified corrosive action produces deep pitting and a serious loss of cross section of the steel rebars. Upon expansion, rust products from corroded rebar occupy a greater volume than the original one, and large internal pressure leads to the cracking and spalling of concrete. As a result, the bond strength between the concrete and steel rebars is drastically reduced. This results the premature deterioration, costly repairs, and ultimately the catastrophic failures of the structures.

Several methods have been adopted to prevent the corrosion process of steel rebars, such as increasing the concrete cover, using additives and admixtures in concrete, cathodic protection, and epoxy coating steel rebars. Of all the methods, use of epoxy coating offers the most effective combination of protection and economy, and spreads to nearly all types of structures where concrete is exposed to a corrosive environment. But, the recent discovery of extensive premature corrosion of epoxy-coated steel rebars in new

bridges indicates that neither a practical nor an efficient approach has been developed yet to prevent corrosion.

A totally different method from those mentioned above could be to use new long-lasting materials with a unique characteristic of high corrosion resistance. Glass-Fiber-Reinforced-Plastic (GFRP) rebars which have been produced in recent years appear to be an ideal candidate and have great potential to fill such a need for concrete structures. These rebars have several important advantages over conventional steel rebars, such as high corrosion resistance, high tensile strength, light weight, non-conductivity, ease of handling and cutting, and good economy on long-term cost.

However, there are many factors that restrict GFRP rebars to be widely accepted among the practical civil engineering fields. One of which is the lack of information concerning the bond property that is one of the most important prerequisites of reinforced concrete structures. Furthermore, the ACI 318-89 codes for bond design of steel rebars to concrete cannot be directly used in that of GFRP rebars since their tensile strength, modulus of elasticity, and rib geometry are different from those of steel rebars.

Therefore, the need for further research to give a better and more complete understanding of the bond problem of GFRP rebars to concrete is apparent. The primary objective of this research project are to study the effect of different kinds of parameters

on bond behavior and establish the practical design guidelines for calculating the development lengths of straight and hooked GFRP rebars to concrete.

1.2 Literature Review

The following is a review of previous relevant research dealing with bond behavior of steel and GFRP rebars to concrete.

1.2.1 Bond of Straight Steel Rebars to Concrete

When plain rebars without surface deformations were used, bond was often thought of as chemical adhesion between concrete paste and rebar surface. Deformed rebars were designed to change this behavior pattern. Adhesion and friction still assist, but the chief reliance has changed to the bearing of lugs on concrete and to the shear strength of a concrete section between lugs.

In the early 1940's, Watstein (1941) examined the distribution of bond stress by testing pullout specimens, concluding that the bond stress at the loaded end of the rebars varied approximately linearly with the applied load. Meanwhile, a report published by the ACI Committee 208 (1945), Bond Stress, about the proposed test procedure for determining relative bond values, introduced the information about dimensions of beam

specimens, casting, curing, and testing, etc. Subsequently, Clark (1946, 1948), Watstein (1947), Collier (1947), Mylrea (1948), and Mains (1951) focused on bond characteristics in concrete pullout and beam specimens. Their experimental research showed that bars cast in the top position were much less effective than those cast in the bottom position.

Investigation of bond behavior in beam and pullout specimens with high-yield strength rebars was conducted by Mathey and Watstein (1961) who found the bond stress decreased with increases in the embedment length for a given diameter. The bond stress also decreased with an increase in the bar diameter for a given embedment length. The ultimate bond stresses in the pullout specimens agreed in general with the values obtained in beams with #4 bars. However, for #8 bars the bond strength in pullout was significantly greater than the values obtained with beams. The "critical" bond stresses were defined as the lesser of the bond stresses according to either a loaded end slip of 0.01 in. or a free end slip of 0.002 in. The study of development length of high strength rebars was reported by Ferguson and Thompson (1962, 1965), ACI Committee 408 (1966), and Ferguson, et al. (1965). Bond strength increases with increased concrete strength, f_c', approximately in proportion to the square root of the f_c'. Clear cover, C_b, was an important factor in the failure mode of bond test. Longer embedment lengths needed to develop high strength rebars. The greater the depth of concrete below a top bar (for bars with over 12 in. of concrete below the bar), the greater the resulting loss in bond strength is.

The distribution of steel stress and bond stress along a reinforcing bar was investigated in eccentric pullout specimens by Perry and Thompson (1966). The point of maximum bond stress moved away from the loaded end as the force in the bar increased. The location of the maximum bond stress for the same force in the bars moved closer to the loaded end as the concrete strength was increased. As a greater force in the bar was produced, more loaded end slip occurred and caused the point of maximum bond to propagate toward the free end.

The study on mechanics of bond and slip of deformed bars in concrete was conducted by Lutz and Gergely (1967), and Lutz (1970) at Cornell University. With the support of the experimental data, they found that the bond of deformed bars was developed mainly by the bearing pressure of the bar ribs against the concrete. Bars having ribs with steep face angles slip mainly by compressing the concrete in front of the bar rib. The concrete is crushed and a concrete wedge forms in front of the bar rib. Bars with flat ribs, however, slip with the ribs sliding relative to the concrete.

ACI Committee 408 (1970) reported that deformed bars greatly improved bond effectiveness. Larger bars and higher strength bars produced more prominent evidences of splitting. The bond behavior was a complicated phenomenon influenced by bar and cross section geometry, and bar confinement. Bond splitting appeared to be a complicated phenomenon involving interactions with shear and flexure. Bond strength

and the mode of failure are influenced by concrete cover over the reinforcement, specimen widths, and restraints of the reinforcement.

Orangun, et al. (1977) reevaluated the test data to develop a development length equation based on a nonlinear regression analysis. The equation reflects the effects of length, cover, spacing, bar diameter, concrete strength, and transverse reinforcement on the strength of anchored bars. Furthermore, Ferguson (1977) pointed out that both bar cover and bar spacing were very critical factors. According to Kemp and Wilhelm (1979) and Kemp (1986), a design equation suitable for ultimate load design has been developed by studying the influence of reinforcing bar embedment length and spacing, stirrups, concrete cover and associated concrete strength.

Edwards and Yannopoulos (1979) compared local bond-stress to slip relationships between deformed bars and mild steel plain bars and concluded that the maximum bond stress developed by plain bars was only 1/2 to 1/3 of that of deformed bars and was reached at a much smaller slip than that for the deformed bars.

Relationship between bond stress and slip was experimentally tested and theoretically analyzed by Somayaji and Shah (1981), and Jiang, et al. (1984). Instead of assuming a bond stress versus slip relationship, a function was assumed to represent the bond stress distribution. The predicted values using the proposed model were

compared satisfactorily with some experimental data on reinforced concrete. The model adequately predicts the end slip and steel stress-elongation curves. The theoretical local bond stress-slip relationship was found to be nonlinear and not unique at every section of the tension member.

Structures under construction are frequently subjected to early loads. In order to study the early loading effects on bond strength, Clark and Johnston (1983), and Chapman and Shah (1987) conducted the bond tests on identical beam end specimens. The ACI bond and development equations were found to be conservative for older concrete but overestimated bond strength for very young concrete, says 1 to 5 days. Little correlation was found between bond strength and compressive strength when smooth steel bars are used. This indicates that the adhesive component of bond relatively independent of the compressive strength. For deformed bar specimens, the mode of failure of bond is dependent on compressive strength and embedment length. Pullout load increases with increasing embedment length, but the average bond strength decreases. This is because the pullout load increase is not proportional to the increase in embedment length. A modified equation gives longer development length than that suggested by using the ACI Code equation for lower concrete strengths.

Direct measurement of slip between steel and concrete reported by Lahnert, et al. (1986) was applied to the determination of the local bond slip in pullout and tension

specimens. In addition, electric bonded strain gages embedded in the bar were used to measure the bar force and the bond stress.

The "top bar" effect first introduced into the ACI code in 1951 in the form of allowable bond stresses for a top-cast bar was 0.7 times that for bottom-cast bar. The "top bar" effect was accounted for by multiplying the development length by a factor of 1.4 in 1971 because the 1971 ACI code replaced the traditional bond stress calculation with expressions for development length. The "top bar" factor remained essentially the same in the ACI code from 1951 to 1983. However, recent investigation of "top bar" effects in beam based on an experimental study was performed by Jeanty, et al. (1988). For the test series of beams, both with and without transverse reinforcement crossing the plan of splitting, the "top bar" factor was found to be about 1.22. The reduction of development length due to presence of transverse reinforcement for both bottom-cast and top-cast bars was 20 percent. The decrease from 1.4 to 1.3 of the "top bar" factor was reflected in 1989 ACI code.

Based on the differential equation of bond stress versus slip, an entirely new solution of the distributions of both slip and bond stress is found by Yang and Chen (1988). A dimensionless parameter that is dependent on the physical and geometrical conditions of the segments is defined. For flexural members, the formulas developed for calculating bond stress, slip, material elongations, and crack width are also tenable by

finding the equivalent tension members. Statistical results show very good agreement between the calculated width and the corresponding test data available in the literature.

Chana (1990) described a beam specimen to determine the bond strength of reinforcement. It enables the bond strength to be determined for both a top cast and bottom cast condition. This type of specimen gives results that relate more closely to practice than do the conventional pull-out type specimens. The value of bond strength from this type of specimen can be compared directly with design codes. In addition, the beam specimen can be used to give a splitting failure mode.

A total of 233 bond strength measurements were compiled from 16 sources by Sozen and Moehle (1990). A simple design procedure to determine development/splice lengths for deformed reinforcing bars was developed. For deformed bars (without epoxy coating) with less than 12-in. of concrete cast beneath them, the proposed method would require a development length of 40 bar diameters if the specified yield stress is 60,000 psi and the compressive strength is 4,000 psi. Moehle et al. (1991) proposes a method for determining tension anchorage lengths that involves a single, simple expression for basic development length that is a function of bar diameter, reinforcement yield stress, and concrete strength. The proposed method offers the advantages of simplicity and safety. An expression that accurately represents development and splice strength is developed by Darwin et al. (1992). The principal changes involve the use of an

expression in which the basic development length is expressed in terms of bar diameter, rather than the bar area. The modified version has a single development length equation and three modification factors. In contract, the provisions offered under the current code format have three development length equations and four modification factors.

ACI Committee 408 (1990), and Lutz et al. (1993) examined changes made to the development length provisions to consider confinement effects. These changes relating to the confinement effects in ACI 318-89 as well as changes for top bars and provisions for epoxy coated bars are discussed.

Because of the lack of test data, ACI 318-89 building code requirements imposed an arbitrary upper limit of 10,000 psi on specified concrete compressive strength that may be used in calculating tension development length and tension splice length. Twelve beam splice specimens using No. 11 rebars and concrete with compressive strength exceeding 14,000 psi (97 MPa) were tested by Azizinamini et al. (1993). It is concluded that the assumption of a uniform bond stress distribution at the ultimate strength may not hold true for high strength concrete (HSC). The top-cast bars as defined by ACI 318-89, resulted in slightly higher bond capacity in specimens with HSC than bottom-cast bars.

Darwin and Graham (1993) studied the effect of deformation pattern on bond strength using 1 in. (25 mm) diameter machined bars with deformation heights of 0.05,

0.075, and 0.10 in. (1.27, 1.91, and 2.54 mm) and deformation spacings ranging from 0.26 to 2.2 in. (6.7 to 56 mm). The combinations of rib height and spacing produce relative rib areas (ratio of projected rib area normal to bar axis to product of nominal bar perimeter and center-to-center rib spacing) of 0.20, 0.10, and 0.05 for each deformation height. The initial stiffness of load-slip curves increases with an increase in the relative rib area. The magnitude of the increase in bond strength increase with an increase in the relative rib area.

Corrosion of reinforcing steel has always been a major problem which can lead to deterioration and damage of concrete structures. When protective coatings are added to the surface of the reinforcing steel, the changes in the bond behavior of steel to concrete have to be considered.

The possibility of protecting steel reinforcing bars from corrosion with organic-type coatings was investigated by Mathey and Clifton (1976) and Clifton and Mathey (1983). In this investigation, 34 pullout specimens, which were comprised of five specimens with uncoated reinforcing rebars, 23 specimens with epoxy-coated rebars, and six specimens with polyvinyl chloride-coated rebars were tested. It was concluded that rebars with epoxy coatings approximately 10 mils (0.025 cm) or less in thickness developed essentially the same bond strengths as the uncoated rebars. When the film thickness of the epoxy coating was 25 mils (0.064 cm) or when polyvinyl coatings were

used, the bond strength was considerably less for these coated rebars than for the uncoated rebars. It was recommended that thick epoxy coatings, greater than 10 mils (0.025 cm), and polyvinyl chloride coatings not be used as protective coatings for reinforcement in concrete flexural members.

In a study conducted by Treece and Jirsa (1989), twenty-one beams with lap splices in a constant moment region were tested in nine groups, and the bond strength of epoxy-coated rebars was compared to that of uncoated rebars. Variables were rebar size, concrete strength, casting position, and coating thickness. In each test group, the only variable was the coating thickness. Based on the results of 21 splice tests with epoxy-coated and uncoated rebars evaluated in this study along with data from previous studies, the following conclusions were made. Epoxy coating significantly reduced the bond strength of reinforcing rebars. If a splitting failure occurred, the bond strength of epoxy-coated rebars was approximately 65 percent of the bond strength of uncoated rebars. If a pullout failure occurred, the bond strength was approximately 85 percent of that for uncoated rebars. The reduction in bond strength was independent of rebar size and concrete strength, and was insensitive to variations in the coating thickness where the average coating thickness was greater than 5 mils and less than about 14 mils. The width and spacing of cracks were significantly increased by epoxy-coating.

The effects of epoxy coating on the bond behavior of reinforcing bars in concrete are described by Hadje-Ghaffari, et al. (1992). The effects of concrete cover and casting position on concrete and the reduction in bond strength between rebars and concrete caused by epoxy coating are described. They conclude that the bond strength of both coated and uncoated bars increases as cover increases, regardless of casting position, bar size, or deformation pattern. As the depth of concrete below a bar increases, the bond strength decreases, regardless of bar size, deformation pattern, or bar surface condition.

1.2.2 Bond of Hooked Steel Rebars to Concrete

Minor and Jirsa (1971, 1975) examined the parameters which influence the anchorage capacities of bent rebars. Eighty specimens containing rebars bent to different geometric configuration were tested to determine the effect of bond length, angle included in the bend, inside radius of bend, and rebar diameter on the deformation and strength of hooked rebar anchorages. The load-slip curves obtained were used to compare the performances of different rebar geometries. The results indicated that at a given rebar stress, the larger the angle of bend or the smaller the radius of bend, the greater will be the slip. Ultimate strength of hooked rebar anchorages is about the same as that of straight rebars.

The performance of hooked bar anchorages in beam-column joints was examined by Marques and Jirsa (1975). The measured results indicated that strength was increased as restraint against side splitting was provided.

According to Pinc, et al. (1977), sixteen specimens were tested to investigate the influence of straight lead embedment on the strength of hooked rebar anchorages. The bars were loaded in tension to failure to establish basic strength and stiffness characteristics. The main contribution of the study is that the proposed approach is a major departure from ACI 318-77 in that it uncouples hooked bar anchorages from straight bar development provisions and gives the total embedment length, l_{hb}, as indicated in ACI 318-83. The experimental results indicated that the failure of a hooked bar was governed primarily by a loss of cover rather than by pullout, and the principal factor affecting anchorage capacity was the length of lead embedment. On the basis of test results obtained by Marques and Jirsa (1975), and Pinc, et al. (1977), Jirsa, et al. (1979) indicate minimum values of l_{hb} to prevent failure by direct pullout in cases where the standard hook may be located very near the critical section.

Ueda et al. (1986) reported the development of a computer program for predications of axial force-loaded end displacement characteristics for beam bars anchored within exterior column-beam connections. Predicted axial force displacement relationships are shown to be in good agreement with results obtained in tests on 22

specimens representing well-reinforced exterior column-beam connections, for which the beam bars were straight or terminated with a standard 90 deg hook. Seven specimens simulating the behavior of beam reinforcement anchoraged by 90-deg standard hooks inside an exterior beam-column connection were tested by Soroushian et al. (1988). From the results of the limited experimental and analytical studies performed in this study, it may be concluded that the hook pullout resistance increases with increasing bar diameter. Confinement of concrete surrounding the hook is an important factor influencing the hook performance.

Bond behavior of epoxy-coated hooked rebars was first studied by Hamad, et al. (1990, 1993). Twenty four specimens, simulating exterior beam-column joints in a structure, were tested, and the effects of bar size, concrete strength, concrete cover, and hook geometry were evaluated. Number 11 hooked bars consistently showed lower stress-slip stiffness than #7 hooked bars. Anchorage capacities and load-slip stiffness of #7 and #11 hooked bars increased with increase in concrete strength. The reduction of side concrete cover caused a reduction in the anchorage strength of #7 hooked bars. Also, 90-degree hooked bars showed greater load-slip stiffness than 180-degree hooked bars at a high level of loading prior to failure. Epoxy-coated hooked bars consistently developed lower anchorage capacities and load-slip stiffness than companion uncoated hooked bars. On the basis of the test results, a 20% increase in the basic development length l_{hb} of an uncoated hooked bar is recommended for epoxy-coated hooked bars.

1.2.3 Bond of Straight GFRP Rebars to Concrete

In cooperation with the Marshall-Vega Corporation of Marshall, Arkansas, Pleiman (1987, 1991) conducted 4 pullout tests with #2 bars, 19 with #3 bars, and 21 with #4 bars, reporting that the bond strength of the bars improved with size. The embedment length may be safely assumed to be given by

$$l_d = \frac{f_u A_b}{20\sqrt{f_c'}}$$

for E-glass rebar, and

$$l_d = \frac{f_u A_b}{18\sqrt{f_c'}}$$

for Kevlar 49 rebar. In the equations above, l_d is the embedment length in inches, f_u is the ultimate stress of rebars in psi, A_b is the cross sectional area of the rebar in in.^{2}, and f_c' is the 28-day strength of the concrete in psi.

Faza and GangaRao (1990), and GangaRao and Faza (1991) investigated the bond behavior of FRP rebars by testing cantilever beam and pullout specimens. The results indicated that the basic development length of FRP rebars should be computed using the equation

$$l_{db} = 0.06 \frac{A_b f_{yf}}{\sqrt{f_c'}}$$

with f_{yf} taken as the effective yield strength of FRP rebars in psi, and f_c' not to exceed 10,000 psi (69 MPa).

Bond stress-slip relationships of FRP rebars in concrete were studied by Larralde and Silva (1990, 1993), and Larralde et al. (1993). In the pullout testing, the concrete surrounding the rebars is under compression reducing the possibility of cracking and increasing the bond strength due to Poisson's effect. In contrast, in concrete beams, the concrete surrounding the rebars is under tension, thus allowing for cracking at lower stresses and reducing friction. As such, the nominal bond strength obtained from pullout tests does not reflect the actual conditions in flexural reinforced concrete members but, should be greater than the nominal bond strength required in rebars under flexural tension. In addition, from the experimental results, it is concluded that the anchorage design for steel rebars is not directly applicable on FRP rebars. For the same test conditions, the average nominal bond stress at failure was greater for the steel rebars than for the FRP rebars. The slips of the rebars relative to the concrete surface was greater for the FRP rebars than for steel rebars.

To study the mechanical properties of fiber reinforced plastic bars, Wu et al. (1991) conducted 136 tests to describe the structural behavior of FRP bars under static loads and characterize their material properties. Stiffness properties of FRP bars are dominated by the fibers' properties and their volume fraction. They are insensitive to

the specimen size and type, matrix, test methods, and manufactures. The Young's moduli in bending and tension are nearly equal and their values are around $7x10^6$ psi, whereas the compression modulus values is close to $5.5x10^6$ psi. The strength properties are strongly affected by fiber properties and its volume fraction. Also, tensile strength of the FRP bars depends on the specimen diameter due to the "shear lag" on interlaminar or tensile forces of fibers across the cross-section.

In a study conducted by Saadatmanesh and Ehsani (1991), five rectangular beams and one T-beam were tested with GFRP rebars used as either flexural or shear reinforcement. The behavior of each beam was characterized by its load-deflection response to failure. The study was mainly focused on experimentally determining the feasibility of GFRP bars as reinforcement for concrete structures. The preliminary results from the tests of concrete beams reinforced with fiber composite rebars and stirrups indicate that great potential exists for the use of synthetic rebars in concrete structures, especially in areas where corrosion is a problem. On the basis of the relatively large number of narrow cracks in the beams it was concluded that the bond between the GFRP rebars and concrete was good. No failure was observed due to debonding of the rebars and concrete. However, as noted earlier, this study did not include any direct measurements of bond stresses.

In another study, by Chaallal, et al. (1992), pullout tests were undertaken to evaluate bond strength as well as development length of glass fiber composite (GFC) rod when embedded in normal strength concrete (NSC) and high strength concrete (HSC). Development length is defined as the minimum embedded length required to develop the ultimate tensile force, F_u, of the rod. It is concluded that development length can be taken to be around 20 d for both NSC and HSC.

Bond strength of fiber-reinforced plastic rebars was experimentally investigated by Daniali (1992). A total of 30 concrete beams was tested, and results showed that a development length of 8 inches was adequate for developing the ultimate tensile strength of a #4 bar. The full strength of a #6 bar could be developed over 18 inches of embedment length if shear reinforcement was provided along the entire length of the specimens.

An overview of GFRP rebars has been presented by Ehsani (1993). This includes the manufacturing and mechanical characteristics of the bar itself, as well as the behavior of structural members reinforced with GFRP rebars. There is no doubt that composites are rapidly becoming the next generation of construction materials.

Mashima and Iwamoto (1993) studied the bond properties of FRP rod and concrete after freezing and thawing deterioration. It is concluded that unevenness of rod

surface and processing method influences on the bond strength. Glass, vinylon, and carbon FRP is not influenced to the bond strength so much by freezing and thawing deterioration. Aramid fiber FRP both of braided and coiled types reduce the bond strength gradually with progress of freezing and thawing.

An experimental program consisting of three series of tests was conducted in order to investigate the bond performance of concrete members reinforced with FRP bars by Kanakubo et al. (1993). Test results from pull-out specimens show that the bond splitting strength can be estimated using the ratio of lug height to diameter of FRP bars.

Erki and Rizkalla (1993) pointed out that GFRP is the least expensive type of FRP reinforcement. Most GFRP reinforcement on the market is proposed for non-prestressed reinforcement, since GFRP has a very low transverse shear strength, which makes it difficult to make prestressing anchorages for GFRP. Surface treatments such as quartz sand to give a rough finish and external fiber windings to produce a ribbed surface have been applied to GFRP rods to improve their bond with concrete.

1.2.4 Bond of Hooked GFRP Rebar to Concrete

To date there has been only one research work done to study the bond characteristics of hooked GFRP rebars to concrete by Maruyama et al. (1993). In this

study, the authors introduced bends into FRP rods and then after embedding them in concrete, applied loads to investigate the tensile strength of the bent portions. The results show that the FRP rods ruptured at the bent portion, the location of the rupture being the beginning of the bend on the loading side. No rupturing at the bend occurred with steel-bar reinforcement. The tensile strength of the bent portion of FRP rods tended to decrease hyperbolically as the curvature of the processed portion increased.

1.3 Scope of the Study

To investigate the bond behavior of GFRP rebars to concrete, the parametric studies on straight and hooked GFRP rebars were presented in APPENDIX A and B, respectively. Furthermore, to determine the practical design guidelines for ACI Code concerning the bond of GFRP rebars to concrete, the analytical study on GFRP rebars was appeared in APPENDIX C.

1.3.1 Parametric Study on Straight GFRP Rebars

To study bond behavior of straight GFRP rebars to concrete, 48 beam specimens and 18 pull-out specimens were constructed and tested. Variables included in the specimens were concrete compressive strength, embedment length, clear concrete cover, rebar diameter, and concrete cast depth. For both beam and pull-out tests, the collected

data included the load values under static loading status, the slip values at loaded and free ends, and mode of failure. In addition, load-slip relationships and ultimate bond stress corresponding to ultimate load values were also obtained.

Based on the experimental results, effects of concrete compressive strength, embedment length, clear concrete cover, and casting position on bond characteristics of straight GFRP rebars to concrete, and comparison of beam and pull-out specimens were discussed in detail and presented in paper one attached in APPENDIX A.

1.3.2 Parametric Study on Hooked GFRP Rebars

To investigate the influence of several parameters on bond behavior of hooked GFRP rebars to concrete, 36 specimens were constructed and tested subjected to static monotonic loading. Variables in hooked rebars specimens included concrete compressive strength, radius of bend, tail length, lead embedment length, and rebar diameter. The load values, the loaded end slip values, and mode of failure were obtained during testing. Subsequently, load-slip relationships and ultimate tensile stresses were determined.

The experimental results were conducted to examine the effects of concrete compressive strength, radius, tail length, and lead embedment length on bond behavior of hooked GFRP rebars to concrete, and reported as paper two in APPENDIX B.

1.3.3 Analytical Study on GFRP Rebars

The main purpose of the research project is to develop the practical design guidelines for ACI Code pertaining to the bond of GFRP rebars to concrete. According to the experimental results obtained from 48 beam, 18 pull-out, and 36 hooked rebar specimens, the basic development length expressions were established for various rebars, including the effect of varying concrete compressive strength. In addition, new criteria for acceptable bond performance of GFRP rebars to concrete were developed. Moreover, the confinement factors were also derived to reflect the influence of the concrete cover and casting position. The paper three listed in APPENDIX C presented the process of analytical study on GFRP rebars to concrete.

2. PRESENT STUDY

The methods, results, and conclusions of this study are presented in the papers one through three appended to this dissertation. All load-slip relationships and experimental results of beam, pull-out, and hooked rebar specimens are given in APPENDIX D and E, respectively. In addition, the dimensions of the grip system are listed in APPENDIX F. The following is a summary of the most important findings in the three papers.

First, for straight GFRP rebars, the ultimate bond stress was found to increase with increasing concrete compressive strength. The applied tensile load approached the ultimate tensile capacity of rebars, f_u, with increases in the embedment length. Compared with pull-out test, beam test data could be more realistic and accurate for use in determination of development length.

Due to the absence of concrete flexural cracks in pull-out specimens, higher ultimate bond stress and greater slip at loaded and free ends were developed. This clearly indicated that it is unconservative to rely on data from pull-out tests for determination of development lengths. It would be more realistic and accurate to use beam test data in such derivations. The test results from pull-out specimens were only used in comparison with beam specimens for the determination of top bar effects.

For steel rebars, the critical bond stress is defined as the smaller of that associated with a loaded-end slip of 0.01 in. (0.25 mm) or a free-end slip of 0.002 in. (0.05 mm). The above slip limitations for steel rebars cannot be directly utilized in evaluation of GFRP rebars which differ from steel rebars in three important aspects. First, lower modulus of elasticity of GFRP rebars results in greater elongation and contributes to the loaded-end slip. Second, due to higher Poisson's ratio, the greater reduction of rebar diameter under uniaxial tension causes a degradation of adhesion and friction to concrete and larger slips at loaded and free ends. Third, the shallower lugs of GFRP bars can not resist large bearing stresses and result in greater loaded end and free-end slips.

Thus, new criteria for bond of GFRP rebars needed to be developed. These criteria were developed based on load-slip relationships. The critical bond stress, new criteria for GFRP rebars, is defined as the smaller of the bond stresses associated with either a free end slip of 0.0025 in. (0.064 mm) or a loaded end slip of 0.015 in. (0.38 mm). The basic development length l_{db} of straight GFRP rebars should be computed using

$$l_{db}=0.047\frac{A_b f_y}{\sqrt{f_c'}}$$

To account for the influence of concrete cover, the factor 1.0 can be used with concrete cover of not less than two times bar diameters. The factor 1.5 shall be used with cover of one bar diameter or less. The development length l_d computed as the product of the

basic development length l_{db} and the confinement factors 1.0 or 1.5 shall not be less than

$$l_{db}=0.00035 d_b f_y$$

The bond strength developed for top rebars is less than that of bottom one. Therefore, the confinement factor 1.25 can be used for top cast rebars. Moreover, the development length l_d, computed as the product of the basic development length l_{db} and the applicable modification factors was assumed to be not less than 15 in. (381 mm) for GFRP rebars.

Second, for hooked GFRP rebars, high concrete compressive strength may result in larger tensile stress of hooked rebars with r/d_b as three and greater initial stiffness. The applied tensile load and initial stiffness increase with an increase in terms of radius of bend or lead embedment length. Very sharp bends should be avoided, larger bend radii may be advantageous to be utilized for the purpose of design. The hooked GFRP rebars manufactured with 12 times bar diameter tail length may be suggested to use in the design of end anchorage.

Meanwhile, the basic development length L_{hb} for hooked GFRP rebars with f_y equal to 75,000 psi (517 MPa) shall be computed by

$$L_{hb}=1820\frac{d_b}{\sqrt{f_c'}}$$

For the rebar yield strength other than 75,000 psi (517 MPa), the modification factor

$f_y/75,000$ can be used. When side cover and cover on bar extension beyond hook are not less than 2-1/2 in. (64 mm) and 2 in. (51 mm), respectively, the modification factor 0.7 shall be used. Moreover, to prevent direct pull out failure in cases where the hooked rebar may be located very near the critical section, the development length L_{dh} computed as the product of the basic development length L_{hb} and the applicable modification factors shall be the greater of eight times bar diameter or 6 in. (152 mm).

APPENDIX A: A COPY OF PAPER ONE

EXPERIMENTAL STUDY OF BOND OF DEFORMED COMPOSITE REBARS TO CONCRETE

M. R. Ehsani, H. Saadatmanesh, and S. Tao

Department of Civil Engineering and Engineering Mechanics
University of Arizona
Tucson, AZ 85721

Submitted for review and publication in the ACI Structural Journal

ABSTRACT

Bond behavior of straight Glass-Fiber-Reinforced-Plastic (GFRP) reinforcing bars to concrete was experimentally investigated. A total of 66 specimens were tested. Results of 48 beam and 18 pull-out specimens constructed with #3, #6, and #9 GFRP rebars are presented. The static tensile load was applied to the rebars in a gradual increment of load level until splitting failure of concrete, rebar pull out failure, or rebar fracture occurred. The slip between the rebars and concrete was measured at the loaded and free ends at each load level. Variables included in the study were concrete compressive strength, embedment length, clear concrete cover, rebar diameter, and concrete cast depth. On the basis of the experimental results, it was concluded that the ultimate bond stress increases with higher concrete compressive strength and clear concrete cover, but decreases with larger concrete cast depth. The ultimate bond stress and the loaded end slip of the pull-out specimens were found to be greater than that of the beam specimens. Beam test data could be more realistic and accurate for use in determining the development length.

Keywords: Glass-Fiber-Reinforced-Plastic (GFRP), rebar, bond strength, reinforced concrete, development length, anchorage.

Concrete reinforced with steel reinforcing bars is widely used in a variety of construction projects such as bridge decks, parking garages, etc. However, corrosion of reinforcing steel is a particularly serious problem in structures located in aggressive environments. Rust from corroded rebars occupies a larger volume than the iron from which it is formed. This results in large internal pressures which lead to cracking and spalling of concrete. With time, deep pitting and a severe loss of cross section of the reinforcing steel can take place. A combination of high stress and intense corrosion may lead to costly repairs or catastrophic failure of the structure.

Several methods have been developed and used to prevent corrosion of steel reinforcement such as the use of additives and admixtures to improve the permeability of concrete and the use of epoxy-coated steel rebars. The latter has been used extensively in bridges and parking structures. However, the recent discovery of extensive premature corrosion of epoxy-coated steel rebars in new bridges points to the shortcomings of this technique (Keesler and Powers, 1988). Therefore, there is a growing interest in developing more durable materials as replacement for steel rebars for construction in severe environments.

Glass-Fiber-Reinforced-Plastic (GFRP) rebars which have been produced in recent years appear to be an ideal candidate and have great potential to fill such a need. These rebars have several important advantages over conventional reinforcing steel, namely, high corrosion resistance, high tensile strength, high strength-to-weight ratio, nonconductivity, ease of handling and cutting, and economy (Ehsani, 1993).

A major shortcoming limiting the use of GFRP rebars is the lack of information and design guidelines on their bond to concrete. Pleimann conducted pull-out tests and reported that the bond strength of the rebars improved with bar diameter (Pleimann, 1987 and 1991).

In a study conducted by Saadatmanesh and Ehsani (1991), five rectangular beams and one T-beam were tested in which GFRP rebars were used as either flexural or shear reinforcement. Based on the relatively large number of narrow cracks in the beams, it was concluded that bond between the GFRP rebars and concrete was good. No failure was observed due to debonding of

the rebars and concrete.

Faza and GangaRao (1990) investigated the bond behavior of FRP rebars by testing cantilever beams and pullout specimens. The results indicated that the decrease in the bond strength with increasing embedment length was attributed to the increase in the perimeter area of the rebars.

In another study by Chaallal, et al. (1992), pullout tests were undertaken to evaluate bond strength as well as development length of glass fiber composite rods embedded in normal strength concrete (NSC) and high strength concrete (HSC). Development length was defined as the minimum embedded length required to develop the ultimate tensile force, F_u, of the rod. It was concluded that development length is approximately twenty times the bar diameter for both NSC and HSC.

Bond strength of fiber-reinforced plastic rebars was experimentally investigated by Daniali (1992). A total of 30 concrete beams were tested and results showed that a development length of 8 in. (203 mm) was adequate for developing the ultimate tensile strength of a No. 4 bar. The full strength of a No. 6 bar could be developed over 18 in. (457 mm) of embedment length if shear reinforcement was provided along the entire length of the specimen. Still, the lack of sufficient information about bond behavior of GFRP rebars to concrete limits their use in field applications.

The principal objective of this research project was to examine the bond behavior of straight and hooked GFRP rebars to concrete. A total of 102 specimens have been tested. Based on the experimental results, the analytical study focused on the derivation of design equations, i.e., basic development length expressions for straight and hooked GFRP rebars. Due to space limitation, this paper will discuss the study of the bond behavior of straight GFRP rebars to concrete only. The study on bond behavior of hooked GFRP rebars to concrete, and the development of design guidelines for bond of GFRP rebars to concrete are presented elsewhere (Tao, 1994).

RESEARCH SIGNIFICANCE

There is a growing interest in the use of composite rebars which lead to more durable structures. However, the lack of data on bond performance has limited the field application of these materials. The findings of this study should be of interest to design engineers, manufactures, and those involved in development of code provisions.

EXPERIMENTAL PROGRAM

The primary objectives of the research program discussed here were to investigate the influence of several parameters on bond behavior of straight GFRP rebars to concrete. Forty eight beam specimens and 18 pull-out specimens were constructed and tested. Variables in both beam and pull-out tests were concrete compressive strength, embedment length, clear concrete cover, rebar diameter, and concrete cast depth. For both beam and pull-out tests, the collected data included ultimate load under static loading, ultimate bond stress, slip at loaded and free ends, mode of failure, and load-slip relationships.

Design and Construction of Specimens

The specimens were divided into two groups, i.e., beam specimens, and pull-out specimens. The test specimens are shown in Fig. 1, and the dimensions of beam specimens are listed in Table 1. It has been suggested that the bond strength of rebars is affected by the unbonded lead length of the bar (Hadje-Ghaffari, et al., 1992). To eliminate this effect, the leading 3 in. (76 mm) of each rebar was covered with a thin conduit to prevent its bonding to concrete (Fig. 1). The unbonded region near the free end of each bar was varied so that, the desired bonded length, L, could be obtained.

The concrete was placed in several lifts, and each layer was compacted with the aid of an electrical vibrator. Sixteen 6 x 12 in. (152 x 305 mm) test cylinders were cast from each batch. They were cured under the same condition as the specimens. At the end of casting, the

top surfaces of all specimens and cylinders were covered with plastic sheets, and allowed to cure for 7 days. At that time, the plywood forms were removed and the specimens and cylinders were stored under the same environmental condition until the day of testing. All specimens were older than 28 days at the time of testing.

Material Properties

Two batches of concrete were ordered from a local ready-mix plant. The mixes were designed to provide a minimum 28-day compressive strength of 4000 and 8000 psi (28 and 56 MPa). Maximum size of the concrete aggregate was 1 in. (25 mm).

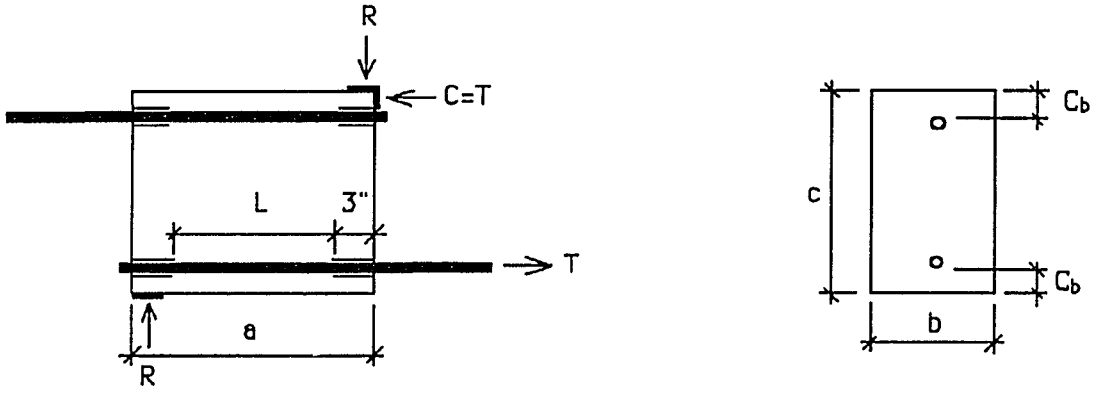

(a) View of Beam Specimens

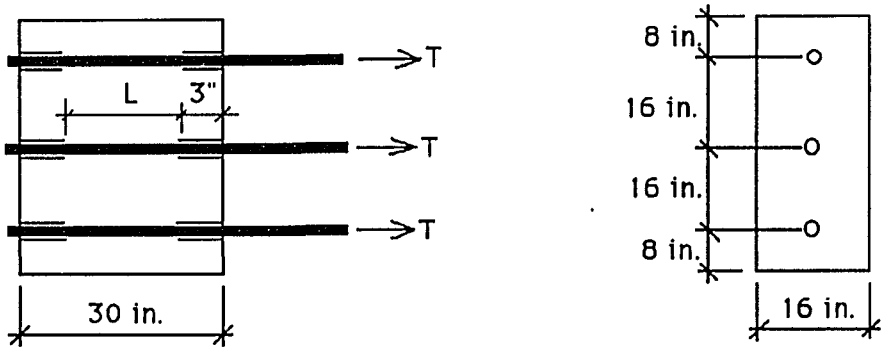

(b) View of Pull-out Specimens

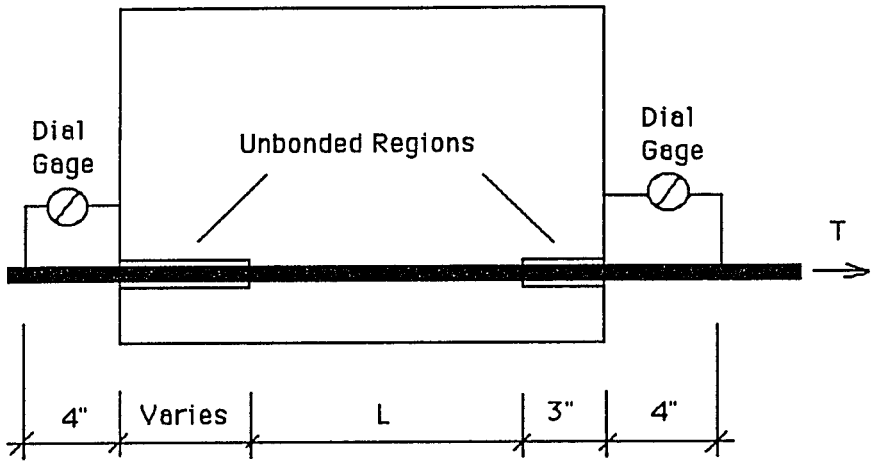

(c) Dial Gage Set Up

Fig. 1 - Test Specimens

Table 1 - Dimensions of Beam Specimens

Rebar Size	a (in.)	b (in.)	c (in.)
No. 3	14	10	14
No. 6	24	20	24
No. 9	36	20	30

Note: 1 in. =25.4 mm

The GFRP rebars used in the tests were supplied by a U. S. manufacture. They were made of polyester resin and type E glass fibers with a glass content of around 60% by weight. No. 3, 6, and 9 GFRP rebars were used in this study (Fig. 2). During manufacturing, the longitudinal fibers are wrapped in a helical pattern with a small strand to induce deformations on the bar and to improve its bond behavior. The width of the strand is usually the same for all rebar sizes. As shown in Fig. 3, the pitch is defined as the distance from the center to center of strands. Larger diameter rebars had longer pitches. Although most manufactures produce GFRP rebars in the same diameters as steel rebars, there are no standard sizes for composite rods. Due to this lack of standards, non-uniformities usually exist in the physical dimensions of GFRP rebars. Some rebars may even have cross-sections that are slightly oval shaped rather than

a true circle (Ehsani, 1993). Representative 6 in. (152 mm) rebar samples were cut and submerged in a graduated cylinder to measure their volumes. Rebar diameter were then calculated from these values assuming a circular cross section for the bars. These measurements are slightly different from the nominal values (Table 2). Rib heights were calculated as an average of one half of the difference between the largest and smallest diameters for several points along the sample. The results are also presented in Table 2.

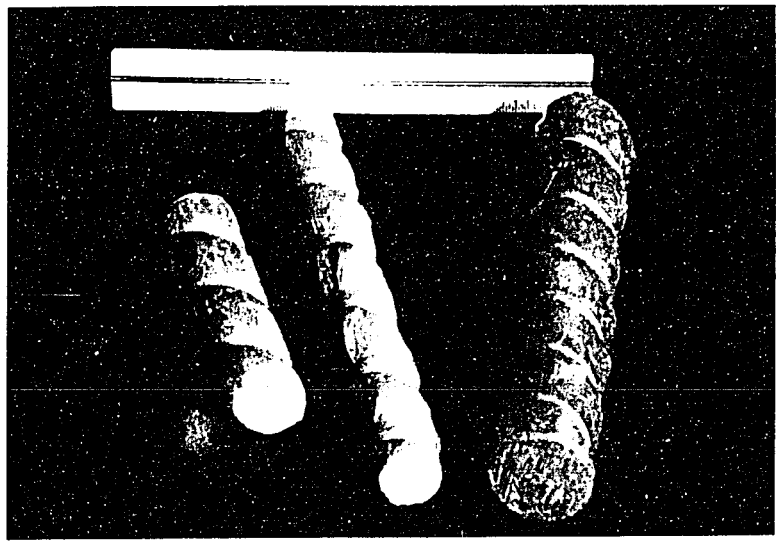

Fig. 2 - No. 6, 3, and 9 GFRP Rebars Used in the Study

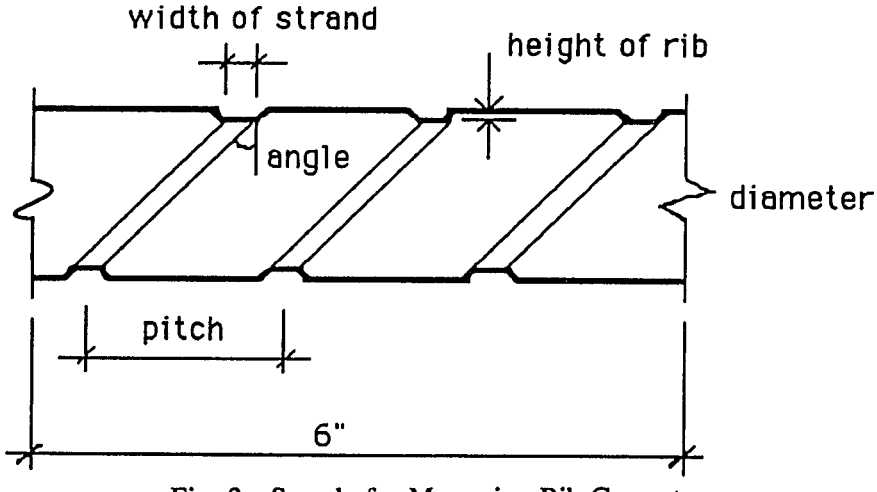

Fig. 3 - Sample for Measuring Rib Geometry

Table 2 - Rib Geometry of GFRP Rebars

Property	No. 3	No. 6	No. 9
Rib Height, in.	0.045	0.051	0.079
Pitch, in.	0.687	0.938	1.063
Angle, Degree	37	25	23
Measured Diameter, in.	0.381	0.726	1.079
Nominal Diameter, in.	0.375	0.750	1.125

Note: 1 in. =25.4 mm

The ultimate tensile strength and the modulus of elasticity of GFRP rebars were measured based on the average values for uniaxial tension tests of three coupons for each bar size. A linear stress-strain relation for the entire range of loading was obtained for all tension tests. The average ultimate tensile strength for No. 3, 6, and 9 bars were 135, 93, and 77 ksi (931, 641, and 531 MPa), respectively. The average modulus of elasticity for No. 3, 6, and 9 bars were 6810, 7050, and 7280 ksi (46950, 48610, and 50200 MPa), respectively.

The modulus of elasticity for GFRP rebars is almost constant and averages about 7000 psi (48270 MPa). However, the results point out that the tensile strength decreases with an increase in the rebar diameter. This reduction in strength is attributed to the "shear lag" phenomenon associated with the tensile force resistance of the core fibers and those at the contact surface of the rebars and the grips (Wu 1991).

Test Set Up and Instrumentation

The beam specimens were tested in the steel reaction frame shown in Fig. 4. This test set up resulted in a state of stress similar to that in a concrete beam, i.e. compression in the top of the section while the GFRP bar is under tension. However, for pull-out tests shown in Fig. 5, the jack was in direct contact with the surface of the specimens, applying a compressive reaction force to the concrete block (Ehsani, et. al 1993).

Due to the low shear strength of GFRP rebars, care must be taken not to harm the rebars during the handling of the specimens and their positioning in the test frame. The tensile load was applied to the rebars using a hydraulic jack. The specimens were loaded under static loading and in a gradual increment of load level until splitting of concrete, rebar pull out, or fracture of rebar occurred. The applied load was monitored by a load cell and the results were automatically recorded and printed at predetermined intervals.

In earlier studies, the design and development of suitable grips to transfer loads to GFRP rebars embedded in concrete have presented some difficulties. Because glass fiber based composites are very weak for loads applied transverse to the fiber direction, the region of the GFRP rebar in the grip must be protected against crushing. The grip must grasp the rebars in a manner as to avoid failure of the rebar at the grips, allowing the failure to take place in the rebar away from the grip region (Faza and GangaRao, 1990). A specially constructed set of sand-coated grips similar to those used in testing of GFRP rebars at West Virginia University were employed. The applied loads are transmitted from the jack to the GFRP rebars through these grips. The tests were successful in avoiding excessive slippage and or rebar failure in the grips. The sand-coated grips have proven effective for all rebar sizes.

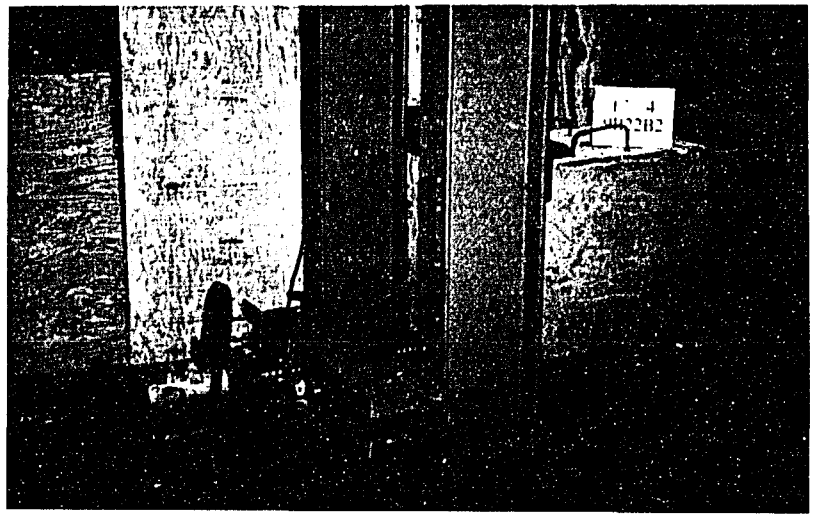

Fig. 4 - Test Set Up for Beam Specimens

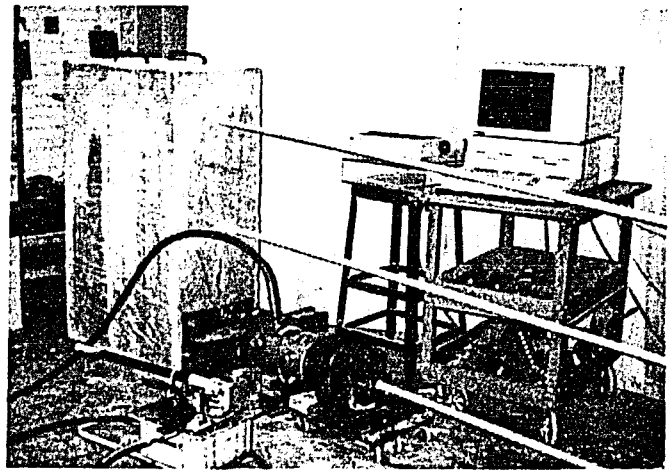

Fig. 5 - Test Set Up for Pull-out Specimens

At each load increment, the slip between the rebar and concrete was recorded at the loaded and free ends of the rebar. As seen in Fig. 1 (c), this was obtained through dial gages which were attached to the loaded- and the free-ends of the rebar.

TEST RESULTS

The bond behavior of straight GFRP rebars to concrete was studied through testing of 66 specimens. The measurements of the load values and slips at loaded and free ends were taken at each increment of static loading. The load values were used to determine the corresponding bond stress. Bond stress is defined as the shear force per unit surface area of the rebar, and computed as

$$u=\frac{T}{\pi d_b l_d} \tag{7}$$

where, u=bond stress, T=applied tension force, d_b=diameter of the rebar, and l_d=embedment length.

A typical curve representing the load values versus slips at loaded and free ends for Specimen 46B18T6 is shown in Fig. 6. Obviously, the slip at the loaded end is significantly larger than that at the free end. The loaded-end slip increased with the increase of load values at the beginning of the loading. However, the free end slips would not take place until the adhesion resistance between the rebar and concrete was broken.

As shown previously in Fig. 1 (c), the dial gage attached to the loaded end of the rebar measured the movement of a point 4 in. (102 mm) away from the concrete block relative to the face of the block. In addition, the first 3 in. (76 mm) of the rebar was always shielded to prevent its bonding to concrete. Therefore, the measured slip at the loaded end of the rebar included the elastic elongation of the 7-in. (178-mm) lead length. Due to the low modulus of elasticity of GFRPs, this elongation is significant and had to be corrected for. Thus, the actual slip, δ_a, was calculated as the difference between the measured slip at the loaded end, δ_m, and the elastic deformation, δ_e.

The test data for beam specimens and pull-out specimens are given in Tables 3 and 4, respectively. The notation for beam specimens is as follows: the first number indicates the concrete compressive strength; the second number, the rebar diameter; the letter "B" for beam specimen; the forth number, the embedment length in inches; the next letter designates the rebar casting position, T: Top, M: Middle and B: Bottom; and the last number, the ratio of the clear concrete cover to rebar diameter. For instance, 43B1.5T1 was a beam specimen cast with 4000-psi (28-MPa) concrete, No. 3 GFRP rebar, 1.5-in. (38-mm) embedment length, top rebar, with a clear concrete cover of one rebar diameter.

For pullout specimens, the first number represents the concrete compressive strength; the second, the rebar diameter; the letter "P" to designate a pull-out specimen; the next character identifies the rebar casting position; B:Bottom, M:Middle, T:Top, and the last number is the embedment length in inches. As shown in Fig. 1, all pull-out specimens had very large clear covers on all sides.

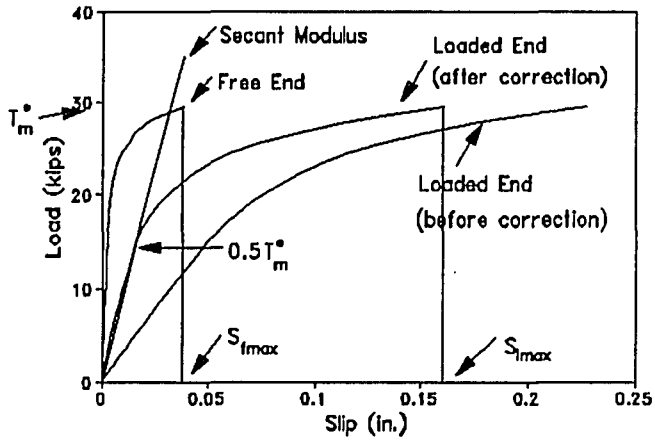

Fig. 6 - Typical Load vs. Slip Relationship

In order to eliminate the effects of the minor variation in the concrete compressive strength for the 4000- and 8000-psi (28- and 56-MPa) specimens, it was decided to normalize the results with respect to the average concrete compressive strength for each group. The procedure carried out was as follows. For each group of specimens which were tested at approximately the same age, three concrete cylinders were tested in compression. For example, for Specimens 43B1.5T1, 43B1.5T2, and 43B3T2, three cylinders were tested which resulted in an average compressive strength of 4010 psi (27.6 MPa). This value is reported in the second column of Table 3 for these three specimens. Next, an average compressive strength, f'_{cavg}, was calculated for all specimens with nominal concrete strength of 4000 or 8000 psi (28 or 56 MPa). These averages were 4810 psi (33 MPa) and 6820 psi (47 MPa), respectively.

It is widely accepted that bond failure is proportional to tensile strength of concrete (Ferguson and Thompson, 1962). Since the tensile strength of concrete is proportional to the square root of its compressive strength, bond expressions also include the $\sqrt{f'_c}$ term (ACI 318-89). For ease of comparison, the maximum load and bond stresses reported in column 3 and 4 of Tables 3 and 4 have been multiplied by the factor $\sqrt{f_{cavg}}/f'_c$ and reported as T_m^* and

u_m^*, respectively. This eliminated any influence the changes in f'_c might have on further analysis of the test results.

The fifth column in Tables 3 and 4 includes the ratio of T_m^*/T_u. The denominator represents the ultimate tensile strength of the rebar which is calculated as the product of the minimum area for each bar from Table 2 times the average tensile strength. The numerator is the maximum load carried by the rebar during the test. The ratio should be less than or equal to one. Occasionally, the ratio is slightly greater than one. This occurs when the mode of failure is due to tension failure of the rebar outside of the specimen and the strength of the rebar is slightly higher than the average value.

During tests, the slip at both ends of the bar increased with an increase in loading. In some specimens which failed by concrete splitting or bar pull out, the load vs. slip curves exhibited a descending portion; i.e., after the maximum load was reached, the bar would continue to slip while the load was reduced. As shown in Fig. 6, the maximum slips reported in columns 6 and 7 of Tables 3 and 4 correspond to those measured at the maximum applied load.

One of the ways to compare the performance of different specimens is in terms of their stiffness. Because the service load stresses in GFRP rebars are expected to remain well below 50% of their ultimate strength, the initial stiffness, E_i, was defined as a secant modulus passing through the point of $0.5T_m^*$ (Fig. 6). The values of initial stiffness are listed in Tables 3 and 4.

Table 3 - Test Data for Beam Specimens

Specimen	f'_c, psi	T_m^*, kips	U_m^*, psi	T_m^*/T_u	S_{fmax}, in.	S_{lmax}, in.	E_i, k/in	Failure Mode
43B1.5T1	4010	5.6	3169	0.50	0.0186	0.0602	312	S
43B1.5T2	4010	7.0	3961	0.63	0.0134	0.0443	646	P
43B3T2	4010	7.6	2150	0.68	0.0245	0.0769	654	P
43B4B2	4330	8.1	1719	0.73	0.0036	0.0198	587	R
43B4T2	4330	8.8	1867	0.79	0.0039	0.0208	508	R
43B6B4	5080	9.7	1372	0.87	0.0039	0.0211	605	R
43B6T4	5080	8.7	1231	0.78	0.0043	0.0221	510	R
43B8B6	5080	10.2	1082	0.92	0.0038	0.0243	641	R
43B8T6	5080	8.6	912	0.77	0.0041	0.0251	549	R
83B4B2	7100	8.2	1740	0.74	0.0057	0.0248	530	R
83B4T2	7100	8.8	1867	0.79	0.0064	0.0259	464	R
83B6B4	7100	9.5	1344	0.86	0.0041	0.0204	610	R
83B6T4	7100	8.3	1174	0.75	0.0043	0.0220	546	R
83B8B6	7100	8.4	891	0.76	0.0031	0.0203	843	R
83B8T6	7100	9.5	1008	0.86	0.0033	0.0211	634	R
46B3B1	4010	15.0	2122	0.51	0.0523	0.1998	907	S
46B3T1	4010	12.0	1698	0.41	0.0639	0.1987	643	S
46B3B2	4010	19.2	2716	0.65	0.0453	0.0893	1250	P
46B3T2	4010	16.0	2264	0.54	0.0492	0.1895	1023	P
46B6B2	4010	20.8	1471	0.71	0.0261	0.0956	1208	P
46B6T2	4010	17.0	1203	0.58	0.0478	0.1406	944	P
46B12B2	5680	21.2	750	0.72	0.0345	0.1343	1242	P
46B12T2	5680	19.8	700	0.67	0.0602	0.1111	1080	P
46B16B4	5680	27.4	727	0.93	0.0599	0.1789	1141	P
46B16T4	5680	25.8	684	0.88	0.0695	0.2111	854	P
46B18B6	5680	28.9	681	0.98	0.0347	0.1436	851	R
46B18T6	5680	29.4	693	1.00	0.0386	0.1607	818	R
86B12B2	6920	23.1	817	0.78	0.0678	0.1871	1444	P
86B12T2	6920	22.4	792	0.76	0.0879	0.1998	1232	P
86B16B4	6920	28.2	748	0.96	0.0564	0.1786	1175	P
86B16T4	6920	27.0	716	0.92	0.0625	0.1733	906	P
86B18B6	6920	30.1	710	1.02	0.0294	0.1556	1286	R
86B18T6	6920	29.4	693	1.00	0.0327	0.1701	1012	R
49B4B1	4010	24.6	1740	0.47	0.0456	0.2131	1891	S
49B4B2	4010	35.0	2476	0.67	0.0567	0.2312	3980	P
49B8B2	4010	39.0	1379	0.75	0.0567	0.1982	2469	P
49B22B2	5760	44.1	567	0.84	0.0421	0.1655	3021	P
49B22T2	5760	43.2	556	0.83	0.1028	0.1479	1982	P
49B26B4	5760	48.1	523	0.92	0.0564	0.2111	3435	P
49B26T4	5760	46.1	502	0.88	0.0876	0.2782	2376	P
49B30B6	5760	51.2	483	0.98	0.0469	0.1248	2960	R
49B30T6	5760	51.8	489	0.99	0.0577	0.1414	1862	R
89B22B2	6490	46.0	592	0.88	0.0458	0.1761	2950	P
89B22T2	6490	44.1	567	0.84	0.0811	0.1986	1916	P
89B26B4	6490	49.7	541	0.95	0.0675	0.2023	3311	P
89B26T4	6490	47.9	521	0.92	0.0539	0.2493	2445	P
89B30B6	6490	51.9	489	0.99	0.0371	0.1189	2851	R
89B30T6	6490	54.0	509	1.03	0.0402	0.1212	2044	R

Table 4 - Test Data for Pull-out Specimens

Specimen	f_c' psi	T_m^* kips	U_m^* psi	T_m^*/T_u	S_{fmax} in.	S_{lmax} in.	E_i k/in.	Failure Mode	Top Bar Ratio
43PB1.5	4670	7.5	4244	0.68	0.0081	0.0512	534	P	1.00
43PM1.5	4670	7.2	4074	0.65	0.0146	0.0624	422	P	1.04
43PT1.5	4670	7.1	4018	0.64	0.0153	0.0667	405	P	1.06
83PB6	6640	10.9	1542	0.98	0.0029	0.0241	688	R	1.00
83PM6	6640	9.6	1358	0.86	0.0031	0.0251	560	R	1.14
83PT6	6640	9.1	1287	0.82	0.0032	0.0253	548	R	1.20
46PB6	4670	23.8	1684	0.81	0.0391	0.1711	1103	P	1.00
46PM6	4670	20.0	1415	0.68	0.0493	0.1988	878	P	1.19
46PT6	4670	19.3	1365	0.65	0.0467	0.1999	876	P	1.23
86PB12	6640	27.1	958	0.92	0.0456	0.2114	1366	P	1.00
86PM12	6640	24.9	881	0.84	0.0889	0.2675	1268	P	1.09
86PT12	6640	23.9	845	0.81	0.0998	0.2781	1258	P	1.13
49PB8	4670	47.9	1694	0.92	0.0653	0.2876	1748	P	1.00
49PM8	4670	42.2	1493	0.81	0.0785	0.2988	1172	P	1.13
49PT8	4670	41.8	1478	0.80	0.0789	0.3307	1162	P	1.15
89PB22	6640	49.3	634	0.94	0.0596	0.2112	2967	P	1.00
89PM22	6640	45.8	589	0.88	0.0873	0.3216	1617	P	1.08
89PT22	6640	45.0	579	0.86	0.0856	0.3118	1613	P	1.09

The modes of failure for the specimens included splitting failure of concrete (S), rebar pull out (P), and rebar fracture (R), as shown in Figs. 7 through 9, respectively. The splitting failure is due to the small concrete cover which can not sustain the circumferencial tensile stresses (Park and Paulay, 1975). For shorter embedment lengths, the pull out failure happens when the slips at loaded and free ends increase rapidly with only a slight increase in the applied load. This signals the initial stage of a pull-out failure. If loading of the specimens is continued, the loads carried by the rebar will start to reduce rapidly. In contrast, under the conditions of longer embedment length and sufficient concrete cover, the load can be applied along the rebar until the rebar tensile stress reaches its ultimate strength. This is referred to as the rebar fracture mode.

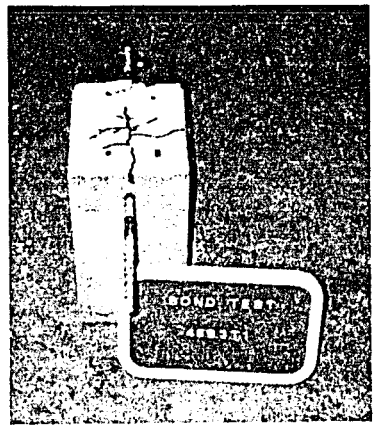

Fig. 7 - Failure of a Specimen by Tension Splitting of the Cover Concrete

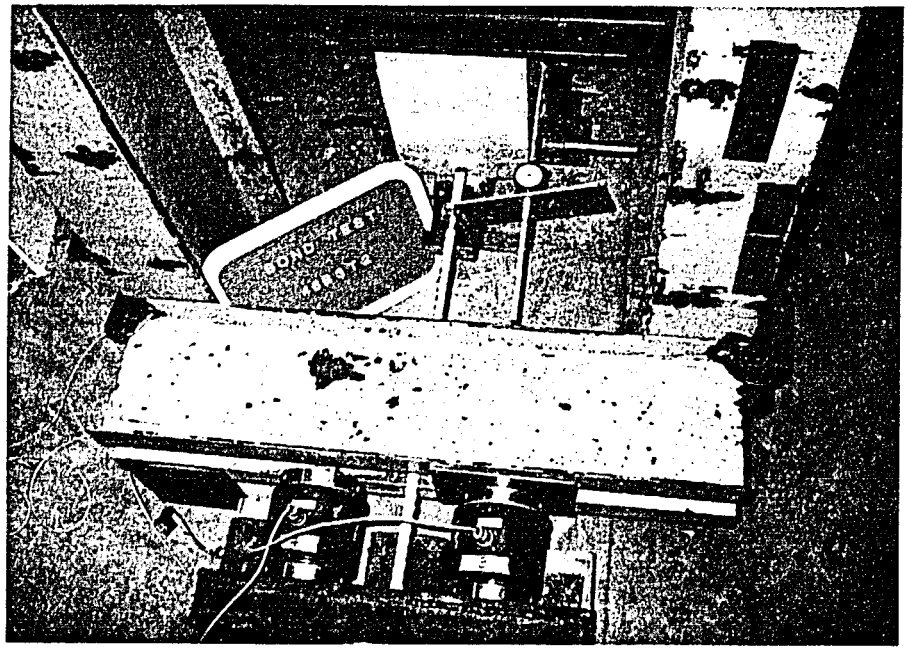

Fig. 8 - Failure of a Specimen due to Pull Out of the Rebar

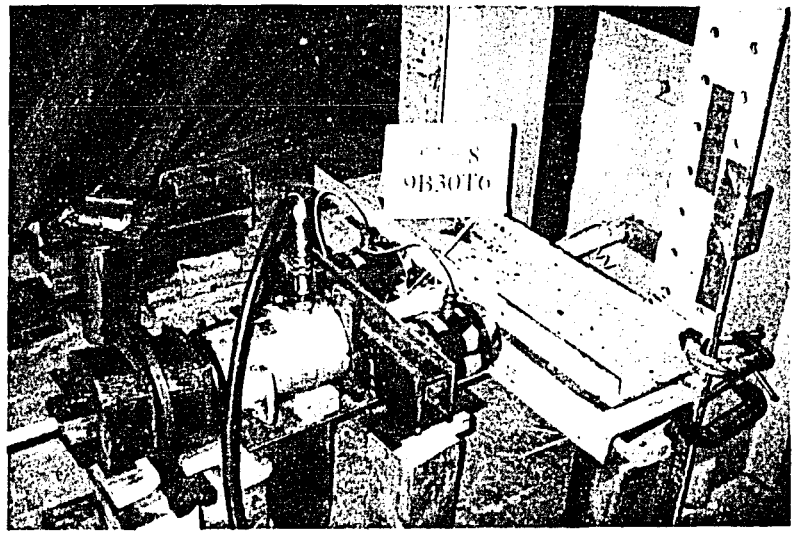

Fig. 9 - Failure of a Specimen by Fracture of the Rebar
Between the Grips and the Concrete Block

Effect of Concrete Compressive Strength

The transfer of the applied load from the rebar to concrete is achieved through the bond mechanism which consists of three components: adhesion, bearing, and friction. Bond failure could be caused by tensile splitting and shearing of the concrete. In these cases, the tensile strength of concrete which is proportional to its compressive strength is considered a key parameter (ACI Committee 408, 1992). The selection of the concrete compressive strength at 4000 and 8000 psi (28 and 56 MPa) was intended to study the effect of this parameter on bond of GFRP rebars to concrete.

Splitting failure and rebar pull out are controlled by concrete strength, but rebar fracture is controlled by the tensile capacity of the rebars only. Examples from three pairs of beam specimens without rebar fracture, i.e., 43B8T6 and 83B8T6, 46B12T2 and 86B12T2, and 49B22B2 and 89B22B2 are shown in Fig. 10. The specimens in each pair had the same conditions except for different concrete strengths. As expected, the ultimate bond stress increased

with the increase in concrete compressive strength, although this increase was not proportional to the square root of the concrete compressive strength. Similar behavior was observed in all other specimens which did not fail due to rebar fracture.

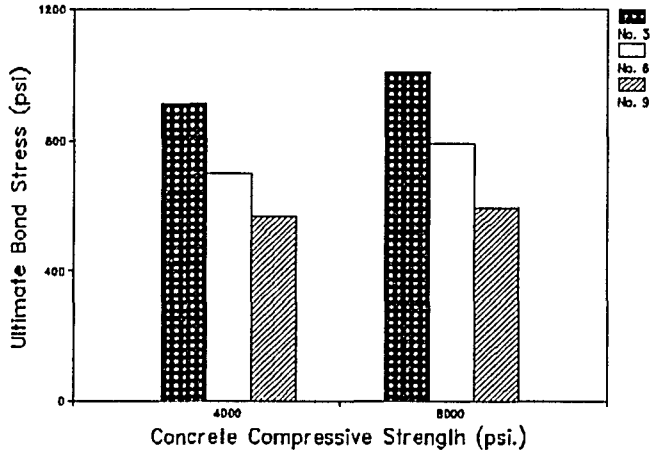

Fig. 10 - Ultimate Bond Stress for Various Concrete Strengths

Effect of Embedment Length

In order to obtain the lower limit for the required embedment length of GFRP rebars, the data from several specimens are compared in Fig. 11. All data are presented for bottom bars in beam specimens constructed with 4000 psi (28 MPa) concrete. The embedment lengths tested for the three different bar diameters ranged as following: No. 3, 4 to 8 in. (102 to 203 mm); No. 6, 3 to 18 in. (76 to 457 mm); and No. 9, 4 to 30 in. (102 to 762 mm). For each specimen, the ratio of the maximum applied load to the ultimate tensile force of the bar is plotted for various embedment lengths. Ideally, the embedment length should be large enough so that this ratio can reach 1.0. As shown in Fig. 11, as the embedment length increases, the applied load does approach the tensile capacity of the rebar.

Based on these data, it is concluded that the minimum embedment length to develop the tensile capacity of No. 3, 6, and 9 rebars must be taken as 8, 18, and 30 in. (203, 457, and 762 mm), respectively. Therefore, in absence of further data, it can be concluded that the minimum embedment length for No. 3, 6, and 9 rebars should be taken as 21, 24, and 27 times their diameters, respectively. Because the analysis of the above data was based on specimens with bottom bars, for top-cast rebars, the required embedment lengths should be multiplied by the top bar factor discussed later.

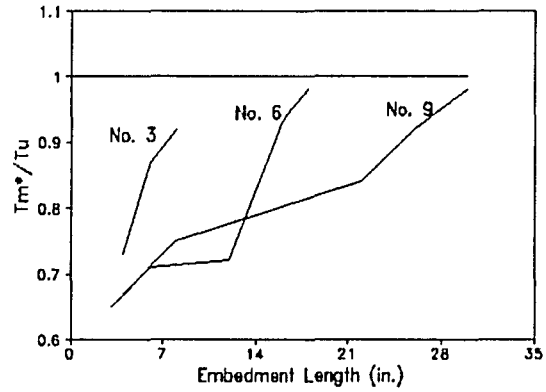

Fig. 11 - Ratio of Maximum Applied Load to Ultimate Tensile Force vs. Embedment Length

Effect of Clear Concrete Cover

The mode of failure observed during testing was strongly dependent on the clear concrete cover. In all specimens with a concrete cover of one rebar diameter, splitting failure occurred. When the cover concrete was twice the rebar diameter, either bar pull out or rebar fracture was observed depending on the embedment length.

For a given embedment length, the ultimate bond stresses in specimens with a clear cover equal to twice the rebar diameter were larger than those for specimens with a clear cover of one rebar diameter, as shown in Fig. 12. The comparison of Specimens 43B1.5T1 and 43B1.5T2

presented in Fig. 13 indicates that smaller clear concrete cover results in lower initial stiffness and greater slip which is caused by the additional internal slip between concrete and rebar, permitted by the splitting cracks along the rebar (Ferguson, et al., 1965). The same trend was observed among all other similar specimens.

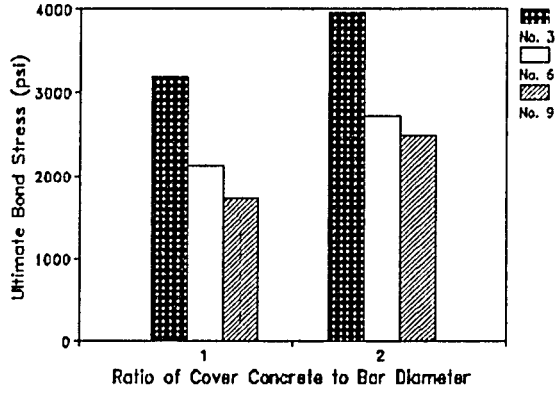

Fig. 12 - Ultimate Bond Stress vs. Clear Concrete Cover

Effect of Casting Position

The influence of casting position on the bond characteristics is significant. Three concrete depths of 8, 24, and 40 in. (203, 610, and 1016 mm) were investigated in the pull- out specimens, and in some of the beam specimens. Top rebars are defined as horizontal rebars soplaced that more than 12 in. (305mm) of concrete is cast below them (ACI Committee 318, 1989). Due to the bleeding of water and air trapped beneath the top rebars, the concrete surrounding these bars is less consolidated than that of bottom bars. For pull-out specimens cast with 4000 psi (28 MPa) concrete and No. 6 GFRP rebars (46PB6, 46PM6, and 46PT6), the data indicate that the higher the casting position, the lower the ultimate bond stress. However, the ultimate bond stress developed in specimens with a casting depth of 24 in. (610 mm) and 40 in. (1016 mm), 46PM6 and 46PT6, respectively, was nearly the same.

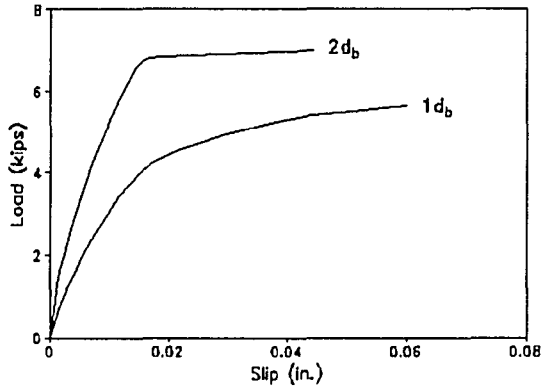

Fig. 13 - Initial Stiffness and Slip for Various Covers

The poor quality of concrete surrounding the top bars also affected the slip of the bars during the test. Therefore, the initial stiffness of top rebars was lower than that of bottom bars, as shown in Table 4. The same general trend was noted for all specimens which failed either by tensile splitting of concrete or pull out of rebar. In the last column of Table 4, the ratios of u_m^* for bottom bars to that for the middle and top bars in each specimen are listed. As seen, these ratios range from 1.04 to 1.23 with an average of 1.13. Therefore, it is recommended that the provided embedment lengths for top bars should be at least 13% larger than that of bottom bars.

Comparison of Beam and Pull-out Specimens

There was a major difference between beam specimens and pull-out specimens. Both concrete and rebar in beam specimens were in tension. However, in pull-out specimens, the rebar was subjected to tension forces while the concrete surrounding the rebar was subjected to compression forces from the reaction of the jack. The latter conditions result in development lengths which are too short or unconservative.

As an example, the results for Specimens 43B1.5T2, 46B6B2, and 49B8B2 are compared with Specimens 43PM1.5, 46PB6, and 49PB8 in Fig. 14. Due to the elimination of concrete

flexural cracks in pull-out specimens, the ultimate bond stresses were increased by 3, 14, and 23 percent for No. 3, 6, and 9 rebars, and an average of 13 percent. This clearly indicates that reliance on data from pull-out tests for determination of development length can result in values which are unconservative. Beam test data would be more realistic and accurate for use in such calculations.

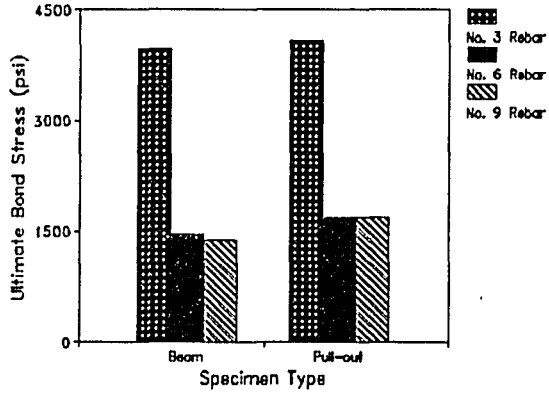

Fig. 14 - Ultimate Bond Stress in Beam & Pull-out Specimens

Moreover, in pull-out specimens, the compressive stresses acting on the concrete surface limit the cracking of concrete and therefore reduce the slip at the loaded end. On the other hand, for beam tests, the tensile cracks in concrete contributed to the measured slip at the loaded end, as shown in Fig. 15.

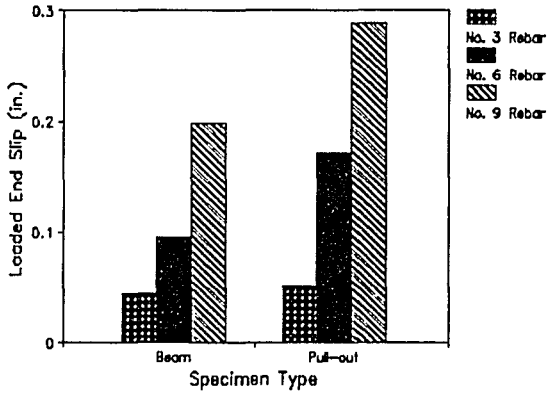

Fig. 15 - Loaded End Slips in Beam & Pull-out Specimens

CONCLUSIONS

Bond behavior was experimentally investigated with 48 beam and 18 pull-out specimens containing No. 3, 6, and 9 straight GFRP rebars. The analysis of the test data led to the following conclusions:

1) The ultimate bond stress increases with an increase in concrete compressive strength.
2) The applied tensile load approached the ultimate tensile capacity of rebars, f_u, as the embedment length increased.
3) For concrete compressive strength of 4000 psi (28 MPa) and higher, the embedment length for No. 3, 6, and 9 bottom rebars is approximately 21, 24, and 27 times bar diameters, respectively. For top rebars the above embedment length should be multiplied by the top bar factor of 1.13.
4) Splitting failure occurred when the clear concrete cover was one rebar diameter; pull out failure and rebar fracture modes were observed when the cover concrete was equal to or larger than twice the rebar diameter.
5) The ultimate bond stress and initial stiffness were found to increase with an increase in clear concrete cover for a given embedment length.

6) The ultimate bond stress and loaded end slip in pull-out specimens were significantly greater than the values observed in beam specimens. Therefore, beam test data are more realistic and accurate for use in determination of development length.

NOTATION

C_b	clear concrete cover, in.
d_b	rebar diameter, in.
E_i	initial stiffness, kips./in.
f_c	concrete compressive strength for each specimen, psi
f'_{cavg}	average of f'_c for all 4,000 or 8,000 psi concrete, psi
L	bonded length of the rebar, in.
l_d	embedment length, in.
S_{fmax}	ultimate slip at free end, in.
S_{lmax}	ultimate slip at loaded end, in.
T	applied tensile load, kips
T_m^*	adjusted ultimate applied tensile load, kips
T_u	ultimate tensile capacity of rebar, kips
u	bond stress, psi
u_m^*	adjusted ultimate bond stress, psi
δ_a	loaded end slip after correction for elastic elongation of rebar, in.
δ_e	elastic elongation of rebar, in.
δ_m	loaded end slip measured during testing, in.

REFERENCES

ACI Committee 318 (1989). "Building Code Requirements for Reinforced Concrete.", (ACI 318-89), American Concrete Institute, Detroit, 181-211.

ACI Committee 408 (1992). "State-of-the-art Report on Bond Under Cyclic Loads." American Concrete Institute, Detroit, 3-7.

Chaallal, O., Benmokrane, B., and Masmoudi, R. (1992). "An Innovative Glass-Fiber Composite Rebar for Concrete Structures," Advanced Composite Materials in Bridges and Structures, Canadian Society for Civil Engineering, 169-177.

Daniali, S. (1992). "Development Length for Fiber-Reinforced Plastic Bars," Advanced Composite Materials in Bridges and Structures, Canadian Society for Civil Engineering, 179-188.

Ehsani, M.R. (1993). "Glass-fiber reinforcing bars." in J.L. Clarke, ed., Alternative Materials for the Reinforcement and Pressing of Concrete, Blackie Academic & Professional, London.

Ehsani, M.R., Saadatmanesh, H. and Tao, S. (1993). "Bond of GFRP Rebars to Ordinary-Strength Concrete." ACI International Symposium on Non-Metallic Continuous Reinforcement, Vancouver, Canada.

Faza, S.S. and GangaRao, H.V.S. (1990). "Bending and Bond Behavior of Concrete Beams Reinforced with Plastic Rebars," Transportation Research Record 1290, 185-193.

Ferguson, P.M., and Thompson, J.N. (1962). "Development Length of High-Strength Reinforcing Bars in Bond." ACI J., 59(7), 887-921.

Ferguson, P. M., Breen, J. E., and Thompson, J. N. (1965). "Pullout Tests on High-Strength Reinforcing Bars." ACI J., 62(8), 933-949.

Hadje-Ghaffari, H., Choi, O.C., Darwin, D., and McCabe, S.L. (1992). "Bond of Epoxy-Coated Reinforcement to Concrete: Cover, Casting Position, Slump, and Consolidation," Structural Engineering and Engineering Materials, SL Report 92-3, University of Kansas, Lawrence, Kansas.

Pleimann, L.G. (1987). "Tension and Bond Pull-Out Tests of Deformed Fiberglass Rods," Final Report for Marshall-Vega Corporation, Marshall, Arkansas, Civil Engineering Department, University of Arkansas, Fayetteville, Arkansas, 5-11.

Pleimann, L.G. (1991). "Strength, Modulus of Elasticity, and Bond of Deformed FRP Rods," Advanced Composites Materials in Civil Engineering Structures, Proceedings of the Specialty Conference, Materials Engineering Division, ASCE, 99-110.

Park, R. and Paulay, T. (1975). "Reinforced Concrete Structures." John Wiley & Sons, New York, 401-404.

Saadatmanesh, H., and Ehsani, M.R. (1991). "Fiber Composite Bar for Reinforced Concrete Construction." J. of Composite Material, 188-203.

Tao, S. (1994). "Bond of Glass-Fiber-Reinforced-Plastic Reinforcing Bars to Concrete," Ph. D. Dissertation, Department of Civil Engineering and Engineering Mechanics, University of Arizona, Tucson, AZ.

Wu, W.P., GangaRao H., and Prucz, J.C. (1991). "Mechanical Properties of Fiber Reinforced Plastics." Research Report, Constructed Facilities Center, College of Engineering, West Virginia University.

APPENDIX B: A COPY OF PAPER TWO

Bond of Hooked GFRP Rebars to Concrete

M. R. Ehsani, H. Saadatmanesh, and S. Tao

Department of Civil Engineering and Engineering Mechanics
University of Arizona
Tucson, AZ 85721

Accepted for publication in ACI Materials Journal

ABSTRACT

The objective of this study was to determine the bond behavior of hooked Glass-Fiber-Reinforced-Plastic (GFRP) reinforcing bars to concrete. Thirty-six 90° hooked rebar specimens were tested to examine the effects of concrete compressive strength, radius of bend, tail length, straight embedment length, and rebar diameter under monotonic static loading. The slip between the rebars and concrete was measured at the loaded end for various load levels. The tensile load was applied to the rebar until splitting of concrete or fracture of rebar occurred. The test results indicated that, with increases in concrete compressive strength, radius of bend, and straight embedment length, the ultimate tensile stress and initial stiffness increased and the maximum slip at failure decreased. The tail length beyond 12 bar diameters had little effect on the ultimate tensile stress. Based on a regression analysis of the test results, it is recommended that the development length of hooked GFRP bars be taken as sixteen times the bar diameter.

Keywords: Glass-Fiber-Reinforced-Plastic (GFRP), rebar, hooked, bond strength, reinforced concrete, development length.

Ninety-degree hooks are commonly used in concrete construction for anchorage of tension reinforcement. The anchorage capacity of hooked rebars is provided by the bond along the straight embedment length, the hook itself, and the tail length.

Concrete reinforced with steel rebars has been successfully used in the civil engineering field for decades. However, the corrosion of these structures, particularly when they are located in aggressive environments such as coastal and marine structures, bridges, chemical plants, water and wastewater treatment facilities, etc. is of concern (Saadatmanesh and Ehsani, 1991). Hundreds of millions of dollars are spent each year to repair corrosion-induced damage in concrete structures. Among methods adopted to prevent or delay the corrosion of steel rebars, inclusion of additives and admixtures to reduce the permeability of concrete and the use of epoxy-coated steel rebars can be named. The latter, when introduced in the early 1970s was expected to be a major breakthrough in eliminating the corrosion of rebars. However, with the recent discovery of the extensive premature corrosion of epoxy-coated steel rebars in new construction (Keesler and Powers, 1988), these hopes have all but diminished. It is clear that no practical and economical approach currently exist to prevent corrosion of rebars. Efficient techniques or new materials are needed to solve this problem.

Recently, Glass-Fiber-Reinforced-Plastic (GFRP) reinforcing bars have been introduced which promise to be more durable than steel rebars. GFRP rebars offer significant advantages over conventional reinforcing steel such as resistance to corrosion, high strength, light weight, ease of handling on job site, and ease of cutting. A major reason limiting the use of GFRP rebars is the lack of information on their bond behavior.

To determine the effect of bond length, bend angle, bend radius, and bar diameter on the deformation and strength of hooked steel bars, Minor and Jirsa (1975) examined eighty specimens containing bars bent to different geometric configurations. The test results indicted that at a given bar stress, the larger the angle of bend or the smaller the radius of bend, the greater was the slip. For practical joint design detailing, 90° hooks are preferable to 180° hooks and to reduce slip, the radius of the hook should be as large as practical.

Bond stress-slip relationships of FRP rebars in concrete were studied by Larralde and Silva (1993). In the pullout testing, the concrete surrounding the rebars is under compression reducing the possibility of cracking and increasing the bond strength due to Poisson's effect. In contrast, in concrete beams, the concrete surrounding the rebars is under tension, thus allowing for cracking at lower stresses and reducing friction. Consequently, the nominal bond strength obtained from pullout tests does not reflect the actual conditions in flexural reinforced concrete members and is greater than the nominal bond strength obtained from rebars under flexural tension. In addition, from the experimental results, it was concluded that the anchorage design for steel rebars is not directly applicable on FRP rebars. For the same test conditions, the average nominal bond stress at failure was greater for the steel rebars than for the FRP rebars. The slips of the rebars relative to the concrete surface were greater for the FRP rebars than for steel rebars.

The principal objective of this research project was to determine the bond behavior of straight and hooked GFRP rebars to concrete. A total of 102 specimens were tested. Based on these data, analytical expressions have been presented for basic development length of straight and hooked GFRP rebars to concrete. Due to space limitation, however, this paper will discuss the study of the bond behavior of hooked GFRP rebars to concrete only. The study on bond behavior of straight GFRP rebars to concrete, and the development of design guidelines for bond of GFRP rebars to concrete are presented elsewhere (Tao, 1994).

RESEARCH SIGNIFICANCE

Few experimental data are available in the literature on bond behavior of hooked GFRP rebars to concrete. In addition, the guidelines provided in ACI 318-89 for bond of hooked steel rebars cannot be directly utilized for GFRP rebars due to the major differences that exist in tensile strength, modulus of elasticity, and deformation patterns of GFRP and steel rebars. The study reported herein provides information about the bond behavior of hooked GFRP rebars to concrete.

EXPERIMENTAL PROGRAM

The main purpose of the research program reported in this paper was to investigate the influence of several parameters on bond behavior of hooked GFRP rebars to concrete. Thirty six specimens were constructed and tested under static monotonic loading. Variables in the specimens included concrete compressive strength, radius of bend, tail length, straight embedment length, and rebar diameter. The ultimate applied load, ultimate tensile stress, loaded end slip, mode of failure, and load-slip relationship were obtained from these tests.

Design of specimens

A sketch of a typical test specimen is shown in Fig. 1, and the corresponding dimensions are listed in Table 1.

Each specimen was cast in the position shown in Fig. 1 with the lead-in portion of the hook in a horizontal position at a distance of three eighths of the height (a) from the bottom surface of the specimen. No transverse reinforcement was used within the specimens.

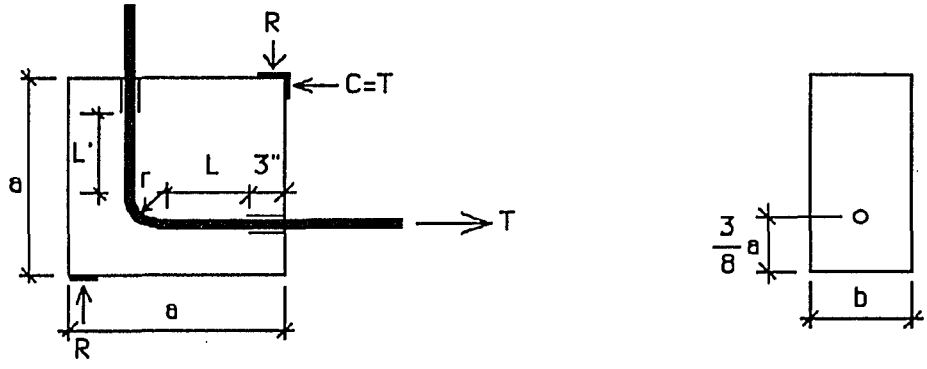

Fig. 1 - Test specimens

Table 1 - Dimensions of test specimens

Rebar size	a, in.	b, in.
No. 3	12	8
No. 6	18	10
No. 9	24	12

Note: 1 in.=25.4 mm

To eliminate the influence of the support reactions on the loaded end, the first 3 in. (76 mm) of the rebar was wrapped in a thin conduit to prevent its bonding to concrete (Fig. 1). Therefore, by careful placement of the rebar prior to casting, the desired straight embedment length (L), i. e. the distance between the beginning of the bend and the point of 3 in. (76 mm) from the concrete face, was obtained for all specimens.

The tail length of standard hooked steel rebars is 12 bar diameters. To investigate the potential benefits of longer tail lengths, some specimens were cast with hooks having a tail lengths (L') of 20 times bar diameter.

Because bending of steel rebars through small radii could result in the fracture of the bar, ACI 318-89 requires minimum radii of bend. In GFRP rebars, however, it is possible to bend the uncured rebar during the manufacturing process through smaller radii. For this study, the ratios of radius to rebar diameter were selected as zero and three to examine the effect of the radius of bend.

Material properties

The concrete used in this study was obtained from a ready-mix plant and specified to have a nominal compressive strength of 4000 and 8000 psi (28 and 56 MPa). The concrete aggregate had a maximum size of 1 in. (25 mm). Sixteen standard 6 x 12 in. (152 x 305 mm) cylinders were cast at the same time and cured under the same condition as the specimens for each concrete batch.

The GFRP rebars used in the research program were supplied by a U. S. manufacturer in the nominal diameters of 0.375, 0.75, and 1.125 in. (10, 19, and 29 mm). These rebars were manufactured using the pultrusion process and were made of polyester resin and type E glass fibers with 60 percent glass, and 40 percent resin by weight, respectively. Additional fiberglass strands were wrapped around the rebars in a helical pattern to enhance bond characteristics. The width of the strands wrapped around the outside diameter is usually the same for all manufactured sizes. As shown in Fig. 2, the pitch is defined as the distance from the center to center of the helical strand. Larger diameter rebars had longer pitches.

The rebar diameters were measured by the volumetric method, cutting a representative 6 in. (152 mm) sample, submerging the sample in a graduated cylinder, and measuring the change in volume. The cross sectional area of the bar was calculated by dividing its volume by the 6-in. (152-mm) length. Assuming a circular cross section for the rebar, the average diameter was calculated. Diameter measurements taken at different sections resulted in slight differences between the measured and nominal diameters, which are listed in Table 2.

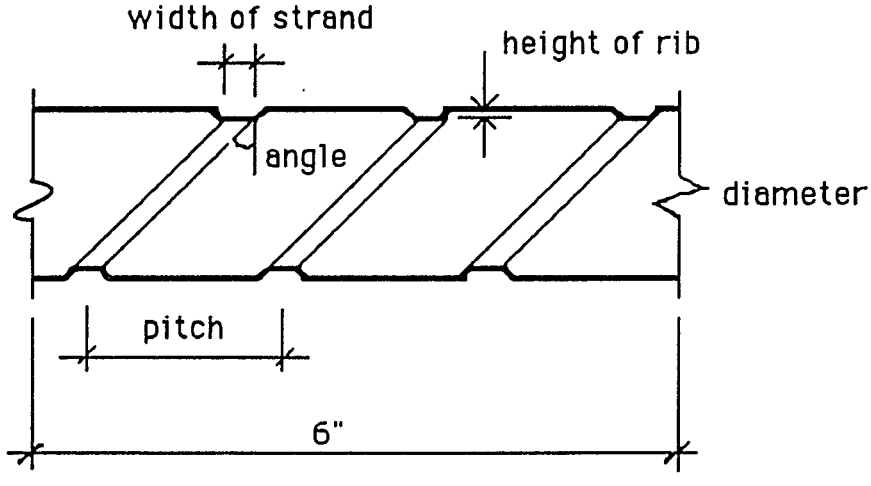

Fig. 2 - Sample for measuring rib geometry

Table 2 - Rebar dimensions

Property	No. 3	No. 6	No. 9
Rib height, in.	0.045	0.051	0.079
Pitch, in.	0.687	0.938	1.063
Angle, degree	37	25	23
Measured diameter, in.	0.381	0.726	1.079
Nominal diameter, in.	0.375	0.750	1.125
Measured dia./Nominal Dia.	1.016	0.968	0.959

Note: 1 in.=25.4 mm

The ultimate tensile strength and stiffness were measured by subjecting GFRP bars to uniaxial tension tests. These bars had a gage length of approximately 20 in. (508 mm). A typical stress-strain curve is shown in Fig. 3. All tension tests of GFRP rebars showed a similar linear relationship for the entire loading range. The test results for modulus of elasticity and ultimate tensile strength of rebars are presented in Tables 3 and 4, respectively.

As seen in Table 3, the modulus of elasticity for GFRP rebars is almost constant and averages around 7000 psi (48,270 MPa). But the results in Table 4 reveal that the ultimate tensile strength is sensitive to rebar diameters, and decreases rapidly with an increase in rebar diameter. Since the tensile load was applied along the GFRP rebar by friction mechanism between the sand-coated grips and the surface of rebar, the loading was likely to induce a parabolic and axisymmetric strain distribution across the cross-section of the rebar (Wu, 1991). Thus the strength reduction with rebar diameter is due to the shear lag phenomenon.

Table 3 - Data for modulus of elasticity

Rebar No.	Sample 1, ksi	Sample 2, ksi	Sample 3, ksi	Average for 3 samples, ksi
3	6750	6824	6857	6810
6	7028	7115	7001	7050
9	7281	7298	7257	7280

Note: 1 ksi=6.895 MPa

Table 4 - Data for ultimate tensile strength

Rebar No.	Sample 1, ksi	Sample 2, ksi	Sample 3, ksi	Average for 3 samples, ksi
3	129	141	135	135
6	98	93	88	93
9	77	76	78	77

Note: 1 ksi=6.895 MPa

Test set up and instrumentation

The test set up for the specimens is shown in Fig. 4. Due to the low shear strength of the rebars, care must be taken not to harm the rebar during the placement of the specimens in the test frame.

In earlier studies, the design and development of suitable grips to pull GFRP rebars embedded in concrete have presented some difficulties. Because glass fiber based composites are very weak for loads applied transverse to the fiber directions, the region of the GFRP rebar in the grip must be protected against crushing (Ehsani, et al. 1993). The grip must grasp the rebar in such a manner as to avoid failure of the rebar at the grips, allowing the failure to take place in the rebar away from the grip region (Faza and GangaRao, 1990). A specially constructed set of sand-coated grips similar to those used in testing of GFRP rebars at West Virginia University was employed. The applied loads are transmitted from the jack to the GFRP rebars through these grips. The tests were successful in avoiding excessive slippage or rebar failure in the grip region. The sand-coated grips proved effective for all rebar sizes.

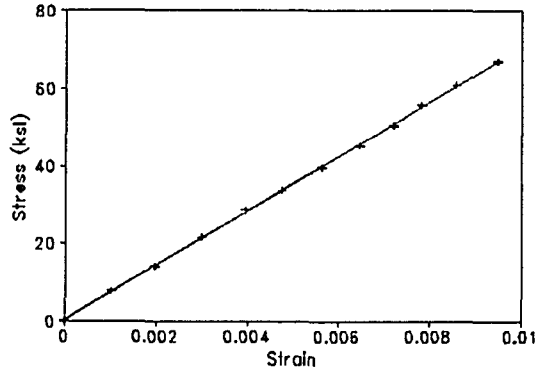

Fig. 3 - Tension stress-strain relationship for GFRP rebars

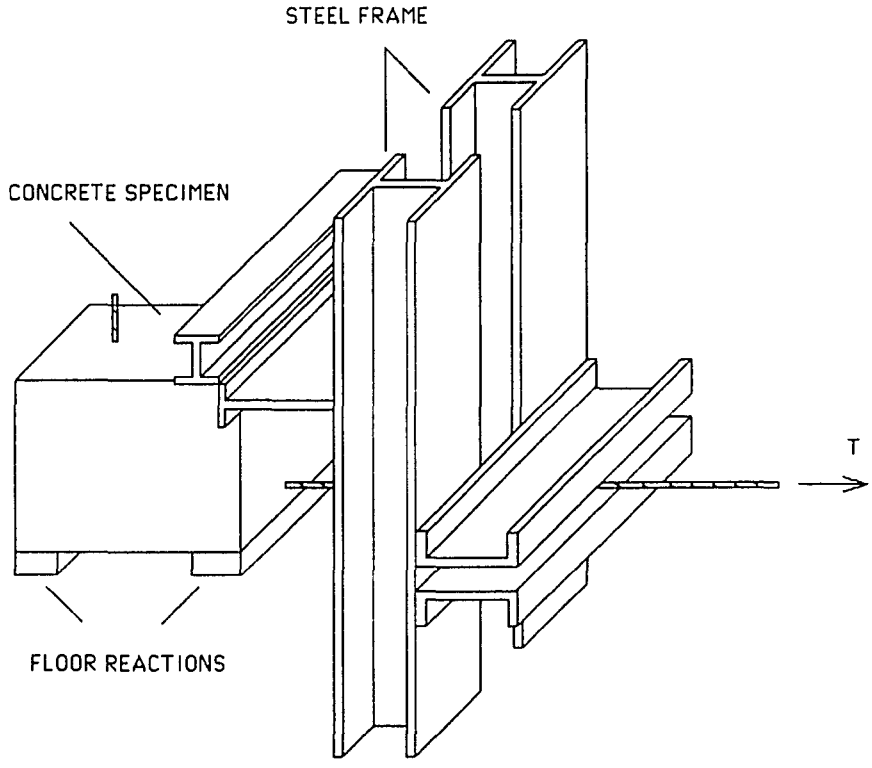

Fig. 4 - Test set up for the specimens

The monotonic static loading was gradually applied in an approximately constant increments of 1000 lbs (4.45 kN) until splitting failure of concrete or fracture of rebar was reached. The load values were measured by two load cells and automatically recorded by an HP-3054A automatic data acquisition/control system. Meanwhile, the slip was measured at each load level during testing by reading a 0.0001" dial gage attached at the loaded end of the rebar as seen in Fig. 5.

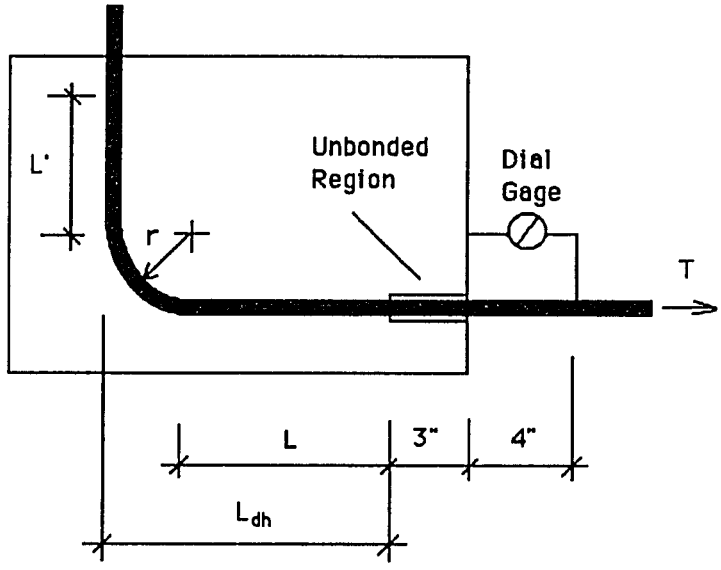

Fig. 5 - Dial gage set up

TEST RESULTS

The results of the 36 specimens were examined to evaluate the bond behavior of hooked GFRP rebars to concrete. Under monotonic static loading, the load values and loaded-end slips were obtained at each load increment. The corresponding nominal tensile stress was calculated as the applied tensile load divided by the nominal cross section of the rebar, or

$$f_s = \frac{4T}{\pi d_b^2} \tag{8}$$

where f_s=tensile stress, T=applied tensile force, d_b=rebar diameter.

Figure 6 shows a typical plot of the applied load vs. the slip at the loaded end of the rebar. As seen in the curve, the loaded end started to slip from the beginning of the loading, and continued until splitting failure or rebar fracture occurred.

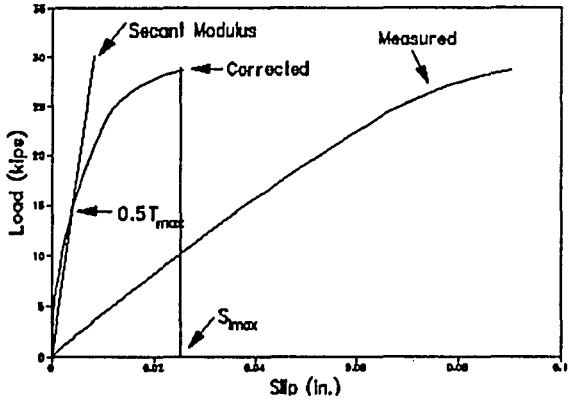

Fig. 6 - Typical load-slip relationship

The measured loaded end slip contains two main components: the elastic elongation of the rebar itself, and the slip of the rebar with respect to the surrounding concrete. It is noted that due to the relatively high modulus of steel, the former component is usually ignored in bond studies of steel rebars. However, in the case of GFRP bars, the contribution of this component to the total measured displacement cannot be ignored.

As shown previously in Fig. 5, the dial gage attached to the loaded end of the rebar measured the movement of a point 4 in. (102 mm) away from the concrete block relative to the face of the block. In addition, the first 3 in. (76 mm) of the rebar was always shielded to prevent its bonding to concrete. Therefore, the measured slip at the loaded end of the rebar included the elastic elongation of the 7-in. (178-mm) lead length. Due to the low modulus of elasticity of GFRPs, this elongation is significant and has to be corrected for. Thus, the actual slip was

calculated as the difference between the measured slip at the loaded end and the elastic deformation, or

$$\delta_a = \delta_m - \delta_e \tag{9}$$

The test results for all specimens are presented in Table 5. The notation for the specimens is as follows: the first number indicates the design concrete compressive strength in units of ksi; the second number, the rebar diameter; the letter "H" denotes a hooked rebar specimen; the third number, the ratio of radius to rebar diameter; the next number, the ratio of tail length to rebar diameter; and the last number the ratio of the development length to rebar diameter. For example, 43H3.12.4 designates a hooked specimen cast with 4000-psi (28-MPa) concrete, No. 3 GFRP rebar, where the ratios of radius, tail length, and development length to rebar diameter were 3, 12, and 4, respectively.

Due to the variations in the concrete strength of specimens, it was necessary to normalize the test results with respect to an average concrete compressive strength in order to allow a reasonable comparison among specimens. The process for determining the average compressive strength was as follows. For specimens 46H3127, 46H31210, 46H31213, and 46H31216, for example, which were tested at approximately the same time, three 6 x 12 in. (152 x 305 mm) cylinder tests resulted in an average compressive strength, f_c', of 4280 psi (29.5 MPa) tabulated in the second column of Table 5 for these four specimens. Next, an average concrete compressive strength, f'_{cavg}, was calculated for all specimens expected to have a nominal concrete strength of 4000 or 8000 psi (28 or 56 MPa). These averages were 4890 psi (34 MPa) and 6810 psi (47 MPa), respectively.

Table 5 - Test results

Specimen	f_c', psi	T_m^*, kips	T_m^*/T_u	f_s^*, ksi	S_{lmax}, in.	E_i, k/in	Failure Mode
43H3124	5080	6.1	0.55	56	0.2234	88	S
43H3204	5080	5.8	0.53	53	0.2231	96	S
43H3127	4280	7.5	0.68	68	0.1453	268	S
43H31210	4280	8.8	0.79	80	0.1342	414	S
43H31213	4280	10.5	0.94	95	0.0388	523	RA
43H31216	4280	11.4	1.03	103	0.0282	776	RA
83H3124	6640	7.0	0.63	63	0.1672	128	S
83H3204	6640	6.9	0.62	62	0.1786	129	S
43H0121	5080	2.4	0.21	21	0.3114	43	RS
43H0201	5080	2.4	0.21	21	0.3165	43	RS
83H0121	6640	2.3	0.21	21	0.3044	45	RS
83H0201	6640	2.4	0.22	22	0.3089	46	RS
46H3124	5680	20.2	0.68	46	0.1786	604	S
46H3204	5680	20.6	0.70	47	0.1678	620	S
46H3127	4280	24.0	0.81	54	0.1111	1111	S
46H31210	4280	25.4	0.86	58	0.0989	2192	S
46H31213	4280	28.7	0.97	65	0.0256	3629	RA
46H31216	4280	29.4	1.00	67	0.0155	4592	RA
86H3124	6920	22.1	0.75	50	0.1231	788	S
86H3204	6920	22.3	0.76	50	0.0988	748	S
46H0121	5680	6.9	0.23	16	0.2514	110	RS
46H0201	5680	6.6	0.23	15	0.2487	109	RS
86H0121	6920	6.5	0.22	15	0.2322	115	RS
86H0201	6920	6.5	0.22	15	0.2291	116	RS
49H3124	5760	31.9	0.61	32	0.1111	1525	S
49H3204	5760	32.2	0.62	32	0.1231	1548	S
49H3127	4280	37.9	0.73	38	0.0897	3508	S
49H31210	4280	41.4	0.79	42	0.0655	4704	S
49H31213	4280	49.1	0.94	49	0.0161	8467	RA
49H31216	4280	51.6	0.99	52	0.0152	9554	RA
89H3124	6860	34.3	0.66	35	0.0876	2174	S
89H3204	6860	35.0	0.67	35	0.0879	2082	S
49H0121	5760	14.2	0.27	14	0.2148	177	RS
49H0201	5760	14.2	0.27	14	0.2177	177	RS
89H0121	6860	14.1	0.27	14	0.2054	185	RS
89H0201	6860	14.0	0.27	14	0.2089	184	RS

Earlier studies have indicated that bond strength varies with the square root of the compressive strength (Ferguson and Thompson, 1962). In order to compare the test results directly, the effects of the slight variations in the concrete compressive strength had to be eliminated. Since the bond strength is proportional to the square root of the concrete strength, the maximum applied load values, T_m, and the corresponding tensile stress, f_s, have been

multiplied by the factor $\sqrt{f_{cavg}}/f_c'$ and listed as T_m^* and f_s^* in columns 3 and 5 of Table 5, respectively.

The ratio T_m^*/T_u is listed in the fourth column of Table 5. The values of T_m^* are the maximum load applied along the rebar during the test. The values of T_u represent the ultimate tensile force of a rebar sample, calculated as the product of the average ultimate tensile strength reported in Table 4 multiplied by the minimum area for each rebar, which was calculated from the minimum bar diameter reported in Table 2. While this ratio is expected to be less than or equal to one, it is occasionally slightly larger. This happens when the rebar fractures outside the specimen and the tensile strength of rebar is slightly higher than its average ultimate tensile strength reported in Table 4.

During testing, the slip at the loaded end is expected to increase with an increase in loading. As shown in Fig. 6, the maximum slips listed in column 6 of Table 5 correspond to those measured under maximum applied load and after the necessary reduction for the elastic elongation of the lead length.

One of the ways to compare the performance of different specimens is in terms of their stiffness. Because the service load stresses in GFRP rebars are expected to remain well below 50% of their ultimate strength, the initial stiffness, E_i, was defined as a secant modulus passing through the point of $0.5T_{max}$ (Fig. 6). These values are also given in Table 5.

Failure of hooked rebar specimens occurred either by splitting failure of concrete (S), or by fracture of rebar (RA-axial, RS-shear). The failure mode for each specimen is also listed in Table 5.

In nearly all splitting failures, such as that shown in Fig. 7, the cracking patterns were quite similar. During testing, horizontal cracks radiated outward from the rebar on the front face and propagated to side faces of the specimens. The vertical cracks appeared on the side faces and continued to the top face of the specimens with subsequent loading. The cracks were

widened, and more cracks occurred with additional loading. Concrete splitting failure was sudden and ended with the side cover spalling away and a reduction in the load. After removing the spalled side cover from a few specimens, close examination at bend region of the bars indicated that the concrete at the inner radius of the bend was crushed completely. This behavior was induced by a wedge mechanism which produced intense compressive stresses to the concrete at the hook location.

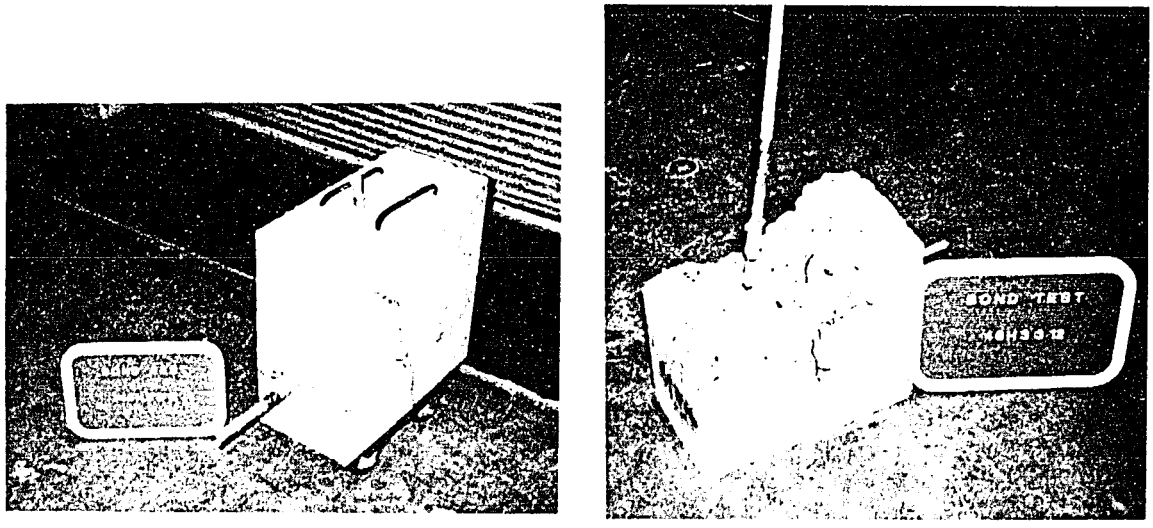

Fig. 7 - Typical cracking pattern and failure of specimens due to splitting of concrete

As seen in Fig. 8, for specimens with r/d_b of zero, the rebars failed in shear at the hook under very low load levels. For specimens with r/d_b of three, however, two modes of failure were observed. When the cover concrete or the straight embedment length were small, the specimens failed by the splitting of concrete. Otherwise, the mode of failure was due to fracture of the rebar outside of the specimen.

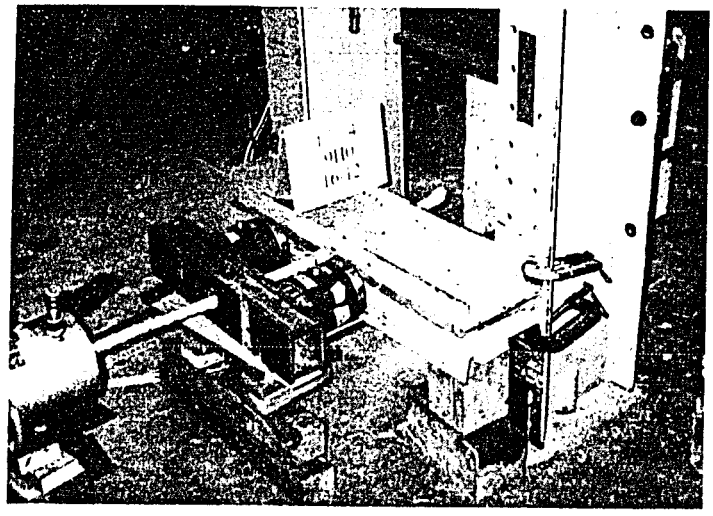

(a). fracture of rebar near bend for specimens with $r/d_b=0$

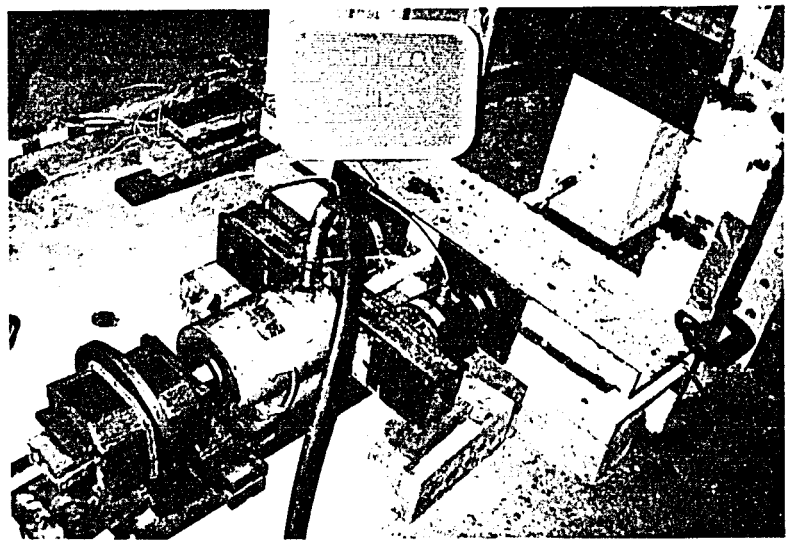

(b). fracture of rebar outside the concrete for specimens with $r/d_b=3$

Fig. 8 - Typical failure of specimens due to fracture of rebar

INFLUENCE OF DESIGN PARAMETERS

Effect of concrete compressive strength

The anchorage capacity of hooked rebars is provided by the bond along the straight embedment length, the hook itself, and the tail length. Bond failure could be caused by tensile splitting of the concrete along the straight portion of the bar. Thus, the tensile strength of concrete, which is approximately proportional to the square root of its compressive strength, is considered a key parameter in bond behavior (ACI Committee 408, 1992). To determine the effect of the concrete strength on the bond behavior of hooked GFRP rebars, compressive strengths of 4000 and 8000 psi (28 and 56 MPa) were selected for this study.

For specimens with r/d_b of three, Fig. 9 illustrates the influence of concrete compressive strength on bond properties. The six specimens shown in this figure, 43H3124 and 83H3124, 46H3124 and 86H3124, and 49H3124 and 89H3124, had the same design parameters except for concrete compressive strength. It can be seen that the tensile stress of the rebar increases slightly with an increase in concrete strength. As shown in Fig. 10, however, the concrete compressive strength has little influence on tensile stress for specimens with r/d_b of zero.

The comparison of Specimens 46H3124 and 86H3124 presented in Fig. 11 indicates that higher concrete compressive strength results in greater initial stiffness and smaller slip. The influence of concrete compressive strength on tensile stress of rebars, initial stiffness, and loaded end slip was found to be similar for all other specimens with identical hook configurations.

Effect of hook radius

For steel rebars, limits have been set for the radius of curvature of the hook to prevent fracture of the rebar. For GFRP rebars, however, this limitation does not apply because the bars are formed into their final shape before the resin is cured (Ehsani, 1993). Two ratios of radius to rebar diameter, three and zero, were chosen to study the effect of hook radius on bond

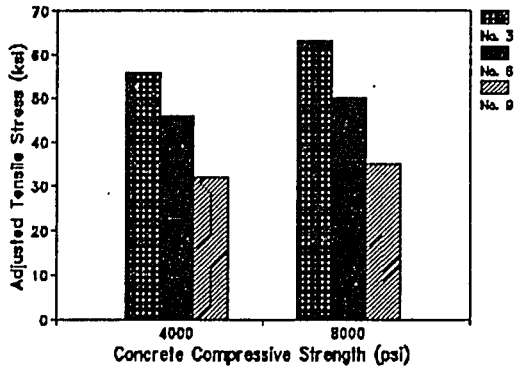

Fig. 9 - Influence of concrete compressive strength on tensile stress for bars with $r/d_b=3.0$

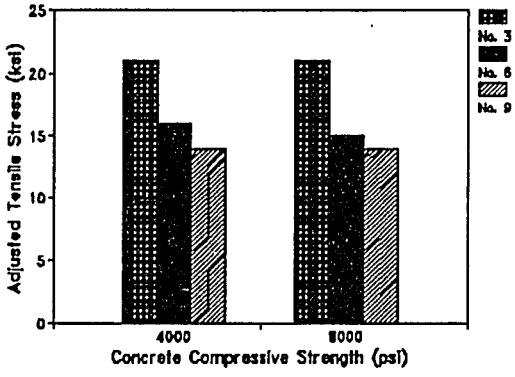

Fig. 10 - Influence of concrete compressive strength on tensile stress for bars with $r/d_b=0.0$

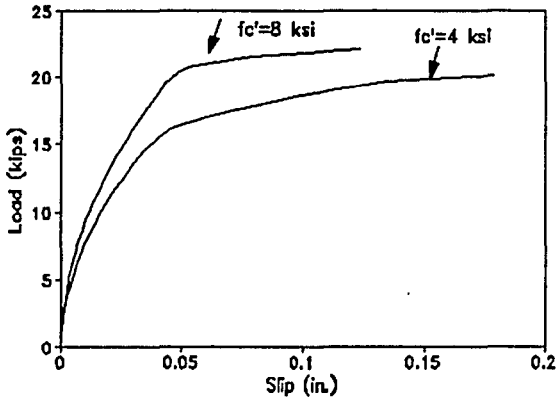

Fig. 11 - Effect of concrete compressive strength on initial stiffness & slip

behavior. Fig. 12 shows the load-slip relation for Specimens 86H0201 and 86H3204. In this case, all hook geometry conditions except for hook radius are the same. As indicated, both the load and the initial stiffness increased with an increase in the hook radius. In addition, for specimens with r/d_b of zero, the rebars failed in shear at very low load levels at the point when the horizontal and vertical legs of the bar intersected. Therefore, although manufacturing of GFRP rebars with sharp bends does not pose any difficulties, the use of such details should be avoided due to the low shear strength of GFRPs. Additional studies are needed to determine the economy of using larger hook radii for GFRP bars and their effect on reducing the required development length.

Effect of tail length

The tensile force applied to the rebar was transferred to the concrete along the straight embedment length, the hook, and the partial tail length near the hook bend. Figures 13 through 15 compare the data for Specimens 43H3124 and 43H3204, 46H3124 and 46H3204, and 49H3124 and 49H3204. As can be seen, a tail length of 20 times the bar diameter had no beneficial effect on the tensile stress of the rebars, the loaded end slip, and the initial stiffness compared to that for a standard hook with a tail length of 12 bar diameters. Therefore, longer

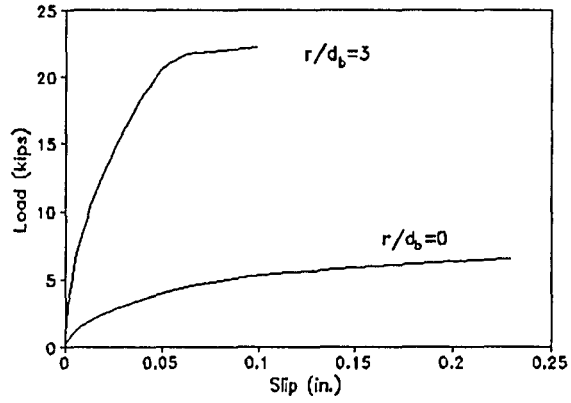

Fig. 12 - Influence of hook radius on load-slip relation

tail lengths, beyond the 12 d_b, had no significant influence on tensile stress and loaded end slip. Moreover, the initial stiffness is independent of longer tail lengths. The tail length of 12 bar diameters is long enough to sustain the applied tensile force during testing for all No. 3, 6, and 9 rebar specimens. Therefore, hooked GFRP rebars manufactured with tail lengths of 12 times bar diameter are recommended for use in design.

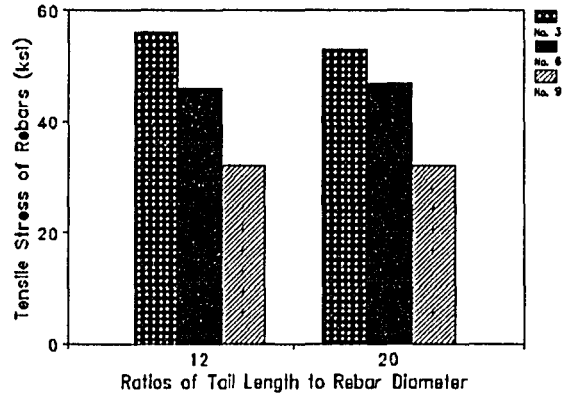

Fig. 13 - Effect of tail length on tensile stress of rebars

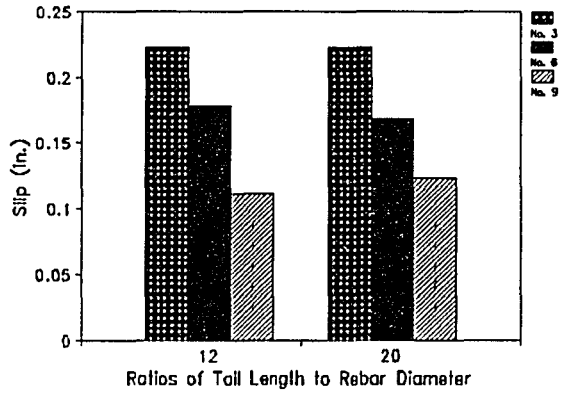

Fig. 14 - Effect of tail length on loaded end slip

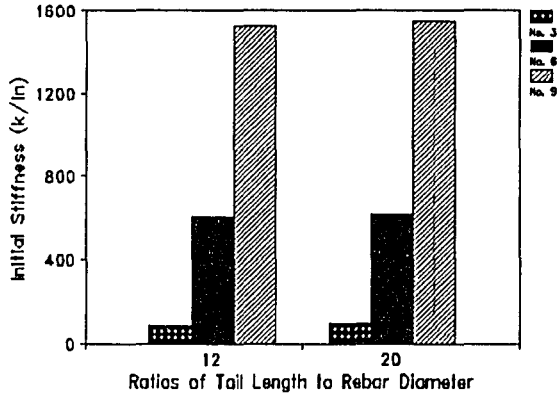

Fig. 15 - Effect of tail length on initial stiffness

Effect of straight embedment length

The straight embedment length refers to that portion of the bar between the beginning of the bend and the point 3 in. (76 mm) away from the concrete surface (Fig. 5). As shown in Figs. 16 through 18, straight embedment length has a significant influence on the applied tensile load, the loaded-end slip, and the initial stiffness. The specimens considered were cast with

4000-psi (28-MPa) concrete. The hooked GFRP rebars were selected with r/d_b of three, and tail lengths of 12 times the bar diameter. As expected, the applied tensile load and initial stiffness increased with the increase in the straight embedment length. The loaded end slip, however, decreased with the increase in the straight embedment length.

DESIGN RECOMMENDATIONS

The overall behavior of the thirty six specimens was examined to develop some preliminary design guidelines. In order to arrive at conservative conclusions, only the response of the specimens with lower strength concrete (i.e. 4000 psi) was considered. Additionally, because the behavior of the specimens with $r/d_b=0$ was unsatisfactory, they were excluded from any further considerations. Similarly, the small gains resulting from longer tail lengths were ignored. This resulted in a sub-set of specimens with designation 4*H312*, where the "*" can take any of the previously described values.

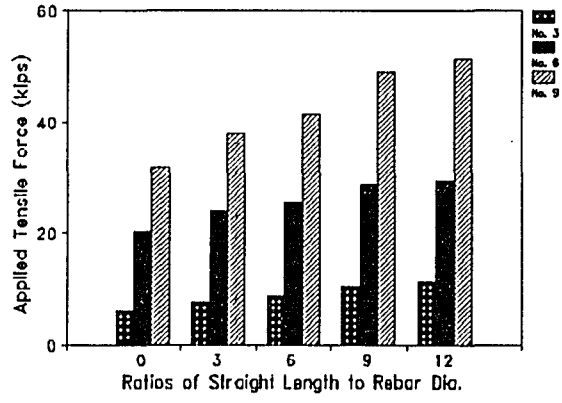

Fig. 16 - Effect of the straight embedment length on tensile force

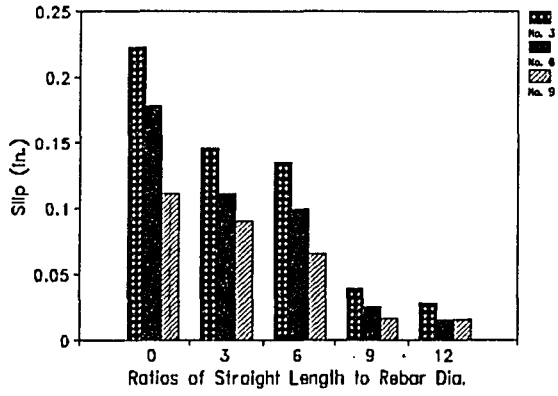

Fig. 17 - Effect of the straight embedment length on slip

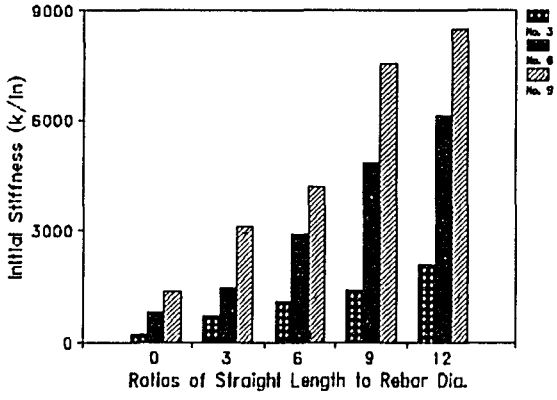

Fig. 18 - Effect of the straight embedment length on initial stiffness

For all specimens in the sub-set, the ratios of the applied tensile force to the ultimate tensile capacity of the rebar (T_m^*/T_u) for various straight embedment lengths have been plotted in Fig. 19. A ratio of at least 1.0 would indicate satisfactory bond performance since the failure would be caused by the fracture of the rebar at a point away from the hook. As shown in Fig. 19, an increase in the straight embedment length improves this ratio. The bond capacity of the

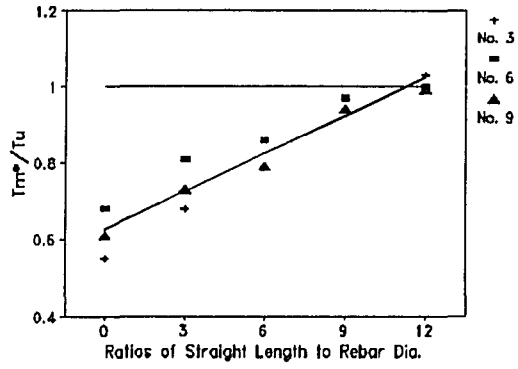

Fig. 19 - Effect of the straight embedment length on the ratio of tensile force to ultimate tensile capacity of rebars

hook itself, i.e. when $L/d_b=0.0$, is not sufficient to develop the tensile capacity of the hook. A regression analysis was performed to obtain the best-fit line passing through all data points in Fig. 19. As shown, a straight embedment length of 11.3 times the bar diameter is adequate to provide a ratio of 1.0.

The ACI 318-89 defines the development length of a hook as the distance measured from the critical section to the back face of the hook. This distance is equal to the sum of the straight embedment length, plus three bar diameters for the hook radius, and an additional bar diameter for the tail portion of the rebar. Therefore, based on the data presented, it is concluded that the development length of 90° GFRP hooks can be taken as $11.3+3+1=15.3$ times the bar diameter. Conservatively, it is recommended to take the embedment length as sixteen times the bar diameter.

It is noted that the above recommendation does not include any capacity reduction factor. Furthermore, these recommendations are to be considered in light of the limitations of the tested specimens. Additional studies are required before comprehensive design guidelines can be developed.

CONCLUSIONS

Thirty six 90-degree hooked GFRP rebar specimens were tested. The effects of concrete compressive strength, radius of bend, tail length, and straight embedment length on the bond behavior were studied. From these tests, it is concluded that:

1. Higher concrete compressive strength, results in little gain in the maximum tensile stress in the bars. For specimens with $r/d_b=3.0$, however, an increase in the compressive strength resulted in higher initial stiffness and lower maximum slip at failure.
2. The strength and stiffness of the specimens with $r/d_b=0$ was very low and it is recommended that a minimum r/d_b of 3.0 be used for GFRP hooks.
3. The additional tail length beyond twelve times the bar diameter had no beneficial effect on the tensile stress, slip, and initial stiffness of the bar. Therefore, it is recommended to use a minimum tail length of twelve bar diameters.
4. An increase in the straight embedment length of the bars, increases the tensile stress and initial stiffness, and reduces the slip.
5. It is recommended that a development length equal to sixteen times the bar diameter be used for 90° GFRP hooks.

ACKNOWLEDGEMENTS

Partial support for this study through NSF Grant No. MSS-9257344 is gratefully acknowledged. However, the results and conclusions are those of the authors and do not necessarily reflect the views of the sponsor. The KODIAK™ reinforcing bars used in this study were manufactured by IGI, Inc., Houston, Texas.

NOTATION

d_b rebar diameter, in.

E_i initial stiffness, kips/in.

f_c' concrete compressive strength for each specimen, psi

f'_{cavg}	average of f_c' for all 4000- or 8000-psi (28- or 56-MPa) concrete, psi
f_s^*	adjusted maximum tensile stress of rebars, ksi
L	straight embedment length, in.
L_{dh}	development length, in.
L'	tail length, in.
r	radius of bend, in.
RA	rebar axial fracture
RS	rebar shear fracture
s_{lmax}	ultimate slip at loaded end, in.
T	applied tensile load, kips
T_m^*	adjusted ultimate applied tensile load, kips
T_u	ultimate tensile capacity of rebars, kips
δ_u	loaded end slip after correction for elastic elongation of rebar, in.
δ_e	elastic elongation of rebar, in.
δ_m	loaded end slip measured during testing, in.

REFERENCES

ACI Committee 318, (1989). "Building Code Requirements for Reinforced Concrete.", (ACI 318-89), American Concrete Institute, Detroit, 181-211.

ACI Committee 408, (1992). "State-of-the-art Report on Bond Under Cyclic Loads." American Concrete Institute, Detroit, 3-7.

Ehsani, M. R., (1993). "Glass-fiber reinforcing bars." in J. L. Clarke, ed., Alternative Materials for the Reinforcement and Pressing of Concrete, Blackie Academic & Professional, London.

Ehsani, M. R., Saadatmanesh, H. and Tao, S., (1993). "Bond of GFRP Rebars to Ordinary-Strength Concrete." ACI International Symposium on Non-Metallic Continuous Reinforcement, Vancouver, Canada.

Faza, S.S. and GangaRao, H.V.S., (1990). "Bending and Bond Behavior of Concrete Beams Reinforced with Plastic Rebars," Transportation Research Record 1290, 185-193.

Ferguson, P. M., and Thompson, J. N., (1962). "Development Length of High-Strength Reinforcing Bars in Bond." ACI J., 59(7), 887-921.

Keesler, R. J., and Powers, R. G. (1988). "Corrosion of epoxy coated rebars-Keys Segmental Bridge-Monroe County." Report No. 88-8A, Florida Department of Transportation, Materials Office, Corrosion Research Laboratory, Gainesville.

Larralde, J., and Silva, R., (1993). "Bond and Slip of FRP Rebars in Concrete." J. of Mat. in Civil Engineering, ASCE, 5(1), NY, 30-40.

Minor, J., and Jirsa, J. O., (1975). "Behavior of Bent Bar Anchorage." ACI J., 72(4), 141-149.

Saadatmanesh, H., and Ehsani, M. R., (1991). "Fiber Composite Bar for Reinforced Concrete Construction." J. of Composite Material, 188-203.

Tao, S., (1994). "Bond of Glass-Fiber-Reinforced-Plastic Reinforcing Bars to Concrete," Ph. D. Dissertation, Department of Civil Engineering and Engineering Mechanics, University of Arizona, Tucson, AZ.

Wu, W. P., GangaRao H. and Prucz, J. C. (1991). "Mechanical Properties of Fiber Reinforced Plastics." Research Report, Constructed Facilities Center, College of Engineering, West Virginia University.

APPENDIX C: A COPY OF PAPER THREE

DESIGN RECOMMENDATIONS FOR BOND OF GFRP REBARS TO CONCRETE

M. R. Ehsani, H. Saadatmanesh, and S. Tao

Department of Civil Engineering and Engineering Mechanics
University of Arizona
Tucson, AZ 85721

Submitted for review and publication in the ASCE Journal of Structural Division

ABSTRACT

To develop design guidelines for bond of Glass-Fiber-Reinforced-Plastic (GFRP) rebars to concrete, a total of 102 specimens were constructed and tested subjected to monotonic static loading. The research program was inclusive of the experimental testing of forty eight beam specimens, eighteen pull-out specimens, and thirty six hooked rebar specimens. The tensile load was applied to the rebars in a gradual increment of load level until splitting of concrete, rebar pull-out failure, or rebar fracture occurred. The slip between the rebars and concrete was measured at the loaded and free ends at each load level. Variables included in the study were concrete compressive strength, embedment length, clear concrete cover, rebar diameter, concrete cast depth, radius of bend, tail length, and lead embedment length. New criteria for acceptable bond performance of GFRP rebars to concrete were developed and were used to evaluate the experimental results. Design guidelines for calculating the development lengths for straight and hooked GFRP rebars to concrete were derived. In addition, confinement factors were calculated to reflect the influence of concrete cover and casting position.

INTRODUCTION

Corrosion of reinforcing steel is a serious problem in concrete structures located in aggressive environments, especially, if the reinforcing steel is subjected to high stresses. With passage of time, corrosion produces deep pitting and a severe loss of cross section of the reinforcing steel. These conditions normally lead to costly repairs and catastrophic failures. Several approaches have been chosen to control the corrosion process such as improving the permeability of concrete by additives and admixtures and epoxy coating steel rebars. The latter has been widely used in bridges and parking garages. However, with recent discoveries of extensive premature corrosion in new bridges, there are concerns regarding the long-term performance of such systems (Keesler and Powers, 1988).

A completely different approach would be to use materials that are highly corrosion resistant, such as reinforcing bars constructed of composite materials (Ehsani, 1993). Glass-Fiber-Reinforced-Plastic (GFRP) rebars which have been produced recently are considered to be an ideal candidate and have great potential to fill such a need. GFRP rebars offer significant advantages over conventional reinforcing steel bars, namely, high corrosion resistance, high tensile strength, high strength-to-weight ratio, nonconductivity, ease of handling and cutting, and economy.

Only a handful of studies on bond of straight GFRP rebars to concrete have been reported in the literature; no studies on bond of hooked GFRP rebars to concrete could be found.

In cooperation with the Marshall-Vega Corporation of Marshall, Arkansas, Pleimann (1987, 1991) conducted 4 pull-out tests with No. 2 bars, 19 with No. 3 bars, and 21 with No. 4 bars. The embedment length was given by

$$l_d = \frac{f_u A_b}{20\sqrt{f'_c}} \qquad (10)$$

for E-glass rebar, and

$$l_d = \frac{f_u A_b}{18\sqrt{f_c'}} \qquad (11)$$

for Kevlar 49 rebar. In these equations, l_d is the embedment length in inches, f_u is the ultimate strength of rebars in psi, A_b is the cross sectional area of the rebar in in.^{2}, and f_c' is the 28-day compression strength of the concrete in psi.

Faza and GangaRao (1990) investigated the bond behavior of FRP rebars by testing cantilever beam and pull-out specimens. The results indicated that the basic development length of FRP rebars should be computed using the expression

$$l_{db} = 0.06 \frac{A_b f_{yf}}{\sqrt{f_c'}} \qquad (12)$$

where f_{yf} is the effective yield strength of FRP rebars in psi, and f_c' not to exceed 10,000 psi (69 MPa).

In another study by Chaallal, et al. (1992), pull-out tests were undertaken to evaluate bond strength as well as development length of GFRP rods embedded in normal strength concrete (NSC) and high strength concrete (HSC). Development length was defined as the minimum embedded length required to develop the ultimate tensile force, F_u, of the rod. It was concluded that development length can be taken to be approximately twenty times the bar diameter for both NSC and HSC.

Bond strength of fiber-reinforced plastic rebars was experimentally investigated by Daniali (1992). A total of 30 concrete beams were tested, and results showed that a development length of 8 in. (203 mm) was adequate for developing the ultimate tensile strength of a No. 4 bar. The full strength of a No. 6 bar could be developed over 18 in. (457 mm) of embedment length if shear reinforcement were provided along the entire length of the specimens. Still, the lack of sufficient information about bond behavior of GFRP rebars to concrete restricts their use in field

applications. Moreover, a direct utilization of the ACI 318-89 for calculation of the development length of GFRP rebars is unwarranted due to the inherent differences between steel and GFRP rebars in terms of their tensile strength, modulus of elasticity, and rib geometry.

The primary objective of this research project was to examine the bond behavior and develop design recommendations for anchorage of straight and hooked GFRP rebars to concrete. A total of 102 specimens were tested. Due to space limitation, this paper focuses on the development of a new criterion for acceptable bond performance and design guidelines for GFRP rebars to concrete only. Detailed results of the experiments on bond behavior of straight and hooked GFRP rebars to concrete are presented elsewhere (Tao, 1994).

EXPERIMENTAL PROGRAM

In order to familiarize the reader with the data used in the development of design guidelines, a brief overview of the experimental set up and the test variables is presented here.

Forty-eight beam specimens, eighteen pull-out specimens, and thirty-six 90° hooked rebar specimens were constructed and tested under static monotonic loading. Variables in both beam and pull-out specimens were concrete compressive strength, embedment length, clear concrete cover, and concrete cast depth. Variables in hooked rebar specimens included concrete compressive strength, radius of bend, tail length, and straight embedment length. The data collected during each test included the applied load, and the slip at the free and loaded ends.

Design of Specimens.-The specimens were divided into three groups as shown in Fig. 1, i.e., beam specimens, pull-out specimens, and hooked specimens. The dimensions of specimens are listed in Table 1.

It has been suggested that the bond strength of rebars is affected by the unbounded lead length of the rebar (Hadje-Ghaffari, et al., 1992). To eliminate this influence, a thin conduit was selected to prevent the bonding of the first 3 in. (76 mm) of all rebars to concrete (Fig. 1).

Table 1. - Dimensions of Specimens

Rebar size (1)	Beam Specimen a, in. (2)	b, in. (3)	c, in. (4)	Hooked Specimen a, in. (5)	b, in. (6)
No. 3	14	10	14	12	8
No. 6	24	20	24	18	10
No. 9	36	20	30	24	12

Note: 1 in.=25.4 mm

Material Properties.-Concrete used in this research program was purchased from a local ready-mix plant and specified to have nominal compressive strengths of 4000 and 8000 psi (28 and 56 MPa). For each batch of concrete delivered, sixteen 6x12 in. (152x305 mm) standard cylinders were cast and cured under the same conditions as the specimens. Cylinder samples were tested in compression at approximately the same time as the specimen were tested.

GFRP rebars used in this research program were supplied by a U. S. manufacture. These rebars have around 60 percent type E glass mixed with 40 percent polyester resin by weight. To improve bond strength between rebars and concrete, the longitudinal fibers are wrapped in a helical pattern with a small strand during manufacturing. The pitch shown in Fig. 2 is defined as the distance from the center to center of strands. For all bar sizes, the width of the helical wrap was the same.

To date, there are no standards for the sizes of GFRP rebars. However, most U.S. manufacturers produce rebars with nominal diameters similar to those for steel rebars. The rebar diameters were measured by the volumetric method, cutting a representative 6 in. (152 mm) sample, submerging the sample in a graduated cylinder, and measuring the change in volume. Assuming a circular cross section, the average area and diameter of the bars were calculated. Diameter measurements reported in Table 2 resulted in a little difference between the measured values and the nominal diameters.

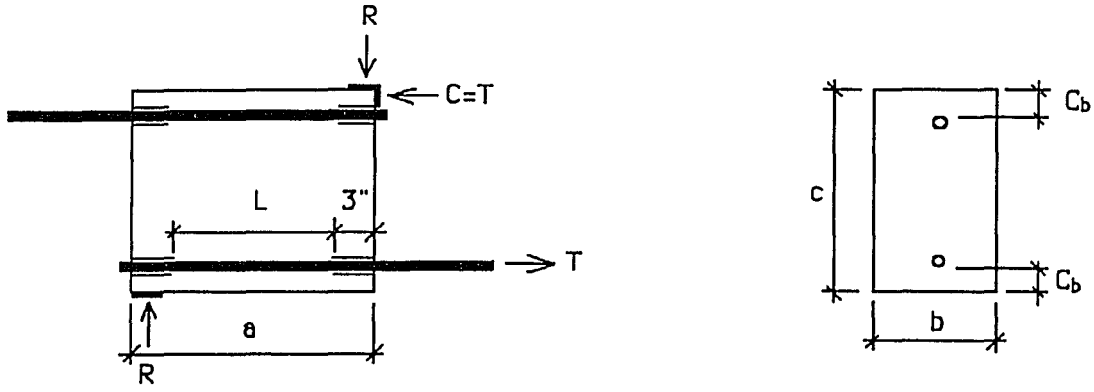

(a) View of Beam Specimens

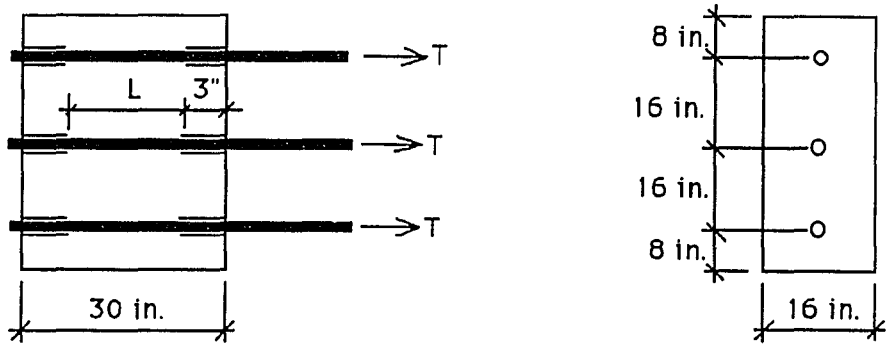

(b) View of Pull-out Specimens

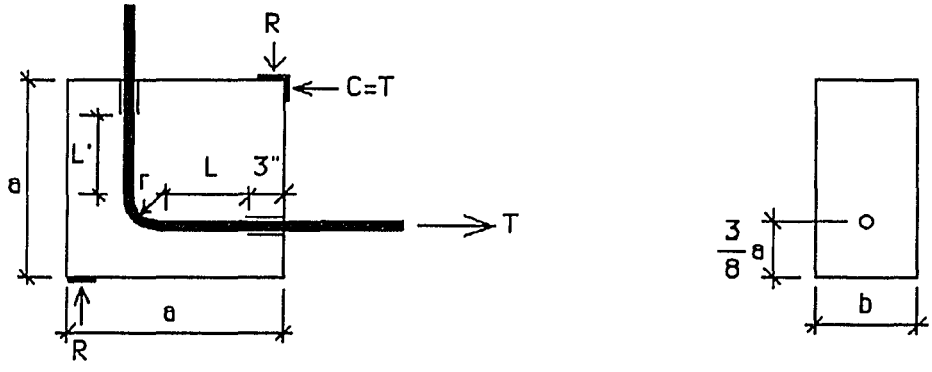

(c) View of Hooked Specimens

Fig. 1. - Test Specimens

The ultimate tensile strength and the modulus of elasticity of GFRP rebars were measured by subjecting coupons to uniaxial tension tests. All coupon samples exhibited a linear tensile stress-strain relationship during the entire loading range. Results for the modulus of elasticity and strength are listed in Table 3 and indicate a mean tensile stiffness of 7000 psi (48,270 MPa).

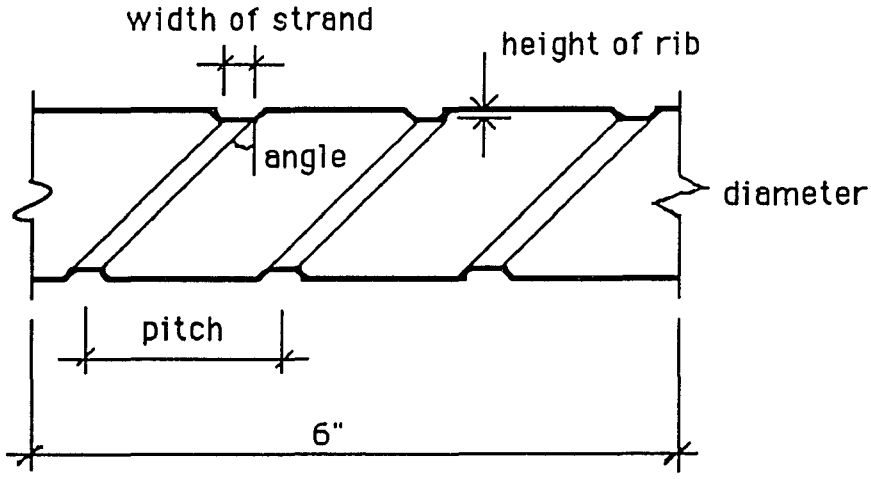

Fig. 2. - Sample for Measuring Rib Geometry

Table 2. - Rib Geometry of GFRP Rebars

Property (1)	No. 3 (2)	No. 6 (3)	No. 9 (4)
Rib height, in.	0.045	0.051	0.079
Pitch, in.	0.687	0.938	1.063
Angle, degree	37	25	23
Minimum diameter, in.	0.324	0.637	0.929
Measured diameter, in.	0.381	0.726	1.079
Nominal diameter, in.	0.375	0.750	1.125
Measured dia./Nominal dia.	1.016	0.968	0.959

Note: 1 in. =25.4 mm

Table 3. - Coupon Test Results for Modulus of Elasticity and Tensile Strength

Rebar No. (1)	Sample 1, ksi (2)	Sample 2, ksi (3)	Sample 3, ksi (4)	Average for 3 samples, ksi (5)
3	6750/129*	6824/141	6857/135	6810/135
6	7028/98	7115/93	7001/88	7050/93
9	7281/77	7298/76	7257/78	7280/77

Note: 1 ksi=6.895 MPa; * For each pair of entries, the first number indicates the modulus of elasticity and the second number is the tensile strength.

The results in Table 3 show that the ultimate tensile strength of GFRP bars is sensitive to rebar diameter, and decreases rapidly with an increase in the diameter of the rebar. This strength reduction is attributed to the "shear lag" phenomenon associated with the tensile force resistance of the core fibers and those at the contact surface of the rebars and the grips (Wu, 1991).

Test Set Up and Instrumentation.-The beam and hooked rebar specimens were tested in a steel reaction frame. This test set-up provided the same state of stresses that a rebar in a real beam would experience. For pull-out tests, however, the compressive reaction force was applied directly to the surface of the concrete specimens (Ehsani, et. al, 1993).

The monotonic static loading was applied along the rebars in a gradual increment until splitting of concrete, rebar pull out from the concrete, or fracture of rebar occurred. The applied load values were measured by two load cells, and automatically recorded. The slip between the rebars and concrete was measured through dial gages and recorded at each load level (Tao, 1994).

ANALYTICAL STUDY

Data from the tests were analyzed to develop design guidelines for anchorage of straight and hooked GFRP rebars to concrete. Due to the absence of concrete flexural cracks in pull-out

specimens, higher ultimate bond stress and greater slip at loaded and free ends were developed. This clearly indicated that it is unconservative to rely on data from pull-out tests for determination of development lengths. It would be more realistic and accurate to use beam test data in such derivations. Therefore, the test results from pull-out specimens were only used in comparison with beam specimens for the determination of top bar effects.

For steel rebars, the critical bond stress is defined as the smaller of that associated with a loaded-end slip of 0.01 in. (0.25 mm) or a free-end slip of 0.002 in. (0.05 mm). Slips greater than these limits are usually accompanied by large crack widths which may not be acceptable (Park and Paulay, 1975). Because the slip is usually measured at both the loaded and free ends of a bar, there will be two stresses each corresponding to the maximum allowable slip at one end of the bar. The smaller of these stresses will be chosen as the critical bond stress (Mathey and Watstein, 1961). Ferguson, et al. (1965) have also concluded that the embedment length has only a minor effect on the stress attained by any steel bar until the loaded-end slip reaches 0.01 in. (0.25 mm).

The above slip limitations for steel rebars cannot be directly utilized in evaluation of GFRP rebars which differ from steel rebars in three important aspects. First, lower modulus of elasticity of GFRP rebars results in greater elongation and contributes to the loaded-end slip. Second, due to higher Poisson's ratio, the greater reduction of rebar diameter under uniaxial tension causes a degradation of adhesion and friction to concrete and larger slips at loaded and free ends. Third, the shallower lugs of GFRP bars can not resist large bearing stresses and result in greater loaded end and free-end slips. Thus, new criteria for bond of GFRP rebars needed to be developed. These criteria were developed based on load-slip relationships and are presented in the following section.

Straight Rebars.-The development of design guidelines for straight GFRP rebars was based on the experimental results of 66 specimens. The load values and the slips at loaded and free ends were measured at each monotonic static loading level. Bond stress, u, is defined as the shear force per unit surface area of the rebar, and computed as

$$u=\frac{T}{\pi d_b l_d} \qquad (13)$$

where T=applied tensile force, d_b=rebar diameter, and l_d=embedment length. Due to the low modulus of elasticity of GFRPs, the elastic elongation of the unbonded lead portion of the bars has to be deducted from the measured slip values. Therefore, the actual slips, δ_a, were calculated as

$$\delta_a=\delta_m-\delta_e \qquad (14)$$

where δ_m=the measured slip at the loaded end of the rebar, and δ_e=the elastic elongation of the 7-in. (178-mm) lead length (Tao, 1994). The test results of beam specimens and pull-out specimens are presented in Tables 4 and 5, respectively. The notation for beam specimens is as follows: the first number indicates the concrete compressive strength; the second number, the rebar diameter; the letter "B" for the beam specimens; the forth number, the embedment length in in.; the next letter presents the rebar casting positions, T:Top, M:Middle, and B:Bottom; the last number represents the ratio of the clear concrete cover to rebar diameter. For example, 43B4B2 is a beam specimen cast with 4000-psi (28-MPa) concrete, No. 3 GFRP rebar, 4-in. (102-mm) embedment length, bottom rebar, with a clear concrete cover of two rebar diameters. For pull-out specimens, the first number represents the concrete compressive strength; the second, the rebar diameter; the letter "P" to designate a pull-out specimen; and the last letter identifies the rebar casting position.

In column 3 of Table 4, the measured bond stresses are listed. These values were calculated from Eq. (4), using the maximum applied load during the test. As can be seen, sum of these stresses, specially those corresponding to specimens with short embedment lengths, are very high, e.g. 1000 to 3700 psi. It is recognized that such high stress values are not safe for design purposes because bond behavior of specimens with short embedment lengths is associated with excessive local damage and slip. Therefore, in design, the average bond stresses over lengths greater than 15 bar diameters should be used (ACI Committee 408, 1992).

Table 4. - Test Data of Beam Specimens

Specimen (1)	f_c', psi (2)	U_m, psi (3)	T_{cr}^*, lbs (4)	T_d^*, lbs (5)	T_c^*/T_u (6)	U_c, psi (7)	K, 1/in. (8)	U, psi (9)	U^*, psi (10)	U^*/U_m (11)	MOF (12)
43B4B2	4330	1673	7060	6840	0.62	1411	0.0396	1188	715	0.4	R
83B4B2	7100	1751	6470	6320	0.57	1356	0.0528	1521	715	0.4	R
43B6B4	5080	1443	8080	7700	0.69	1147	0.0528	1287	715	0.5	R
83B6B4	7100	1356	7780	7260	0.65	1038	0.0689	1521	715	0.5	R
43B8B6	5080	1137	7780	7550	0.68	843	0.0717	1287	715	0.6	R
83B8B6	7100	905	7980	7630	0.69	818	0.0874	1521	715	0.8	R
43B8T6	5080	956	6870	7010	0.62	767	0.0789	1287	715	0.7	R
83B8T6	7100	1020	7520	7420	0.67	796	0.0899	1521	715	0.7	R
46B3B1	4010	1937	10510	11230	0.36	1358	0.0198	572	381	0.2	S
46B3B2	4010	2480	17090	16810	0.57	2171	0.0124	572	572	0.2	P
46B6B2	4010	1342	18320	17980	0.61	1161	0.0231	572	572	0.4	P
46B12B2	5680	815	18770	18320	0.62	704	0.0454	680	680	0.8	P
86B12B2	6920	824	18780	19110	0.64	671	0.0526	751	715	0.9	P
46B16B4	5680	789	19010	17540	0.60	506	0.0633	680	680	0.9	P
86B16B4	6920	754	18230	17710	0.60	473	0.0746	751	715	0.9	P
46B18B6	5680	742	19890	18790	0.64	481	0.0664	680	680	0.9	R
86B18B6	6920	715	19460	18570	0.63	441	0.0800	751	715	1.0	R
49B4B1	4010	1550	22520	22990	0.43	1419	0.0126	381	254	0.2	S
49B4B2	4010	2208	33020	33540	0.63	2081	0.0086	381	381	0.2	P
49B8B2	4010	1230	35120	34670	0.66	1093	0.0164	381	381	0.3	P
49B22B2	5760	606	36150	35590	0.68	487	0.0441	457	457	0.8	P
89B22B2	6490	582	37230	35890	0.69	454	0.0502	485	485	0.8	P
49B26B4	5760	559	38680	36000	0.69	418	0.0513	457	457	0.8	P
89B26B4	6860	547	39000	36660	0.70	404	0.0581	498	498	0.9	P
49B30B6	5760	516	37110	36140	0.69	364	0.0590	457	457	0.9	R
89B30B6	6860	495	38830	35920	0.69	343	0.0684	498	498	1.0	R
43B1.5T1	4010	2982	4110	3980	0.36	2106	0.0255	1143	572	0.2	S
43B1.5T2	4010	3698	6530	6620	0.59	3456	0.0156	1143	572	0.2	P
43B3T2	4010	2007	6380	6720	0.57	1688	0.0318	1143	572	0.3	P
43B4T2	4330	1823	6910	6650	0.60	1371	0.0407	1188	572	0.3	R
83B4T2	7100	1894	6620	6210	0.56	1332	0.0537	1521	572	0.3	R
43B6T4	5080	1293	6810	6420	0.58	956	0.0633	1287	572	0.4	R
83B6T4	7100	1187	7360	6940	0.63	993	0.0721	1521	572	0.5	R
46B3T1	4010	1545	8500	9000	0.29	1098	0.0245	572	305	0.2	S
46B3T2	4010	2063	13570	14610	0.46	1753	0.0153	572	457	0.2	P
46B6T2	4010	1099	14010	13870	0.47	896	0.0300	572	457	0.4	P
46B12T2	5680	760	13890	14340	0.47	534	0.0599	680	544	0.7	P
86B12T2	6920	799	14510	15350	0.49	517	0.0683	751	572	0.7	P
46B16T4	5680	743	13880	13450	0.46	388	0.0825	680	544	0.7	P
86B16T4	6920	722	14790	14170	0.48	379	0.0932	751	572	0.8	P
46B18T6	5680	754	15210	14120	0.48	362	0.0884	680	544	0.7	R
86B18T6	6920	698	15110	14550	0.49	346	0.1021	751	572	0.8	R
49B22T2	5760	594	27310	28750	0.52	375	0.0572	457	365	0.6	P
89B22T2	6490	558	28440	28970	0.54	360	0.0633	485	388	0.7	P
49B26T4	5760	536	29160	26950	0.52	313	0.0686	457	365	0.7	P
89B26T4	6860	528	27890	28790	0.53	307	0.0763	498	399	0.8	P
49B30T6	5760	521	29510	27920	0.53	281	0.0764	457	365	0.7	R
89B30T6	6860	515	29410	28470	0.55	272	0.0863	498	399	0.8	R

Table 5. - Test Data of Pull-out Specimens

Specimen (1)	f_c', psi (2)	Top bar (3)	U_m, psi (4)	MOF (5)
43PB	4670	N	4270	P
43PM	4670	Y	4103	P
43PT	4670	Y	4058	P
83PB	6640	N	1504	R
83PM	6640	Y	1334	R
83PT	6640	Y	1260	R
46PB	4670	N	1661	P
46PM	4670	Y	1396	P
46PT	4670	Y	1343	P
86PB	6640	N	944	P
86PM	6640	Y	868	P
86PT	6640	Y	834	P
49PB	4670	N	1630	P
49PM	4670	Y	1436	P
49PT	4670	Y	1423	P
89PB	6640	N	631	P
89PM	6640	Y	586	P
89PT	6640	Y	576	P

The ACI Code expressions for bond of steel rebars are presented for the more common conditions. Additional factors are then provided to account for special considerations due to top bar effects, confinement of the concrete, etc. A similar approach will be followed here. Since the effects of top bar and concrete cover are determined based on the measured bond stresses during the test (reported in Column 3 of Table 5), these considerations will be examined next, followed by the basic bond expressions for the more general conditions.

The casting position has been shown to significantly influence bond strength under monotonic static loading. In the current ACI Code, the top bar effect is accounted for by multiplying the development length of steel reinforcement by a factor of 1.3 (ACI 318-89). The top bar factor is defined as the ratio of the ultimate bond strength reached in pulling out the bottom bar to that reached in pulling out the top bar.

Table 6 indicates 21 pairs of specimens in which pull-out failure rather than rebar fracture controlled. The distribution of ratios of measured bond strength of bottom bars to that of top bars reported in Table 6 is shown in Fig. 3. All values are less than 1.25. Therefore, it is recommended that a factor of 1.25 be used to account for the top bar effect.

Table 6. - Top Bar Factor of GFRP Rebars

Bottom bar specimen (1)	Top bar specimen (2)	Height of concrete below bar, in. (3)	U_m@bottom/ U_m@top (4)
46B3B1	46B3T1	23	1.25
46B3B2	46B3T2	22	1.20
46B6B2	46B6T2	22	1.22
46B12B2	46B12T2	22	1.07
86B12B2	86B12T2	22	1.03
46B16B4	46B16T4	20	1.06
86B16B4	86B16T4	20	1.04
49B22B2	49B22T2	27	1.02
89B22B2	89B22T2	27	1.04
49B26B4	49B26T4	24	1.04
89B26B4	89B26T4	24	1.04
43PB	43PM	24	1.04
43PB	43PT	30	1.05
46PB	46PM	24	1.19
46PB	46PT	30	1.24
86PB	86PM	24	1.09
86PB	86PT	30	1.13
49PB	49PM	24	1.13
49PB	49PT	30	1.15
89PB	89PM	24	1.08
89PB	89PT	30	1.10

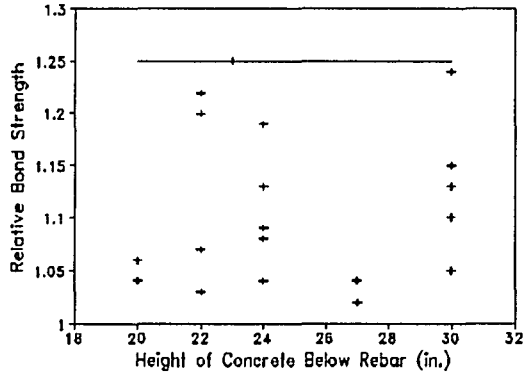

Fig. 3. - Top Bar Effect

To account for the confinement provided by various concrete cover thicknesses, ACI 318-89 specifies confinement factors of 1.0, 1.4, and 2.0 for steel rebars. The concrete cover has a significant effect on the type of bond failure for GFRP rebars. If the cover is one bar diameter, a splitting failure will occur. If the cover equals or exceeds two bar diameters, a pull-out failure or rebar fracture was observed. Other factors such as the presence of stirrups have also shown to improve the confinement in tests of steel bars. However, the effect of this variable was not studied in this investigation.

The distribution of the ratios of measured bond strength in specimens with concrete cover of two bar diameters to those with one bar diameter is shown in Fig. 4. The largest ratio is 1.42. Therefore, a confinement factor of 1.5 will cover all cases when the concrete cover is one bar diameter or less. Thus, to account for the influence of concrete cover, the basic development length l_{db} must be multiplied by the confinement factors 1.0 or 1.5 depending on the amount of concrete cover provided.

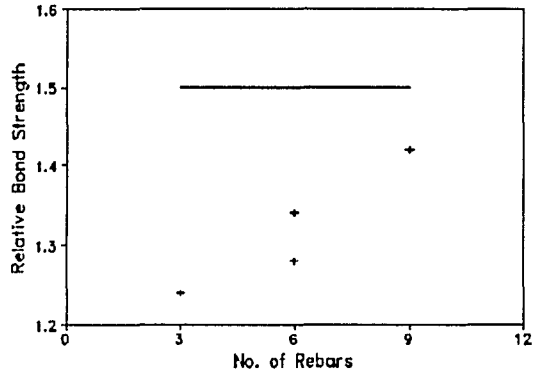

Fig. 4. - Concrete Cover Effect

Having accounted for the effects of top bar and concrete cover, the following discussions will focus on the evaluation of bond of GFRP rebars under the more common conditions. An examination of typical load-slip relationships for four specimens with different embedment lengths shown in Fig. 5 indicates that various embedment lengths have only a minor influence on the load values until the free-end slip is 0.0025 in. (0.064 mm) or the loaded-end slip is 0.015 in. (0.38 mm). The beam specimens considered in this figure were cast with 4000-psi (28-MPa) concrete, No. 9 bottom GFRP rebars, with embedment lengths varying from 8 to 30 in. (203 to 762 mm), and with a clear concrete cover of two rebar diameters or larger. A similar trend was observed in all other beam specimens. It is noted that larger slip limits will cause wider cracks in GFRP specimens compared to ordinary steel reinforced concrete structures. However, considering the corrosion resistance of GFRP rebars, these wider cracks can be permitted.

The critical load values corresponding to a free-end slip of 0.0025 in. (0.064 mm), T_{cf}, and a loaded-end slip of 0.015 in. (0.38 mm), T_{cl}, were obtained from the test data. The smaller of these two numbers was considered the critical load, T_c.

To eliminate the effects of the variation of concrete compressive strength, f_c', the above T_{cf}, T_{cl}, and T_c values were modified by multiplying them by the factor $\sqrt{f'_{cavg}}/f_c'$, where f'_{cavg} is

an average compressive strength for all specimens with nominal concrete strength of 4000 or 8000 psi (28 or 56 MPa). These adjusted values are reported as T_{cf}^* and T_{cl}^* in columns 4 and 5 of Table 4, respectively.

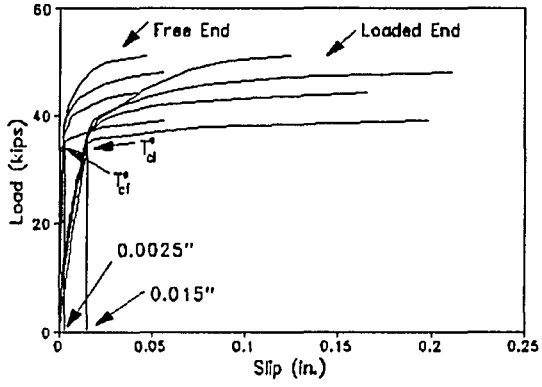

Fig. 5. - Load-Slip Relationships

In the next column in Table 4, the critical load, T_c^*, is presented as a ratio of the ultimate tensile capacity of the bars, T_u. For the bottom-cast bars the average ratio is 0.63, and for top-cast bars, the ratio is 0.51.

The ACI expressions for calculating the development length of steel reinforcement have undergone significant changes since the early 1960s. In the ACI 318-63, the bond strength was taken as

$$u=\frac{9.5\sqrt{f_c'}}{d_b} \qquad \textbf{(6a)}$$

for splitting failure, and

$$u=800psi \qquad \textbf{(6b)}$$

for pull-out failure. In 1971, the expressions were revised to calculate the required development length rather than the bond stress values. Due to the actual strength of steel being greater than

the nominal value, the development length was based on 125 percent of the nominal yield strength (Orangun, et al., 1977). Combining Eqs. (4) and (6) with the 125 percent factor and rewriting the expression in terms of the required development length, the following two expressions were presented (ACI 318-71):

$$l_{db}=0.04\frac{A_b f_y}{\sqrt{f_c'}} \tag{7a}$$

and

$$l_{db}=0.0004 d_b f_y \tag{7b}$$

where f_y=specified yield strength of nonprestressed reinforcement in psi.

For GFRP rebars, the basic development length, l_{db}, was calculated by equating the critical bond strength over the surface of rebar to the ultimate tensile force in the rebar:

$$u_c \pi d_b l_{db}=A_b f_y \tag{8}$$

and by using ACI basic development length equation:

$$l_{db}=K\frac{A_b f_y}{\sqrt{f_c'}} \tag{9}$$

where u_c=critical bond stress in psi. The value of u_c reported in Column 7 of Table 4 was calculated from Eq. 4, when the applied tensile force was replaced with T_c. Because Eq. 9 does include the effect of the concrete compressive strength, it was decided to use the term T_c rather than T_c^* in calculation of u_c. From Eqs. (8) and (9), the factor K listed in Table 4 was calculated as

$$K=\frac{\sqrt{f_c'}}{u_c \pi d_b} \tag{10}$$

The next objective was to determine a factor K and an upper limit for the bond stress, such that after the application of the relevant factors for top bar, concrete cover, etc., the resulting equations would yield a conservative development length. These will result in a pair of equations similar to Eqs. (7a) and (7b) of the ACI code. Therefore, the basic development length equation was modified for the use of GFRP rebars as

$$l_{db}=0.047\frac{A_b f_y}{\sqrt{f'_c}} \qquad (11)$$

which was based on the test results of beam specimens and is similar to Eq. (7a). The 0.047 coefficient ensures that all development lengths calculated based on Eq. (11) will be larger than the measured ones. This equation can be rearranged and presented in terms of bond stresses in a format similar to Eq. (6a) as:

$$u=6.77\frac{\sqrt{f'_c}}{d_b} \qquad (12)$$

In column 10 of Table 4, adjusted bond stress values, u*, are listed. These values were obtained from the bond stresses given in column 9, and include the following three modifications. First, all stresses corresponding to top bars were divided by 1.25 to account for the top bar effect. Second, the stresses for those specimens with concrete cover of one bar diameter or smaller were divided by 1.5 to account for the small cover. Even with these conditions, some of the bond stresses were still too high, resulting in unconservative development length calculation. Therefore, the third modification was to impose a maximum bond stress limit on these values, similar to the 800 psi limit given by Eq. (6b) for steel bars. Analysis of the data indicated that an upper limit of 715 psi for GFRP bars could ensure that all development lengths calculated based on adjusted bond stresses from column 10 of Table 4 will be larger than the measured ones.

The above bond stress limit of 715 psi can be incorporated in Eq. (8) and re-written in a form similar to Eq. (7b) which is more familiar to design engineers as:

$$l_{db}=0.00035 d_b f_y \qquad (13)$$

The ratios of the adjusted bond stress to the measured values are listed in Column 11 of Table 4 and plotted in Fig. 6. As can be seen, all calculated values are less than measured. In the distribution of ratios for all forty eight beam specimens, all ratios are less than or equal to unity. Therefore, in an approach similar to that used by the ACI Code for calculating the development length of rebars, it is recommended that the development length of GFRP rebars be calculated from the product of Eq. (11) times modification factors of 1.25 for top-cast bars and 1.5 for small covers. This value must be compared with the result of Eq. (13) and the larger figure selected. In addition, it is recommended that a minimum development length of 15 in. (381mm) be provided. This limit, which is slightly larger than the ACI recommended 12 in. (305 mm) value for steel rebars, is intended to account for the inherent lower bond strength of GFRP rebars.

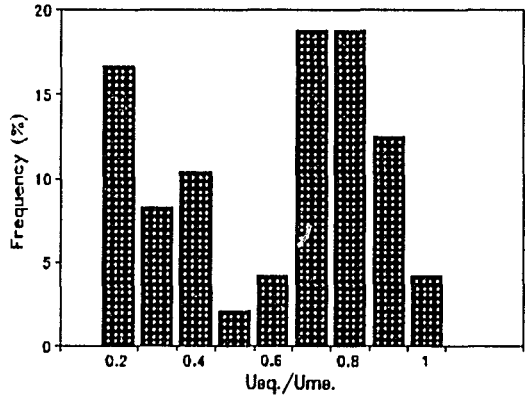

Fig. 6. - Bond Strength Ratio vs. Frequency

Hooked Rebars.-The test results of 24 specimens with a hook radius of three bar diameters were analyzed to develop design guidelines for hooked GFRP rebars. At each monotonic static load increment, the load values and the loaded-end slips were measured. The corresponding nominal tensile stress was calculated as the tensile applied load divided by the nominal cross section of the rebar, as:

$$f_s = \frac{4T}{\pi d_b^2} \qquad (14)$$

The test results are reported in Table 7. The notation for the specimens is as follows: the first number indicates the concrete compressive strength; the second number the rebar diameter; the letter "H" for the hooked rebar specimens; the fourth number is the ratio of hook radius to bar diameter; the next number the ratio of tail length to rebar diameter; and the last number the ratio of the development length to the bar diameter. For example, 43H3124 was a hooked rebar specimen cast with 4000 psi (28 MPa) concrete, No. 3 GFRP rebar, where the ratios of hook radius, tail length, and development length to rebar diameter were 3, 12, and 4, respectively.

Similar to the critical bond stress approach presented for straight GFRP rebars, the critical tensile stress, f_{sc}, is defined as the tensile stress associated with a loaded-end slip of 0.015 in. (0.38 mm). The critical tensile load values and the corresponding critical tensile stresses are listed in Table 7 as T_c and f_{sc}, respectively.

The ACI Code for design of hooked steel rebars underwent a major revision with the ACI 318-83. In ACI 318-77, the tensile stress developed by the hook was calculated as

$$f_h = \xi\sqrt{f'_c} \qquad (15)$$

where ξ was a factor which included the effects of the rebar diameter, tensile strength, and casting position. However, the application of this provision was somewhat difficult because the adjustments in ξ for top bars, lightweight concrete, etc., were not clearly defined (Jirsa, et al.,

1979). In addition, in practice, the development length is of greater interest to the designer than the stress carried by the bar over a given length. Thus, ACI 318-83 required a total embedment length L_{dh} (Fig. 1. c) which was computed as the product of the basic development length L_{hb} and the applicable modification factors. For a hooked bar with f_y equal to 60,000 psi (414 MPa), the basic development length L_{hb} was calculated as

$$L_{hb}=1200\frac{d_b}{\sqrt{f'_c}} \qquad (16)$$

For bars with f_y other than 60,000 psi (414 MPa), L_{hb} was multiplied by a modification factor

Table 7. - Test Data for Hooked Rebar Specimens

Specimen (1)	f'_c, psi (2)	L_{dh}, in. (3)	T_c, lbs (4)	f_{sc}, psi (5)	K (6)	$L_{eq.}$, in. (7)	$L_{eq.}/L_{dh}$ (8)	MOF (9)
43H3124	5080	1.5	2130	19364	0.0147	12.0	8.0	S
43H3204	5080	1.5	2040	18545	0.0154	12.0	8.0	S
43H3127	4280	2.6	3670	33364	0.0137	13.1	5.0	S
43H31210	4280	3.8	4980	45273	0.0145	13.1	3.5	S
43H31213	4280	4.9	6260	56909	0.0149	13.1	2.7	R
43H31216	4280	6.0	7850	71364	0.0147	13.1	2.2	R
83H3124	6640	1.5	2490	22636	0.0144	10.5	7.0	S
83H3204	6640	1.5	2410	21909	0.0149	10.5	7.0	S
46H3124	5680	3.0	10460	23773	0.0127	15.6	5.2	S
46H3204	5680	3.0	10360	23545	0.0128	15.6	5.2	S
46H3127	4280	5.3	13460	30591	0.0150	18.0	3.4	S
46H31210	4280	7.5	19300	43864	0.0149	18.0	2.4	S
46H31213	4280	9.8	24270	55159	0.0154	18.0	1.8	R
46H31216	4280	12.0	27110	61614	0.0170	18.0	1.5	R
86H3124	6920	3.0	11640	26455	0.0126	14.2	4.7	S
86H3204	6920	3.0	11840	26909	0.0124	14.2	4.7	S
49H3124	5760	4.5	20680	20680	0.0147	19.4	4.3	S
49H3204	5760	4.5	20970	20970	0.0145	19.4	4.3	S
49H3127	4280	7.9	28980	28980	0.0158	22.5	2.9	S
49H31210	4280	11.3	33320	33320	0.0196	22.5	2.0	S
49H31213	4280	14.6	45000	45000	0.0189	22.5	1.5	R
49H31216	4280	18.0	47530	47530	0.0220	22.5	1.3	R
89H3124	6860	4.5	23580	23580	0.0141	17.8	4.0	S
89H3204	6860	4.5	23670	23670	0.0140	17.8	4.0	S

of f_y/60,000, and determined as

$$L_{hb}=0.02\frac{d_b f_y}{\sqrt{f_c'}} \quad (17)$$

For hooked GFRP rebars, considering strength and serviceability, the factor K reported in Table 7 was computed as

$$K=\frac{L_{dh}/d_b}{f_{sc}/\sqrt{f_c'}} \quad (18)$$

Figure 7 shows a plot of L_{dh}/d_b versus $f_{sc}/\sqrt{f_c'}$. Through linear regression analysis, a conservative line through the data produces the following equation

$$L_{eq.}=0.017\frac{d_b f_y}{\sqrt{f_c'}} \quad (19)$$

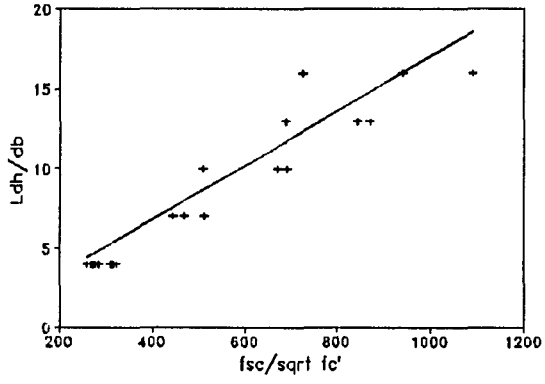

Fig. 7. - Linear Regression Analysis for Hooked GFRP Rebars

This indicates that a value of K=0.017 is adequate for GFRP hooked bars. As can be seen, Eq. (19) is similar to the code-based Eq. (17), which includes the effect of the bar yield strength. In all hooked specimens considered, side cover and cover on bar extension beyond hook were not less than 2-1/2 in. (64 mm) and 2 in. (51 mm), respectively. Meanwhile, the hooked GFRP rebars used in this research program were No. 3, 6, and 9 rebars which had yield strengths, f_y, of 135, 93, and 77 ksi (931, 641, and 531 MPa), respectively. The factor K obtained in Eqs. (18) and (19) already includes the conditions of the relatively large yield strengths of the bars and large covers.

To account for the influence of bar yield strength and cover for steel reinforcement, the modification factors of f_y/60,000 and 0.7 were specified as the multipliers of the basic development length in ACI 318-89. Similar to the ACI Code, the applicable modification factors of f_y/75,000 and 0.7 are recommended for GFRP hooked rebars to take into account bar yield strengths other than 75,000 psi (517 MPa) and large covers. Therefore, the basic development length L_{hb} was determined from Eq. (19) after considering the above two corrections as follows:

$$L_{hb}=1820\frac{d_b}{\sqrt{f'_c}} \qquad (20)$$

Thus, it is recommended that the development length of hooked GFRP bars be calculated as the product of the basic length from Eq. (20) times modification factors of f_y/75,000 and 0.7, if applicable.

Moreover, to prevent direct pull-out failure in cases where the hooked rebar may be located very near the critical section, the above figure shall be no less than 8 times the bar diameter or 6 in. (152 mm).

Ratios of calculated to measured development lengths for hooked rebar specimens listed in Table 7 are plotted in Fig. 8. All ratios were above unity indicating the conservative values obtained from Eq. (19).

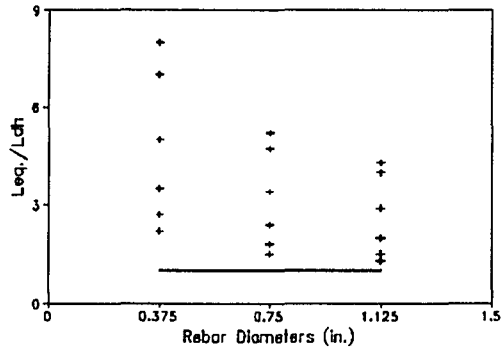

Fig. 8. - Ratios of Calculated to Measured Development Lengths vs. Rebar Diameters

SUMMARY AND CONCLUSIONS

To develop design guidelines for bond of straight and hooked GFRP rebars to concrete, 102 specimens were tested. Based on the theoretical analysis of the test results, the following conclusions were drawn:

1). It is recommended that the allowable slips at the loaded-end and free-end of GFRP bars be limited to 0.015 in. (0.38 mm) and 0.0025 in. (0.064 mm), respectively.

2). For straight GFRP rebars, the development length l_d should be computed as a product of Eq. (12) times modification factors of 1.25 for top bars and 1.5 for cases when the concrete cover is less than or equal to one bar diameter. This figure shall not be less than the values obtained from Eq. (13). Finally, a minimum development length of 15 in. (381 mm) must be provided.

3). For hooked GFRP rebars, the development length is calculated from the product of Eq. (19) times a factor of $f_y/75{,}000$ for bars with yield strengths higher than 75,000 psi (517 MPa) and a factor of 0.7 for larger concrete covers. The resulting value shall not be less than eight times the bar diameter or 6 in. (152 mm).

APPENDIX I. - REFERENCES

ACI Committee 318, (1963). "Building Code Requirements for Reinforced Concrete.", (ACI 318-63), American Concrete Institute, Detroit.

ACI Committee 318, (1971). "Building Code Requirements for Reinforced Concrete.", (ACI 318-71), American Concrete Institute, Detroit.

ACI Committee 318, (1977). "Building Code Requirements for Reinforced Concrete.", (ACI 318-77), American Concrete Institute, Detroit.

ACI Committee 318, (1989). "Building Code Requirements for Reinforced Concrete.", (ACI 318-89), American Concrete Institute, Detroit, 181-211.

ACI Committee 408, (1992). "State-of-the-art Report on Bond Under Cyclic Loads." American Concrete Institute, Detroit, 3-7.

Chaallal, O., Benmokrane, B., and Masmoudi, R., (1992). "An Innovative Glass-Fiber Composite Rebar for Concrete Structures," Advanced Composite Materials in Bridges and Structures, Canadian Society for Civil Engineering, 169-177.

Daniali, S., (1992). "Development Length for Fiber-Reinforced Plastic Bars," Advanced Composite Materials in Bridges and Structures, Canadian Society for Civil Engineering, 179-188.

Ehsani, M. R., (1993). "Glass-fiber reinforcing bars." in J. L. Clarke, ed., Alternative Materials for the Reinforcement and Pressing of Concrete, Blackie Academic & Professional, London.

Ehsani, M. R., Saadatmanesh, H., and Tao, S., (1993). "Bond of GFRP Rebars to Ordinary-Strength Concrete." ACI International Symposium on Non-Metallic Continuous Reinforcement, Vancouver, Canada.

Faza, S.S. and GangaRao, H.V.S., (1990). "Bending and Bond Behavior of Concrete Beams Reinforced with Plastic Rebars." Transportation Research Record 1290, 185-193.

Ferguson, P. M., Breen, J. E., and Thompson, J. N., (1965). "Pullout Tests on High-Strength Reinforcing Bars." ACI J., 62(8), 933-949.

Hadje-Ghaffari, H., Choi, O. C., Darwin, D., and McCabe, S. L., (1992). "Bond of Epoxy-Coated Reinforcement to Concrete: Cover, Casting Position, Slump, and Consolidation," Structural Engineering and Engineering Materials, SL Report 92-3, University of Kansas, Lawrence, Kansas.

Jirsa, J. O., Lutz, L. A., and Gergely, P., (1979). "Rational for Suggested Development, Splices, and Standard Hook Provisions for Deformed Bars in Tension," Concrete International, 47-61.

Keesler, R. J., and Powers, R. G. (1988). "Corrosion of epoxy coated rebars-Keys Segmental Bridge-Monroe County." Report No. 88-8A, Florida Department of Transportation, Materials Office, Corrosion Research Laboratory, Gainesville.

Mathey, R. G., and Watstein, D., (1961). "Investigation of Bond in Beam and Pull-Out Specimens with High-Yield-Strength Deformed Bars," ACI J., 32(9), 1071-1089.

Park, R. and Paulay, T., (1975). "Reinforced Concrete Structures." John Wiley & Sons, New York, 401-404.

Pleimann, L. G., (1987). "Tension and Bond Pull-Out Tests of Deformed Fiberglass Rods," Final Report for Marshall-Vega Corporation, Marshall, Arkansas, Civil Engineering Department, University of Arkansas, Fayetteville,Arkansas, 5-11.

Pleimann, L. G., (1991). "Strength, Modulus of Elasticity, and Bond of Deformed FRP Rods," Advanced Composites Materials in Civil Engineering Structures, Proceedings of the Specialty Conference, Materials Engineering Division, ASCE, 99-110.

Tao, S., (1994). "Bond of Glass-Fiber-Reinforced-Plastic Reinforcing Bars to Concrete," Ph. D. Dissertation, Department of Civil Engineering and Engineering Mechanics, University of Arizona, Tucson, AZ.

Wu, W. P., GangaRao H., and Prucz, J. C. (1991). "Mechanical Properties of Fiber Reinforced Plastics." Research Report, Constructed Facilities Center, College of Engineering, West Virginia University.

APPENDIX II. - NOTATION

The following symbols are used in this paper:

A_b	nominal cross section area of rebars, $in.^2$
d_b	rebar diameter, in.
f_c'	concrete compressive strength for each specimen, psi
$f_{cavg.}'$	average of f_c' for all 4000- or 8000-psi (28- or 56-MPa) concrete, psi
f_h	tensile stress of hook, psi
f_s	tensile stress of rebars, ksi

f_{sc}	critical tensile stress of rebars, psi
f_y	yield strength of steel rebars or tensile strength of GFRP rebars, psi
l_d	embedment length, in.
l_{db}	basic development length of straight rebars, in.
L_{dh}	modified development length of hooked rebars, in.
$L_{eq.}$	development length calculated in Eq. (19), in.
L_{hb}	basic development length of hooked rebars, in.
MOF	mode of failure
T	applied tensile load, lbs
T_c^*	defined as the smaller of T_{cf}^* and T_{cl}^*, lbs
T_{cf}^*	adjusted applied tensile load at free-end slip of 0.0025 in. (0.064 mm), lbs
T_{cl}^*	adjusted applied tensile load at loaded-end slip of 0.015 in. (0.38 mm), lbs
T_u	ultimate tensile capacity of rebar, lbs
U	bond stress, psi
U^*	adjusted bond stress, psi
U_c	critical bond stress, psi
U_m	measured bond stress, psi
δ_a	loaded-end slip after correction for elastic elongation of rebar, in.
δ_e	elastic elongation of rebar, in.
δ_m	loaded-end slip measured during testing, in.

APPENDIX D: ILLUSTRATIONS

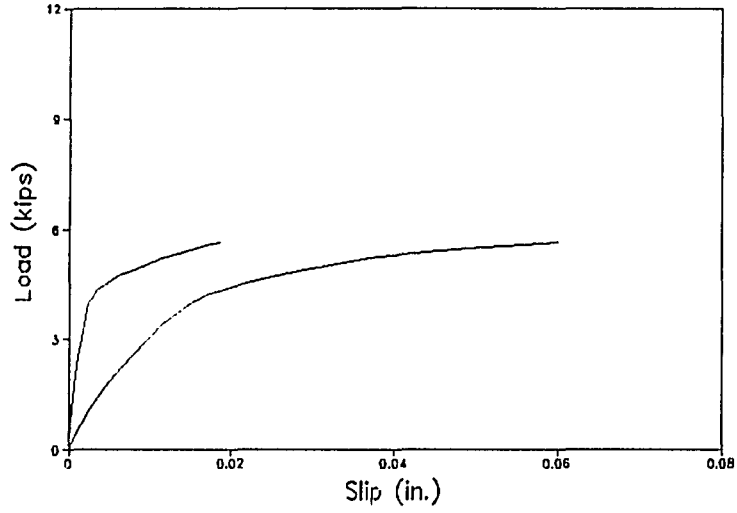

FIGURE 1, Load-slip relationship of specimen 43B1.5T1

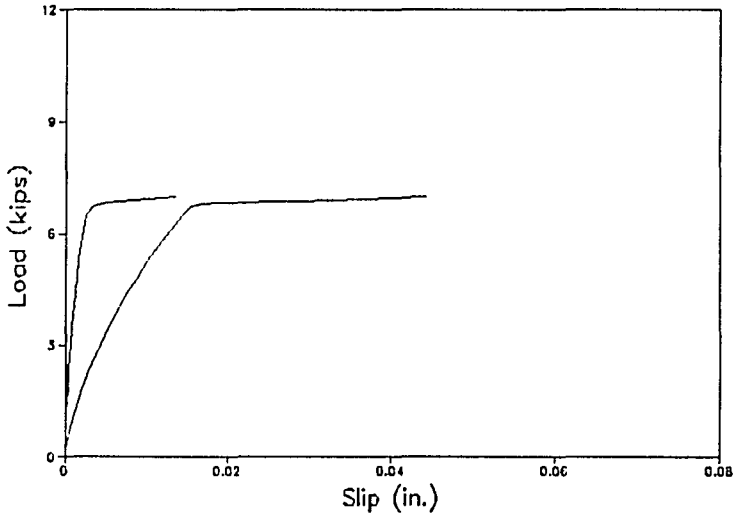

FIGURE 2, Load-slip relationship of specimen 43B1.5T2

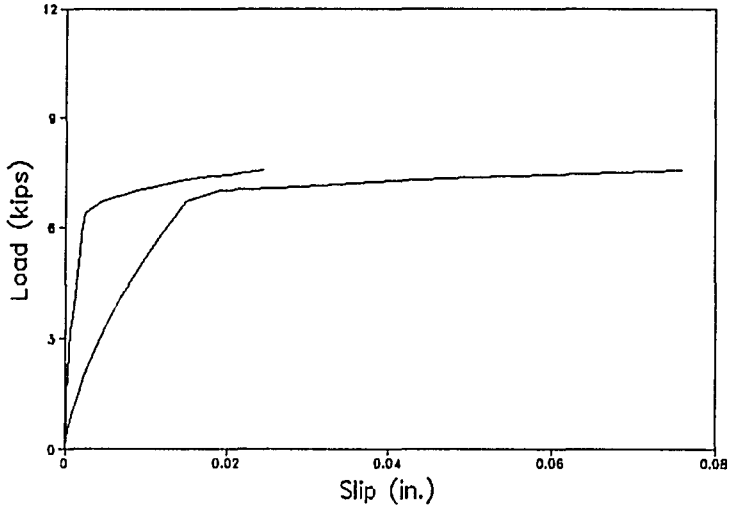

FIGURE 3, Load-slip relationship of specimen 43B3T2

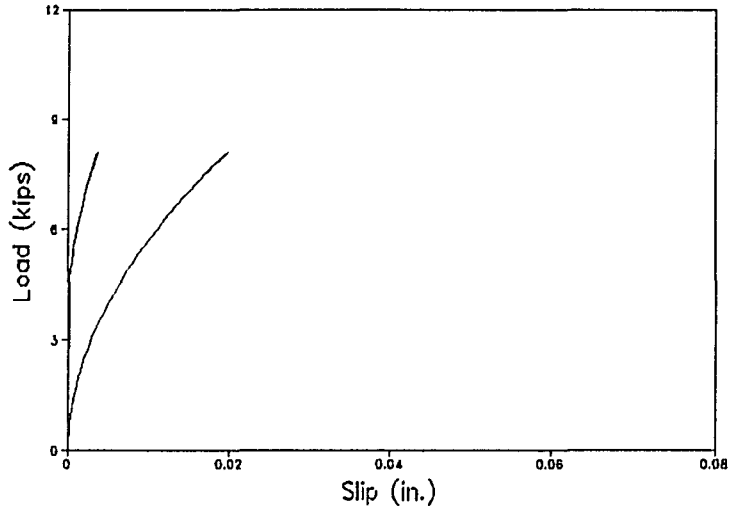

FIGURE 4, Load-slip relationship of specimen 43B4B2

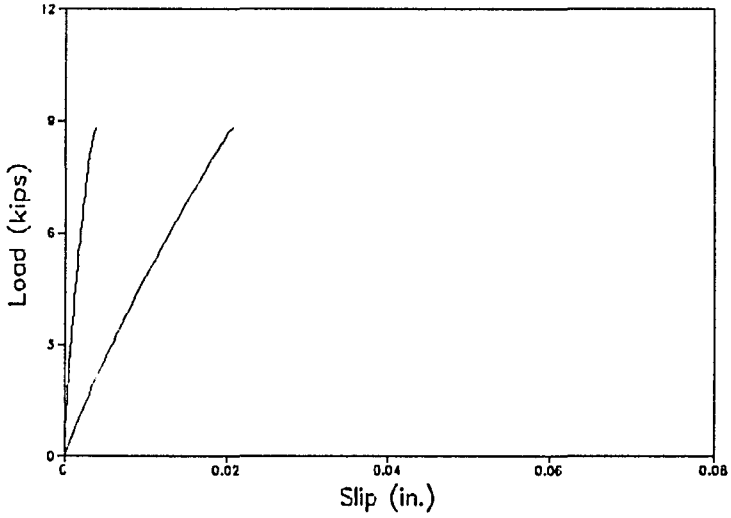

FIGURE 5, Load-slip relationship of specimen 43B4T2

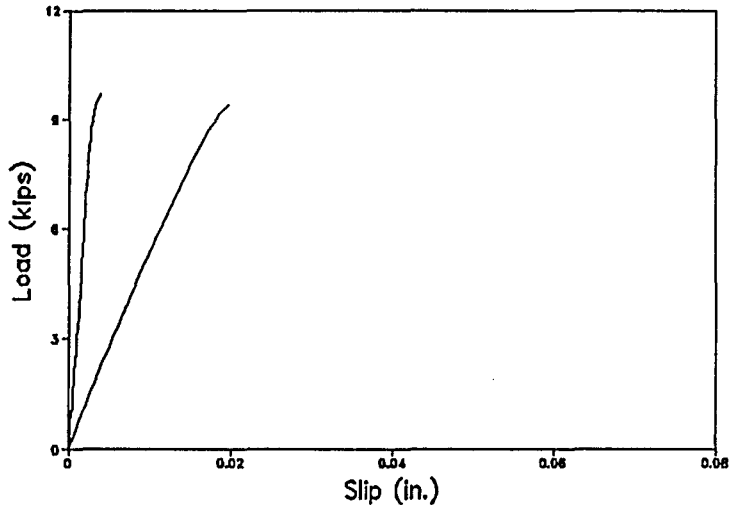

FIGURE 6, Load-slip relationship of specimen 43B6B4

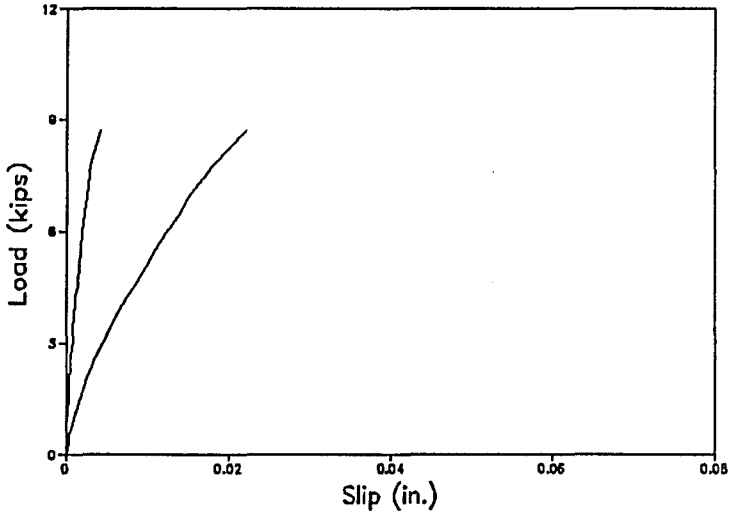

FIGURE 7, Load-slip relationship of specimen 43B6T4

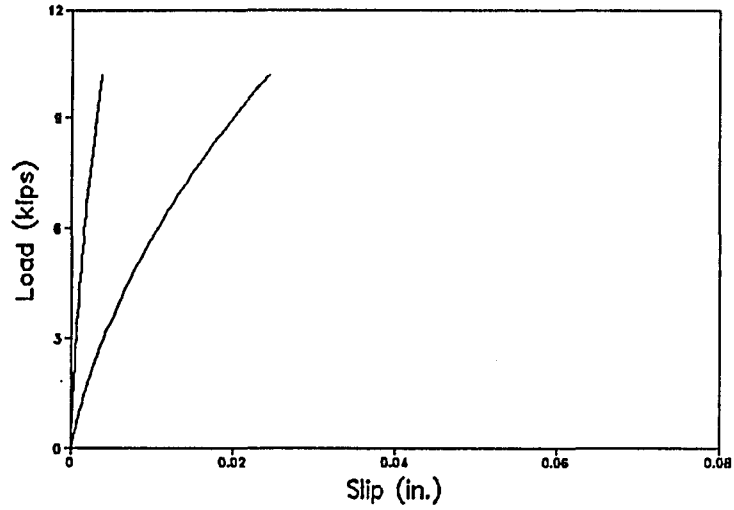

FIGURE 8, Load-slip relationship of specimen 43B8B6

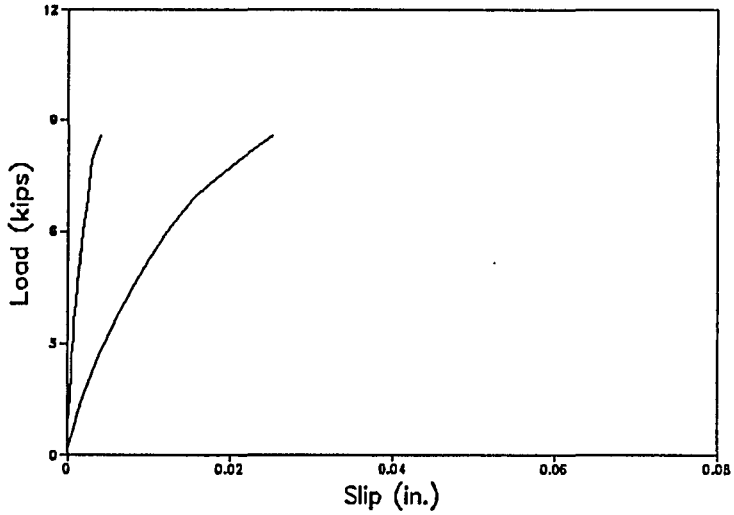

FIGURE 9, Load-slip relationship of specimen 43B8T6

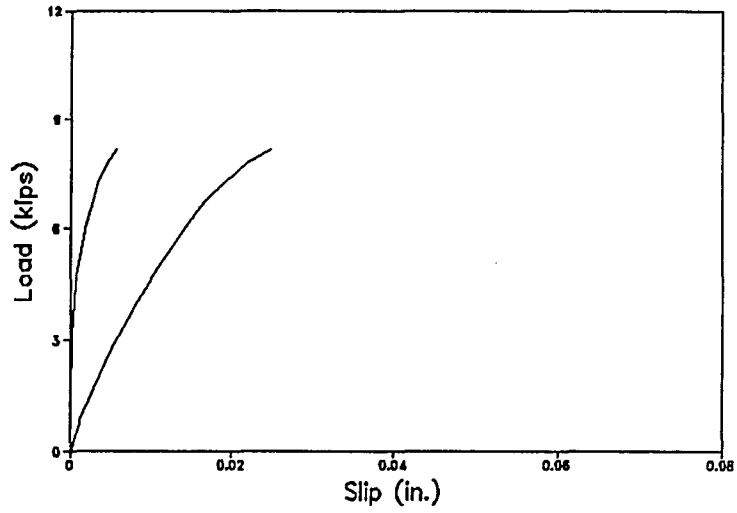

FIGURE 10, Load-slip relationship of specimen 83B4B2

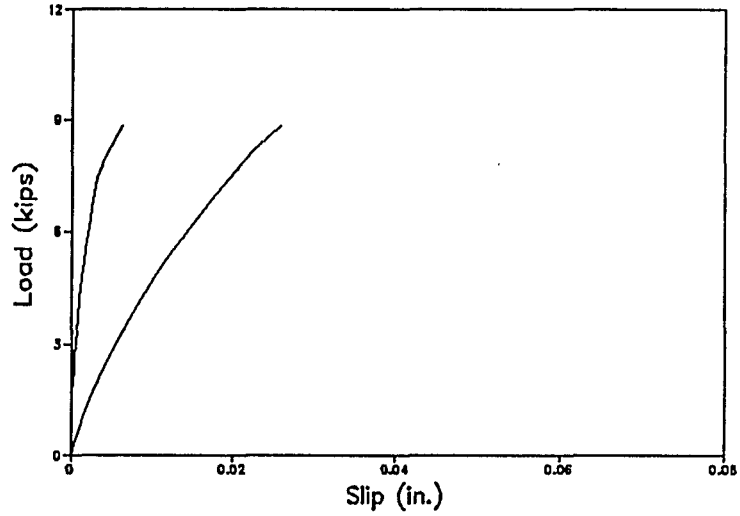

FIGURE 11, Load-slip relationship of specimen 83B4T2

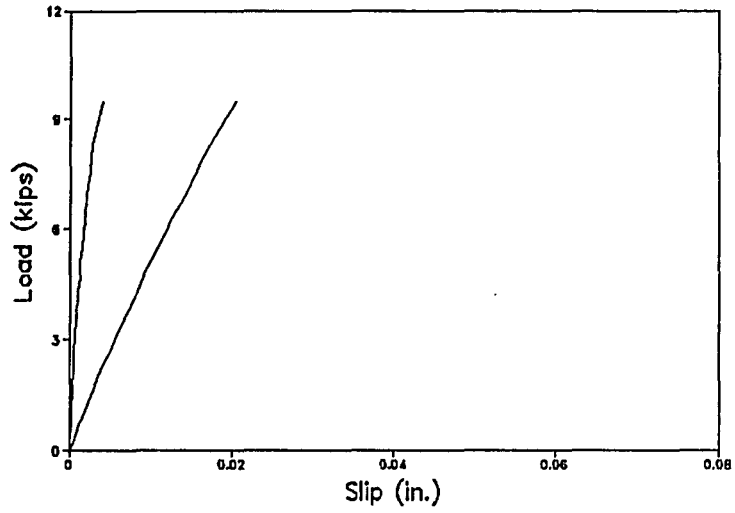

FIGURE 12, Load-slip relationship of specimen 83B6B4

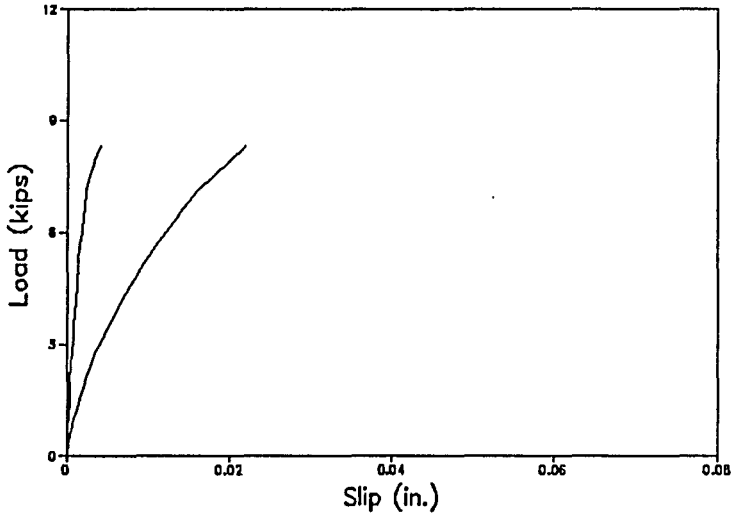

FIGURE 13, Load-slip relationship of specimen 83B6T4

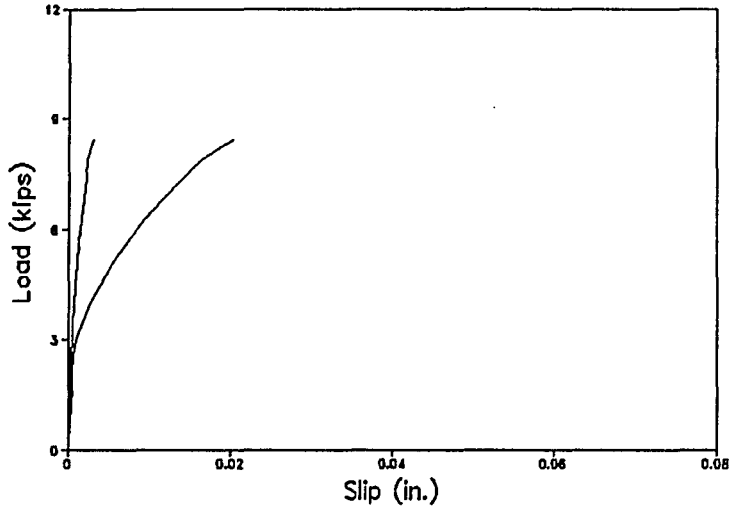

FIGURE 14, Load-slip relationship of specimen 83B8B6

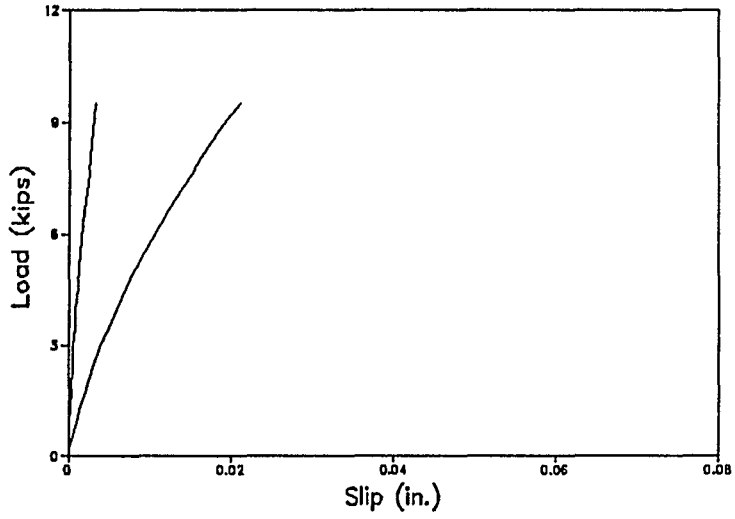

FIGURE 15, Load-slip relationship of specimen 83B8T6

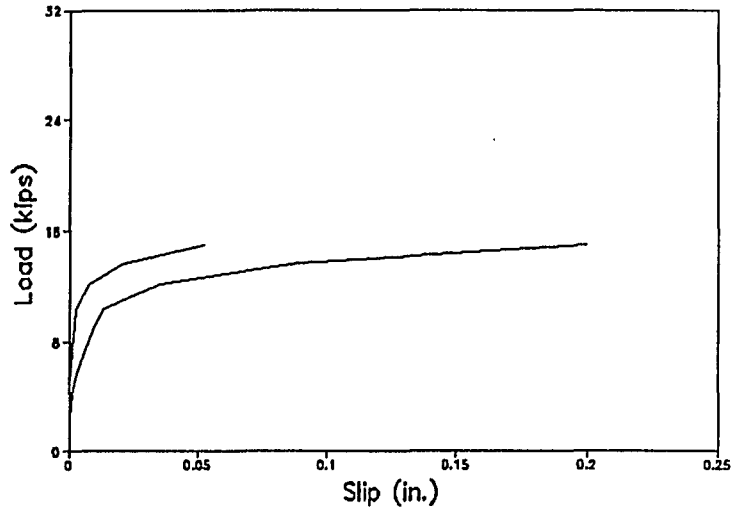

FIGURE 16, Load-slip relationship of specimen 46B3B1

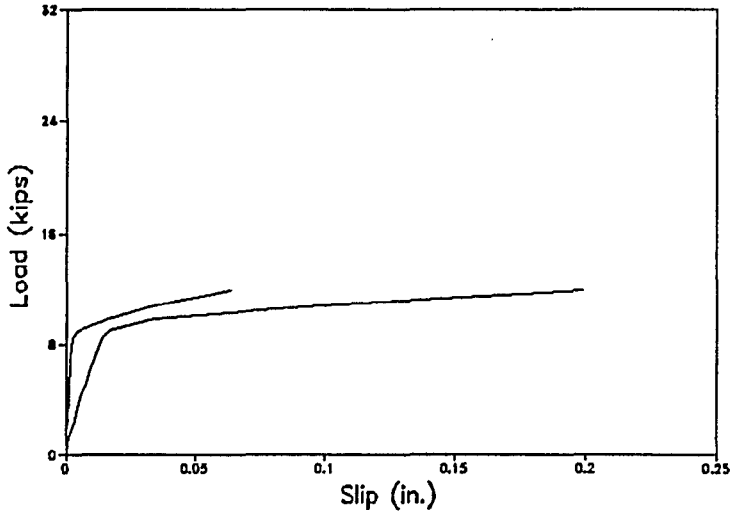

FIGURE 17, Load-slip relationship of specimen 46B3T1

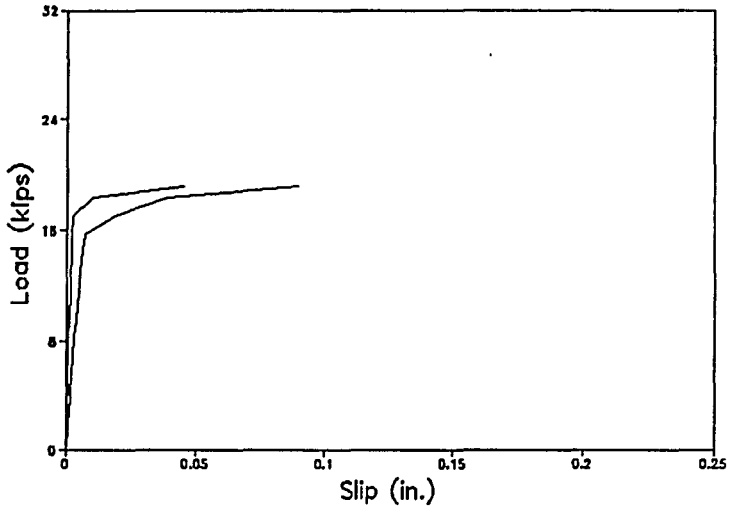

FIGURE 18, Load-slip relationship of specimen 46B3B2

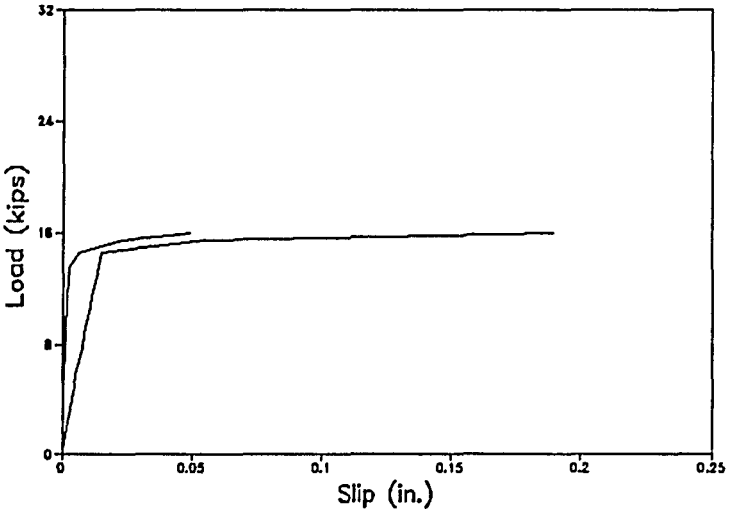

FIGURE 19, Load-slip relationship of specimen 46B3T2

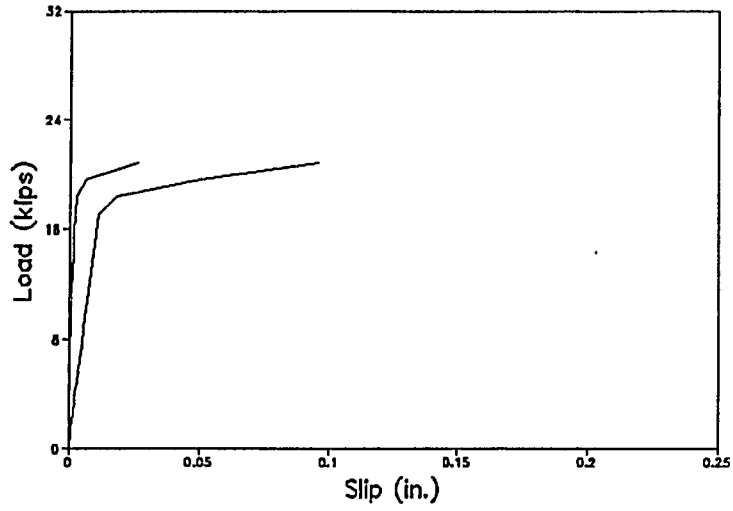

FIGURE 20, Load-slip relationship of specimen 46B6B2

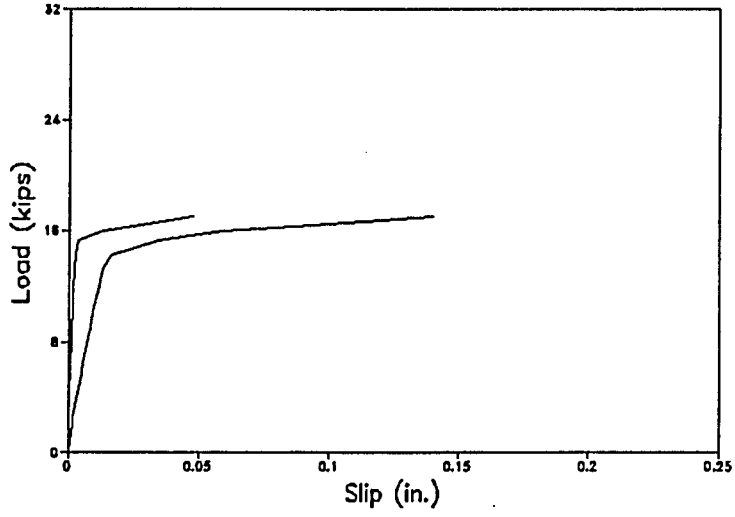

FIGURE 21, Load-slip relationship of specimen 46B6T2

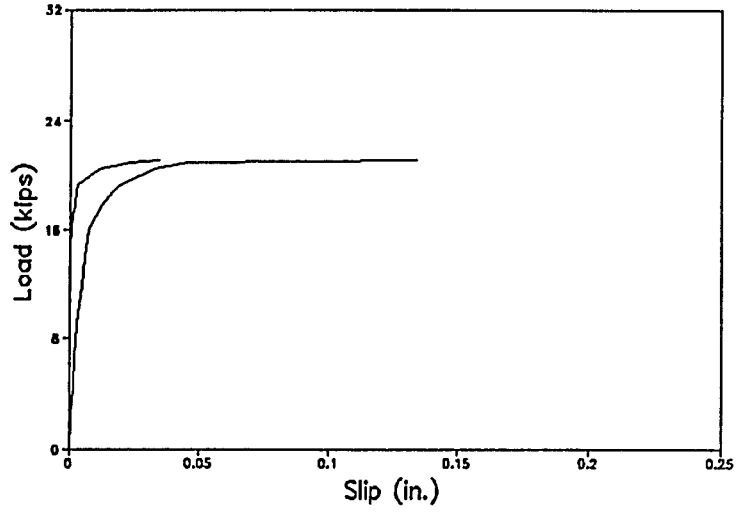

FIGURE 22, Load-slip relationship of specimen 46B12B2

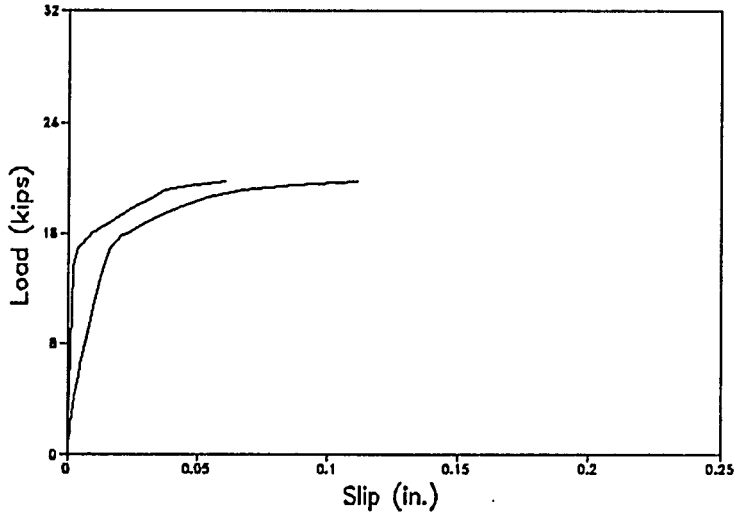

FIGURE 23, Load-slip relationship of specimen 46B12T2

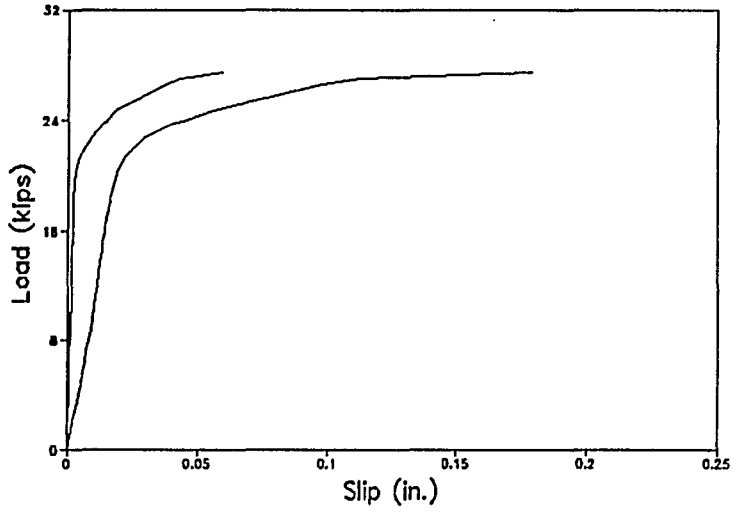

FIGURE 24, Load-slip relationship of specimen 46B16B4

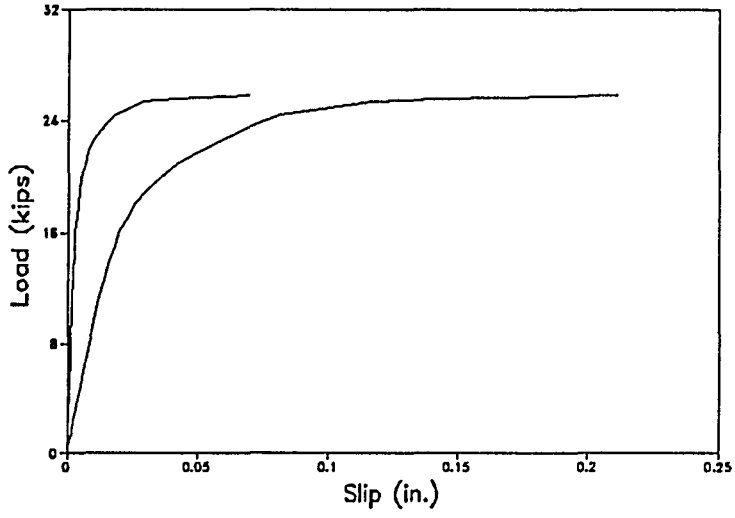

FIGURE 25, Load-slip relationship of specimen 46B16T4

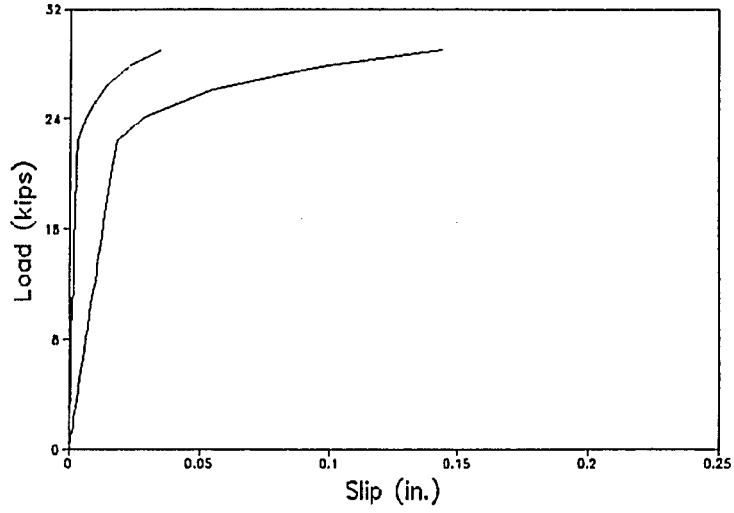

FIGURE 26, Load-slip relationship of specimen 46B18B6

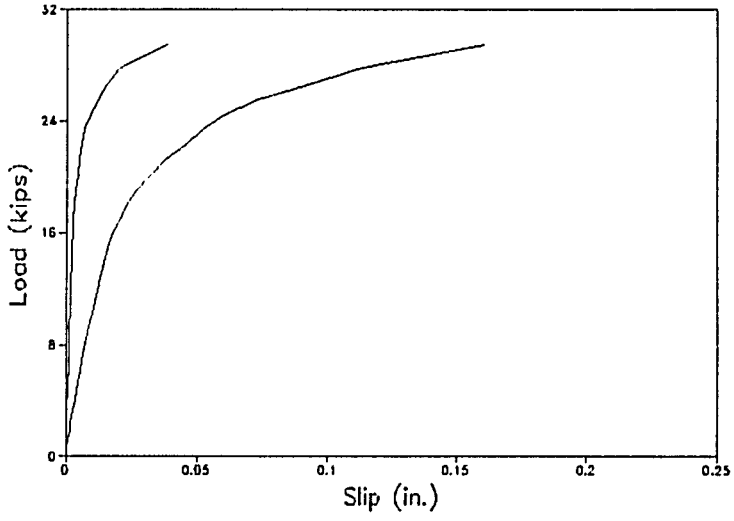

FIGURE 27, Load-slip relationship of specimen 46B18T6

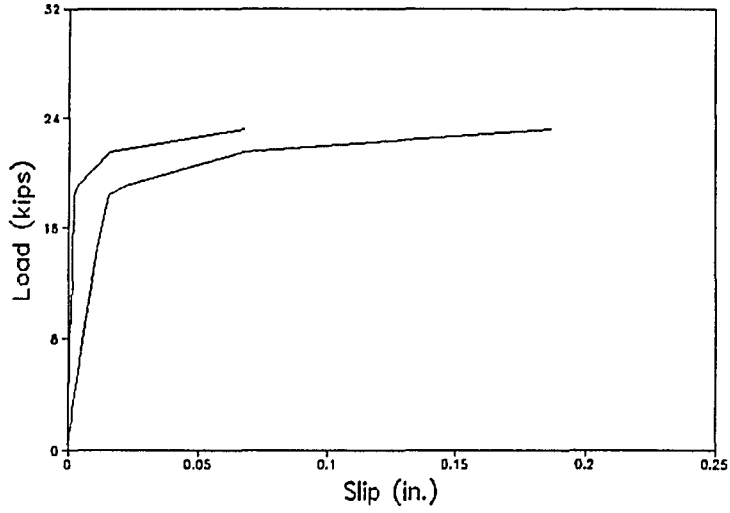

FIGURE 28, Load-slip relationship of specimen 86B12B2

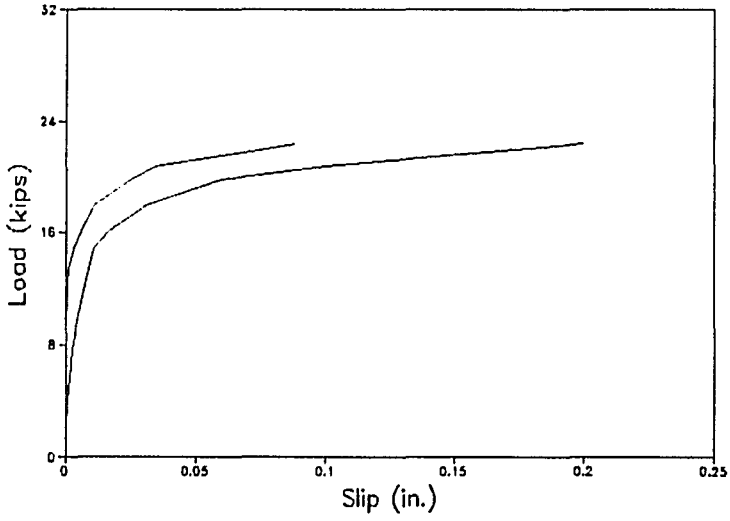

FIGURE 29, Load-slip relationship of specimen 86B12T2

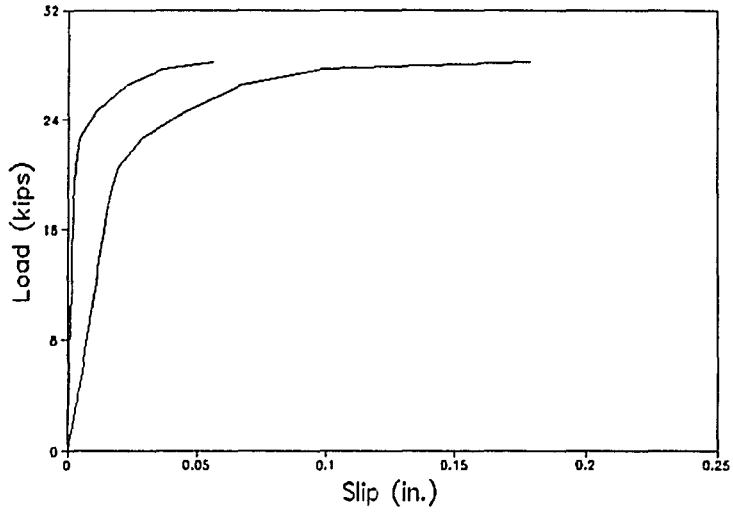

FIGURE 30, Load-slip relationship of specimen 86B16B4

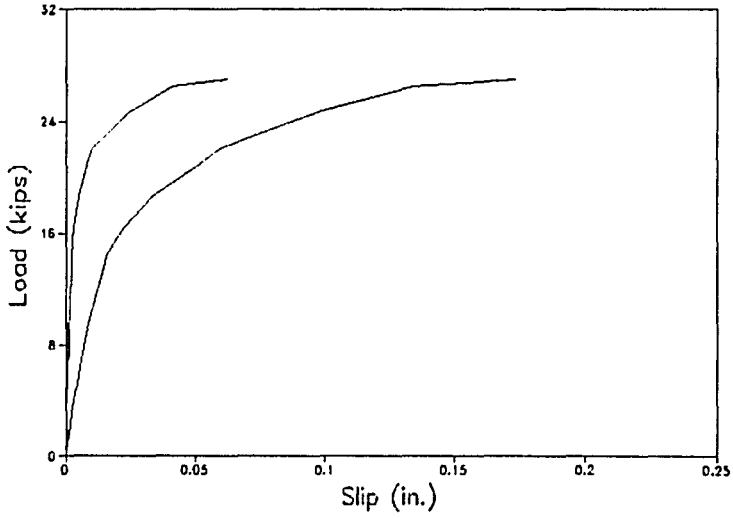

FIGURE 31, Load-slip relationship of specimen 86B16T4

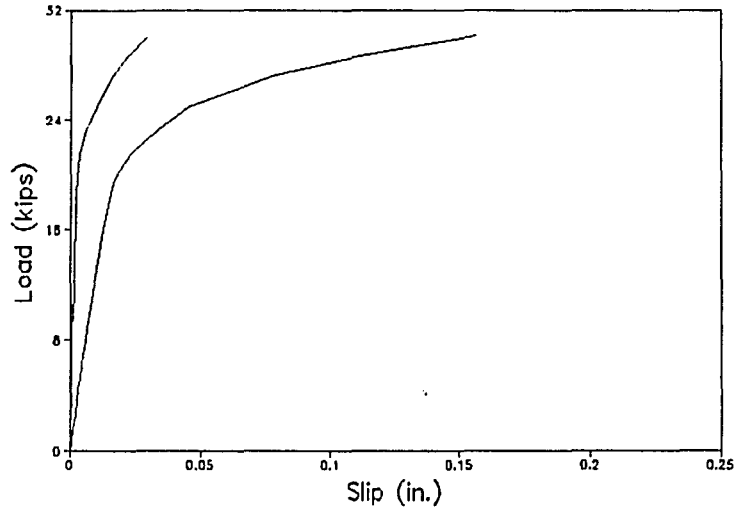

FIGURE 32, Load-slip relationship of specimen 86B18B6

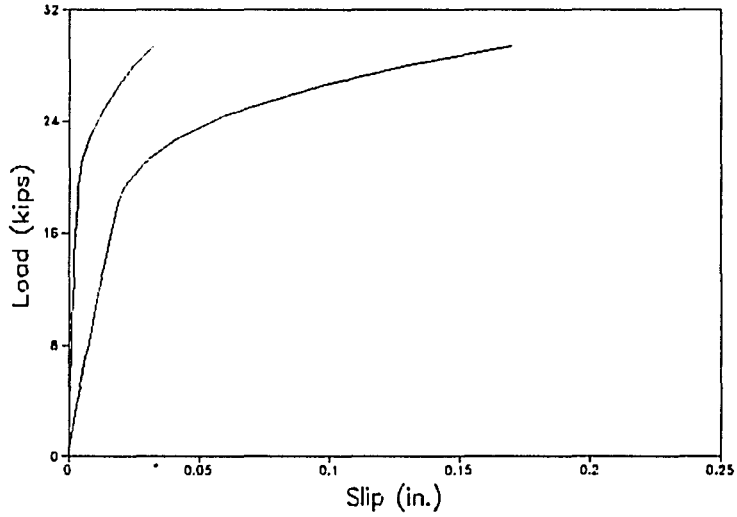

FIGURE 33, Load-slip relationship of specimen 86B18T6

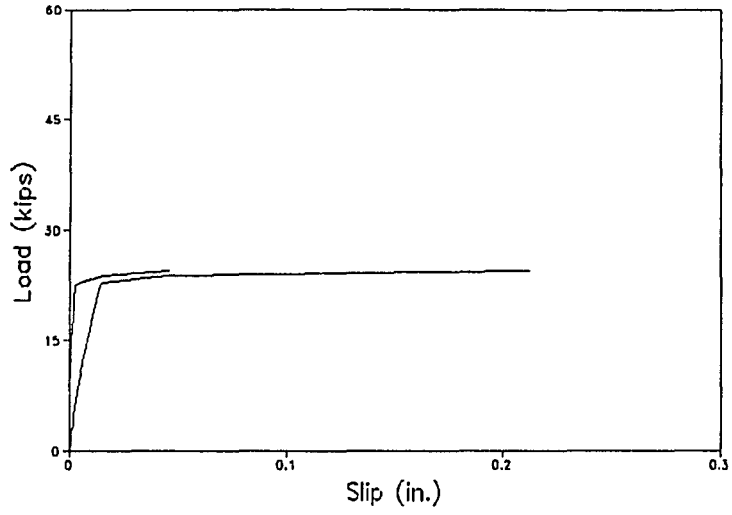

FIGURE 34, Load-slip relationship of specimen 49B4B1

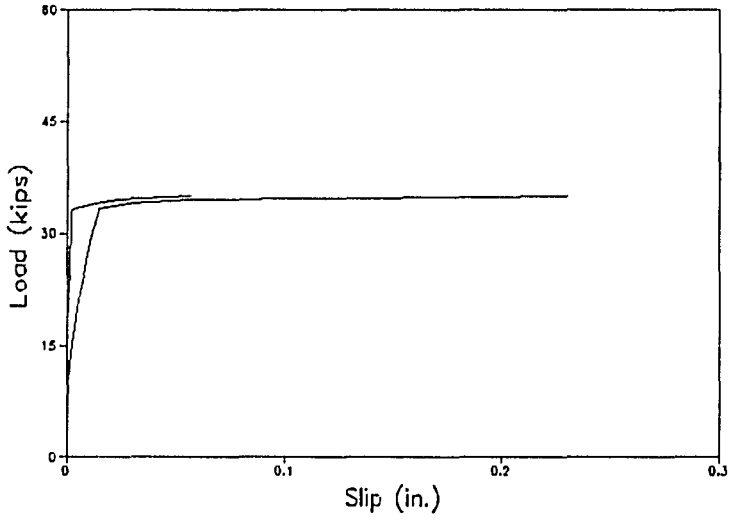

FIGURE 35, Load-slip relationship of specimen 49B4B2

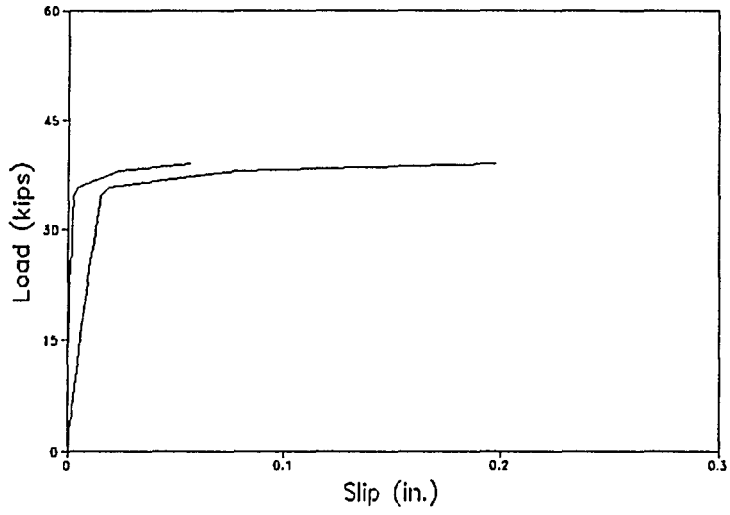

FIGURE 36, Load-slip relationship of specimen 49B8B2

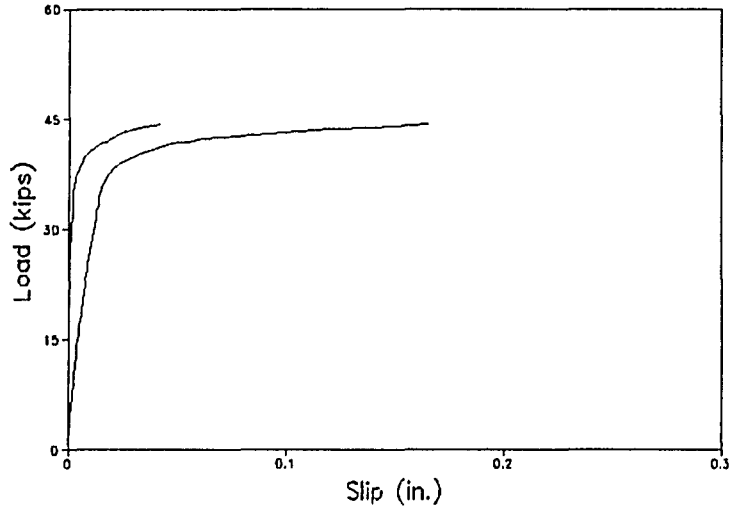

FIGURE 37, Load-slip relationship of specimen 49B22B2

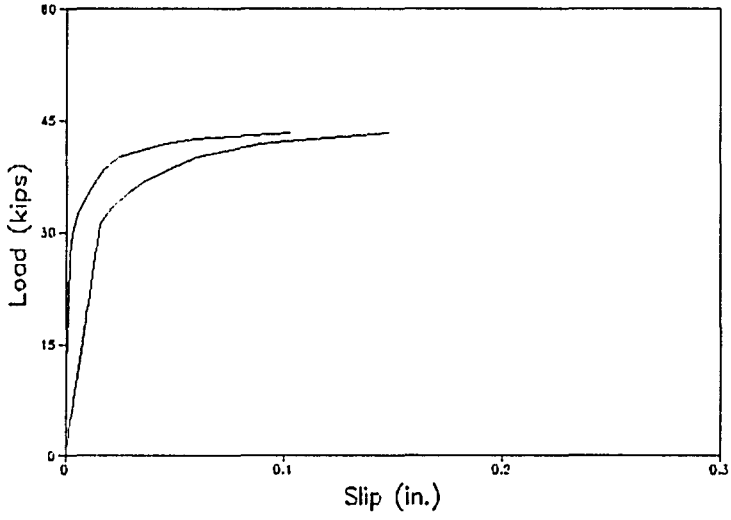

FIGURE 38, Load-slip relationship of specimen 49B22T2

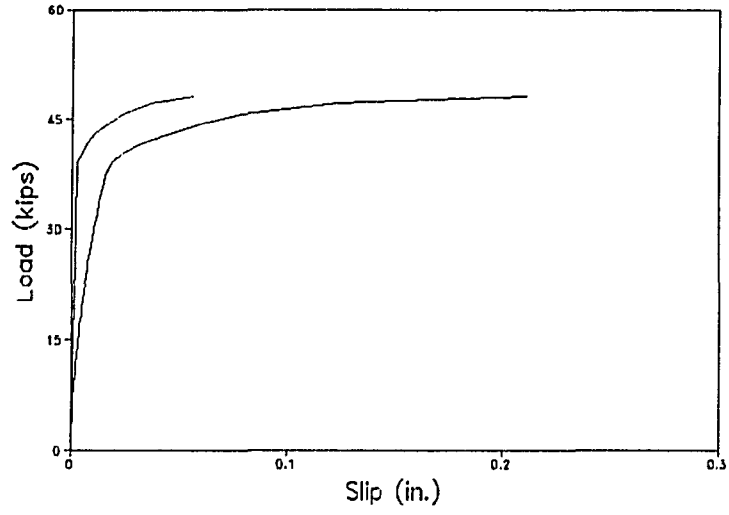

FIGURE 39, Load-slip relationship of specimen 49B26B4

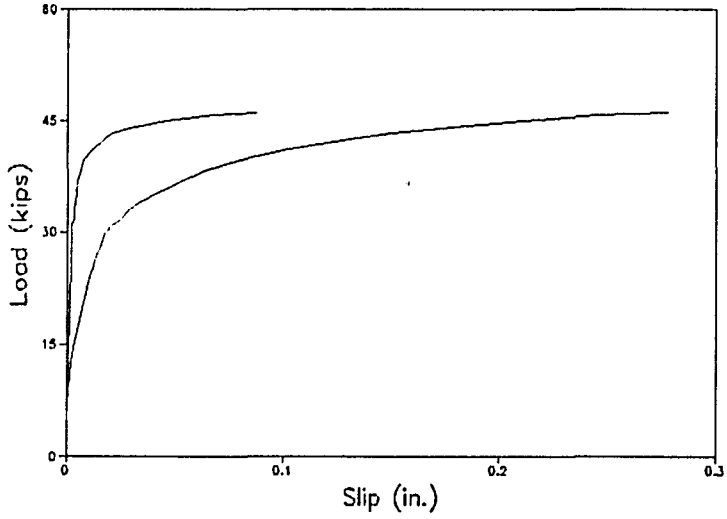

FIGURE 40, Load-slip relationship of specimen 49B26T4

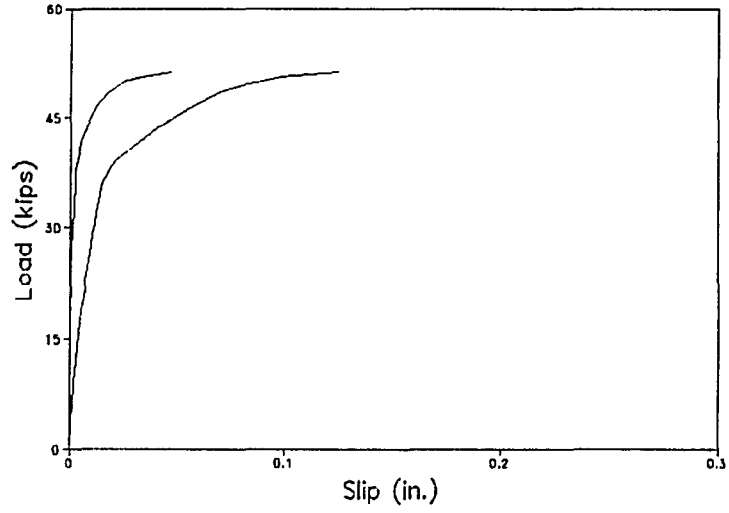

FIGURE 41, Load-slip relationship of specimen 49B30B6

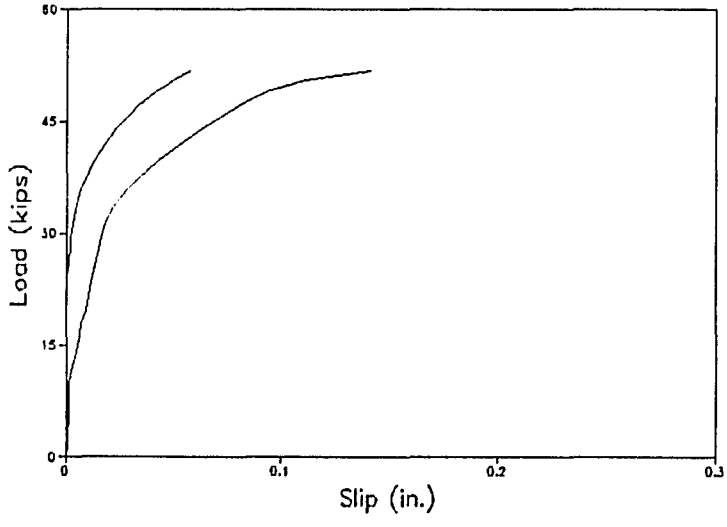

FIGURE 42, Load-slip relationship of specimen 49B30T6

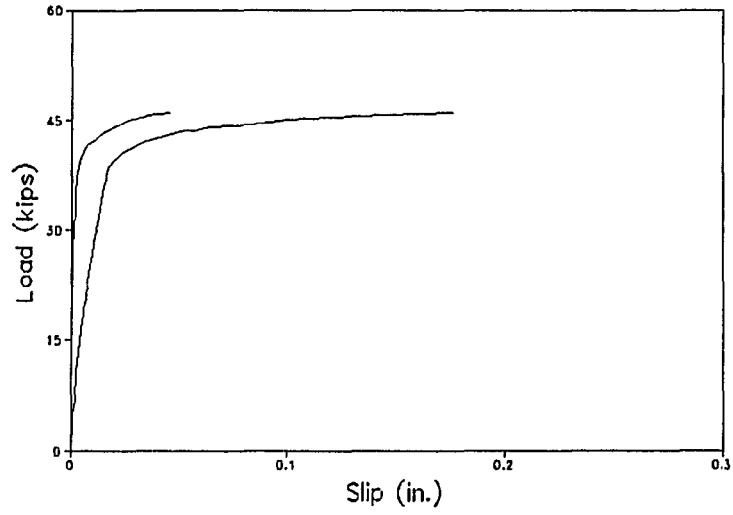

FIGURE 43, Load-slip relationship of specimen 89B22B2

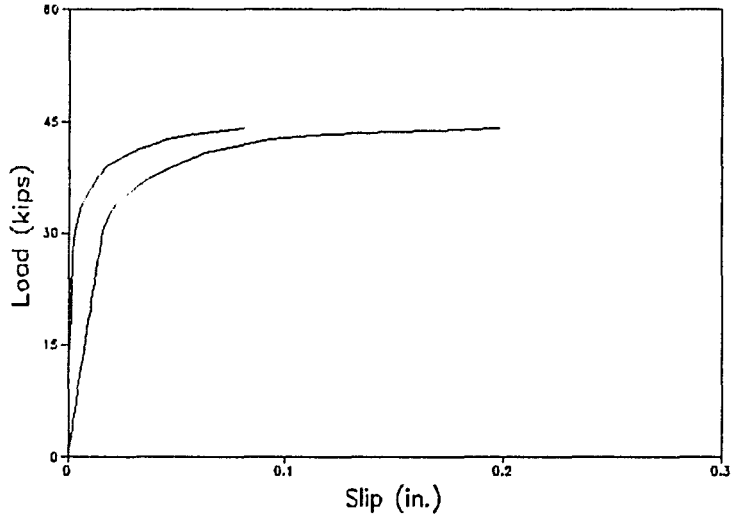

FIGURE 44, Load-slip relationship of specimen 89B22T2

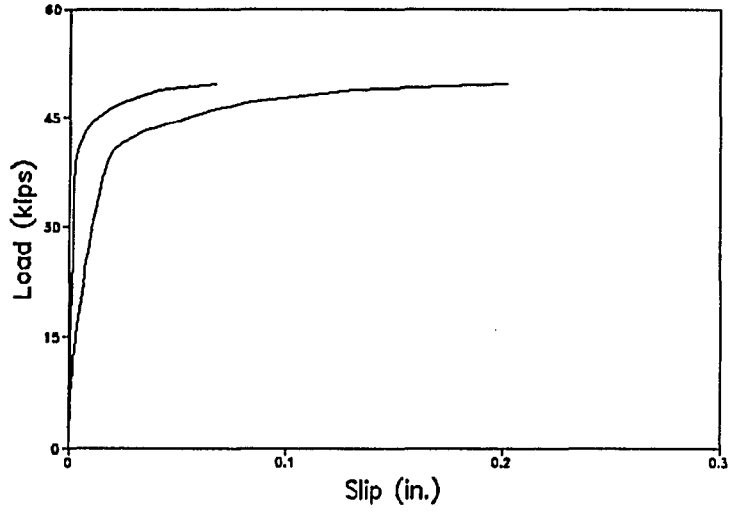

FIGURE 45, Load-slip relationship of specimen 89B26B4

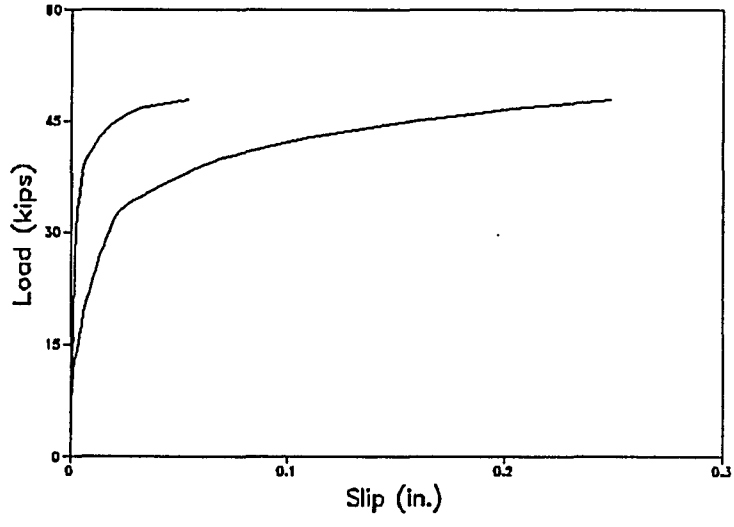

FIGURE 46, Load-slip relationship of specimen 89B26T4

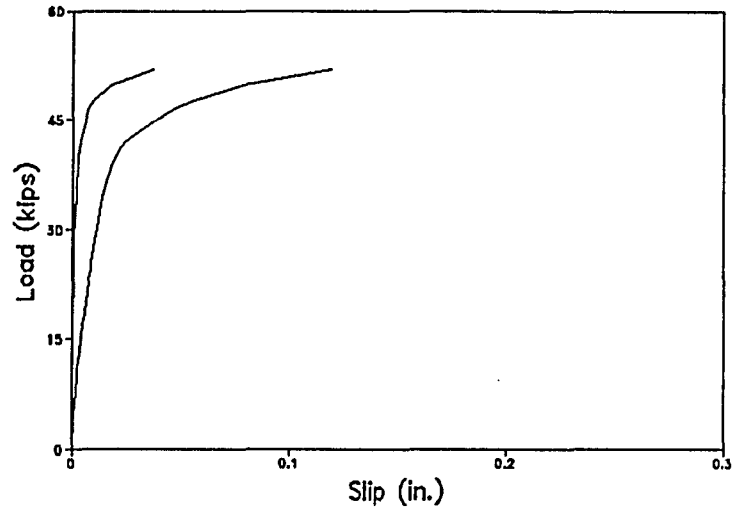

FIGURE 47, Load-slip relationship of specimen 89B30B6

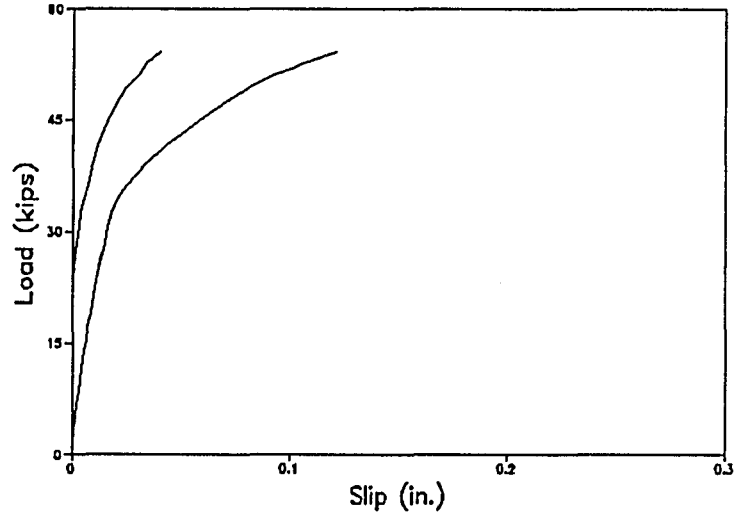

FIGURE 48, Load-slip relationship of specimen 89B30T6

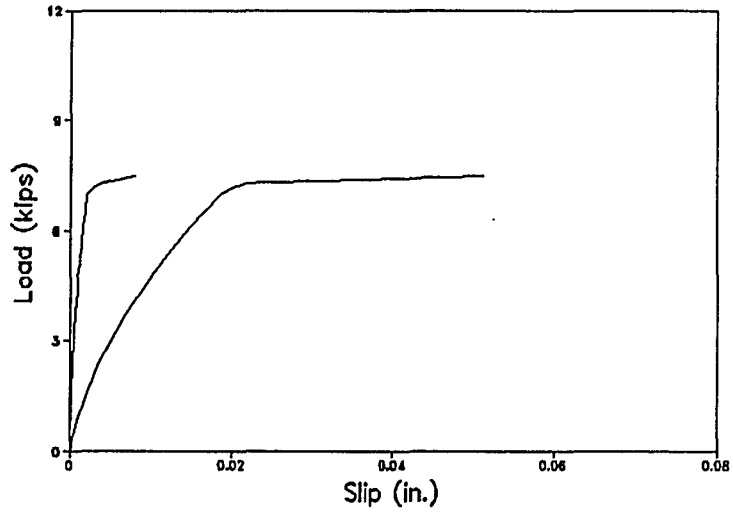

FIGURE 49, Load-slip relationship of specimen 43PB1.5

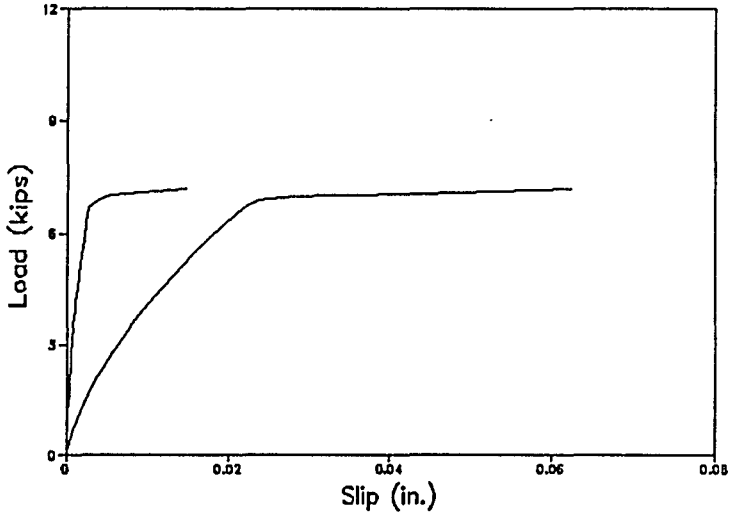

FIGURE 50, Load-slip relationship of specimen 43PM1.5

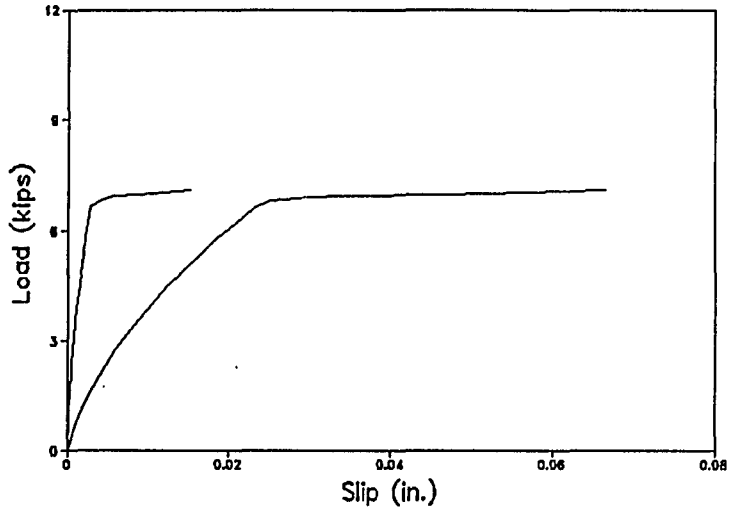

FIGURE 51, Load-slip relationship of specimen 43PT1.5

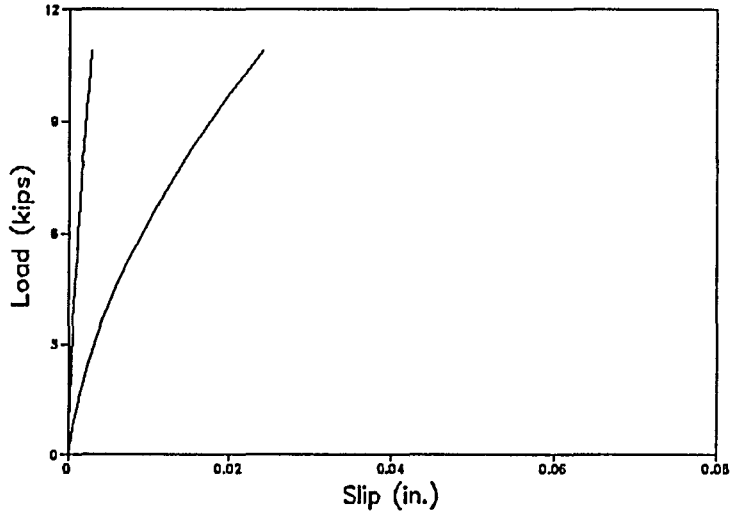

FIGURE 52, Load-slip relationship of specimen 83PB6

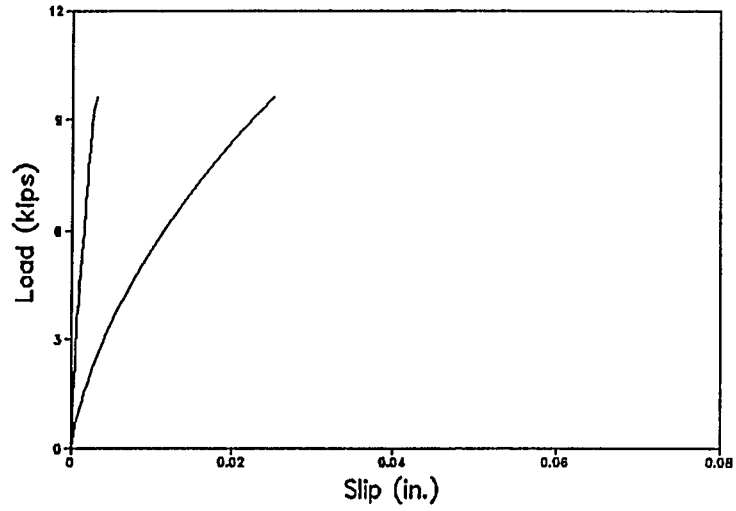

FIGURE 53, Load-slip relationship of specimen 83PM6

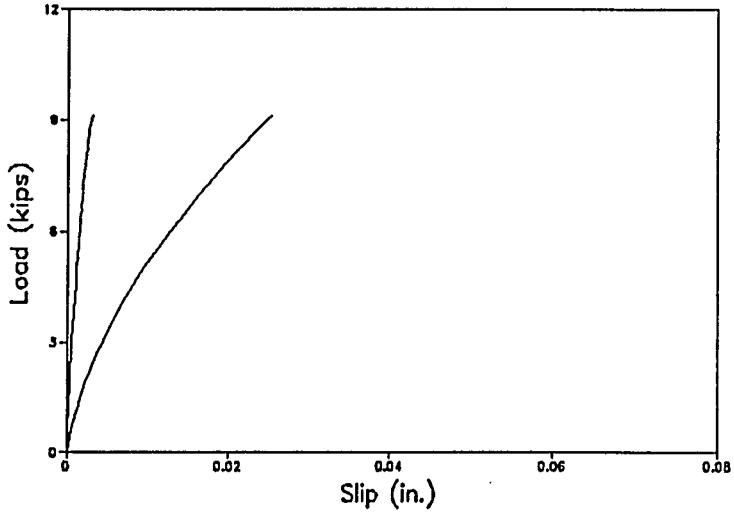

FIGURE 54, Load-slip relationship of specimen 83PT6

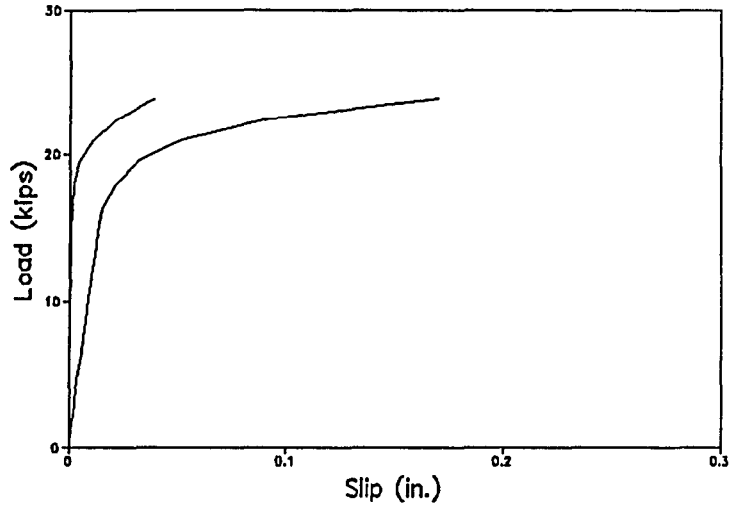

FIGURE 55, Load-slip relationship of specimen 46PB6

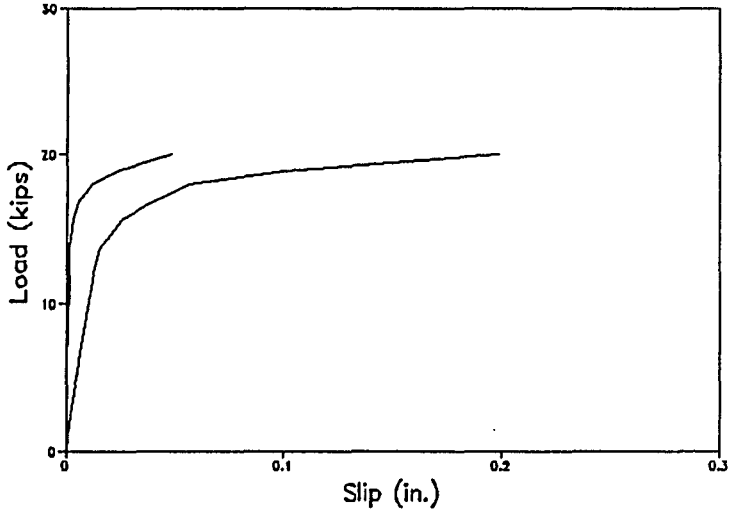

FIGURE 56, Load-slip relationship of specimen 46PM6

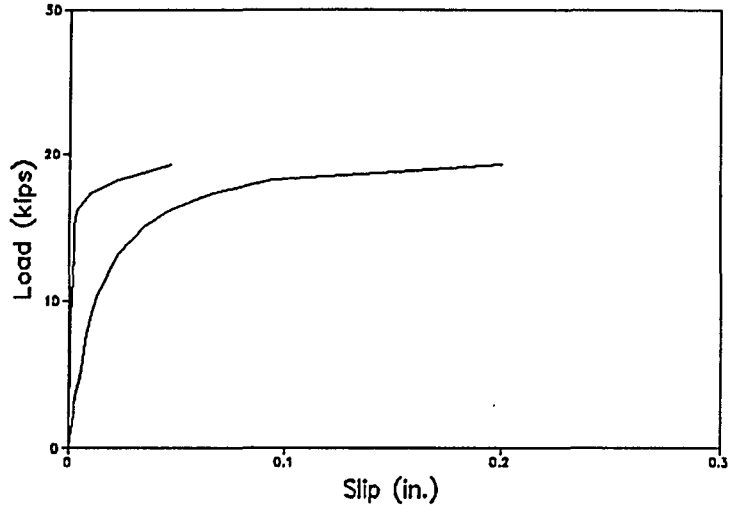

FIGURE 57, Load-slip relationship of specimen 46PT6

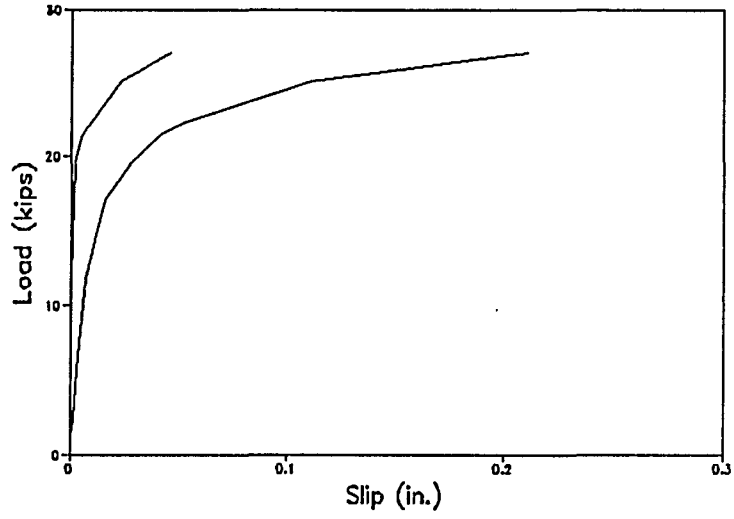

FIGURE 58, Load-slip relationship of specimen 86PB12

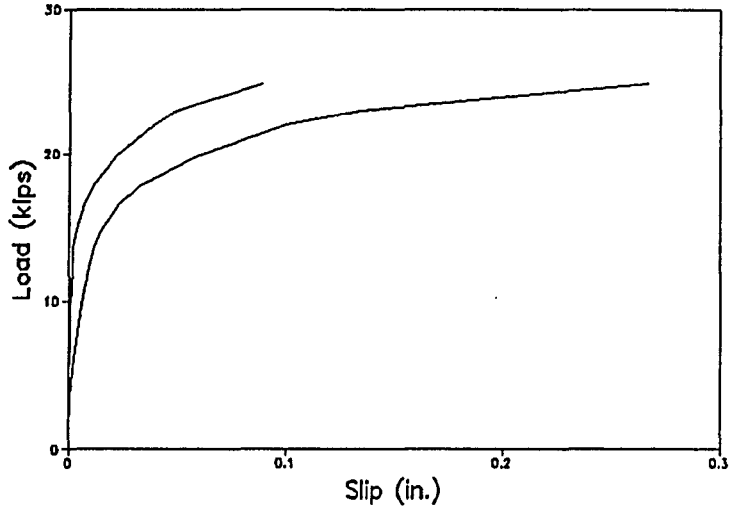

FIGURE 59, Load-slip relationship of specimen 86PM12

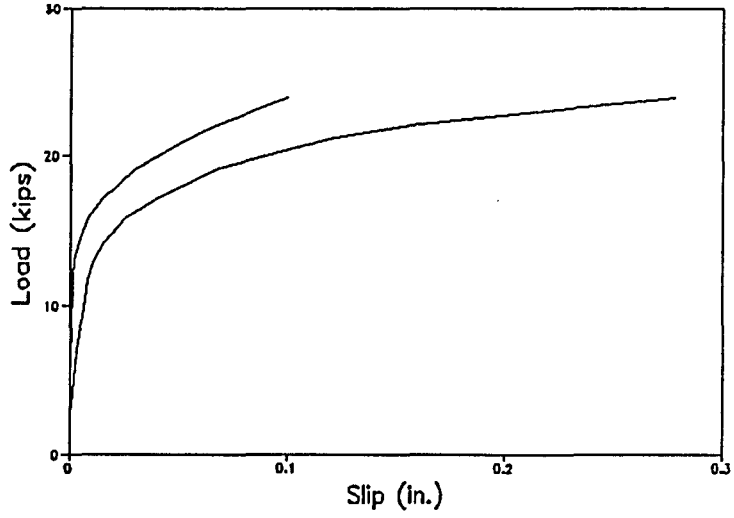

FIGURE 60, Load-slip relationship of specimen 86PT12

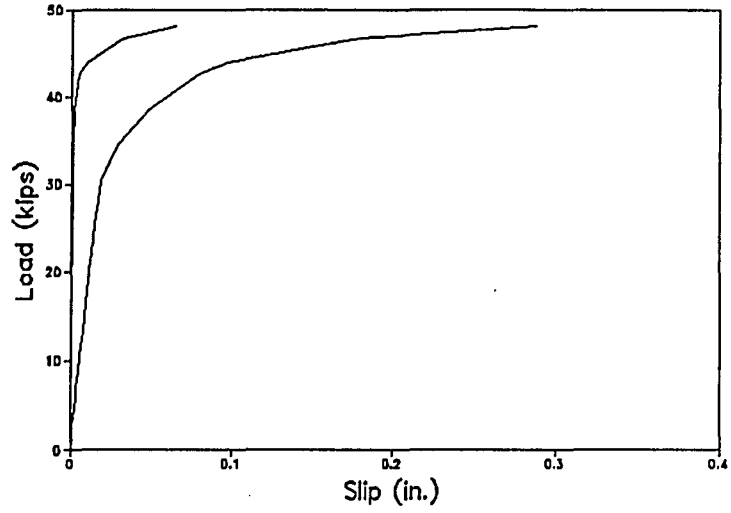

FIGURE 61, Load-slip relationship of specimen 49PB8

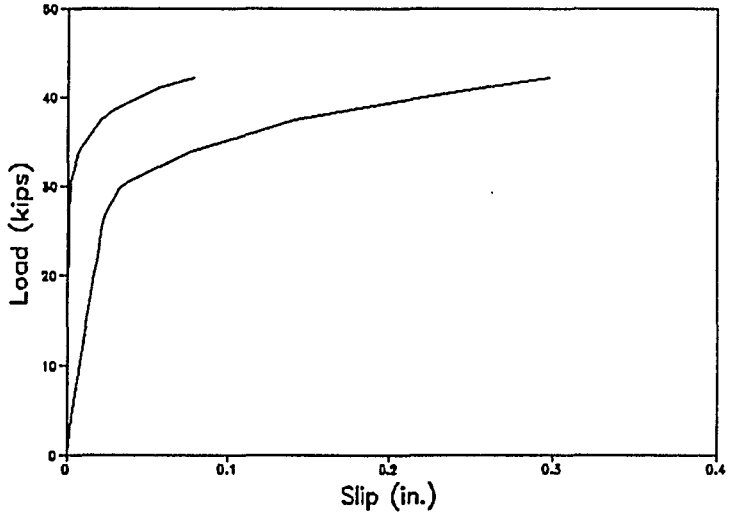

FIGURE 62, Load-slip relationship of specimen 49PM8

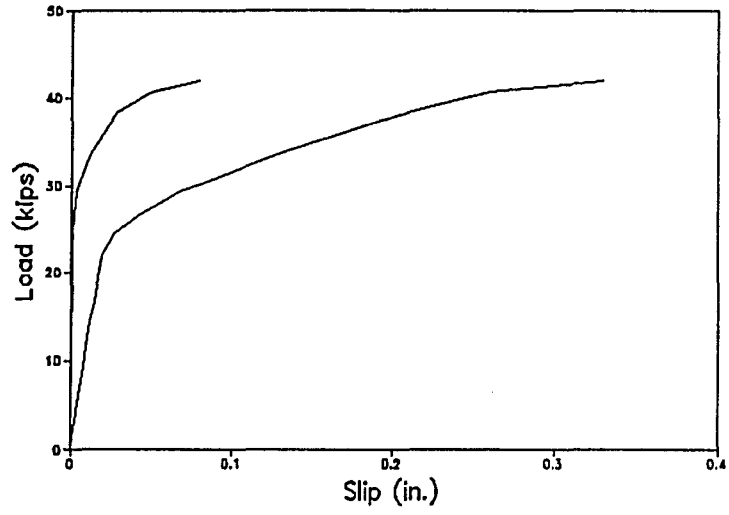

FIGURE 63, Load-slip relationship of specimen 49PT8

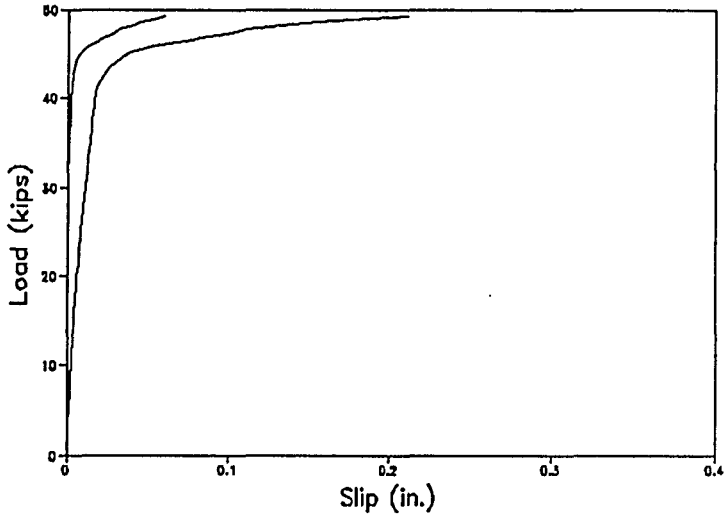

FIGURE 64, Load-slip relationship of specimen 89PB22

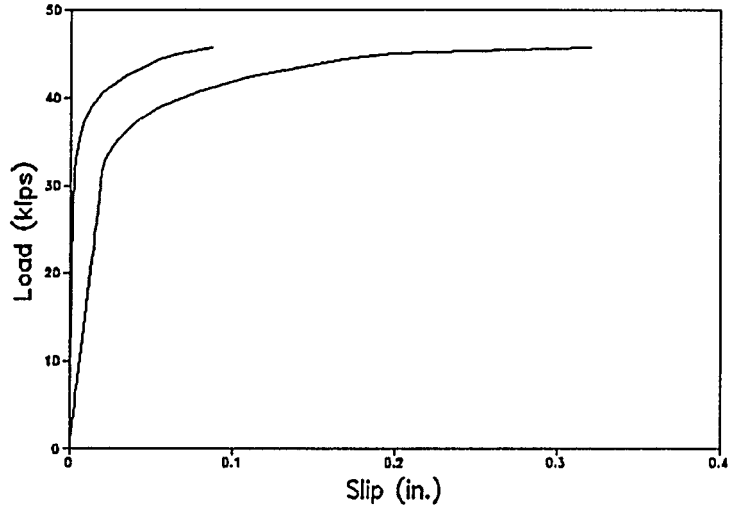

FIGURE 65, Load-slip relationship of specimen 89PM22

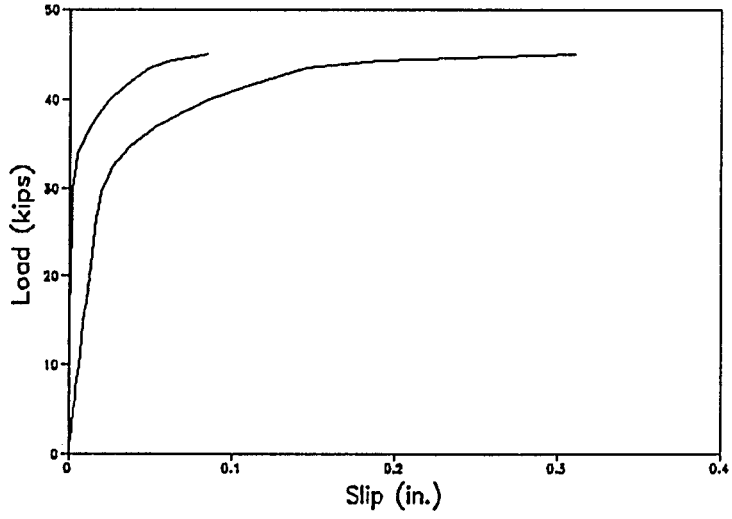

FIGURE 66, Load-slip relationship of specimen 89PT22

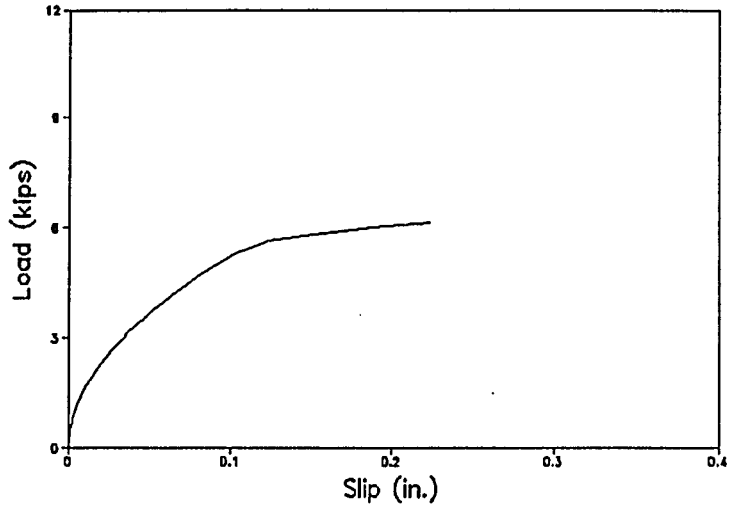

FIGURE 67, Load-slip relationship of specimen 43H3124

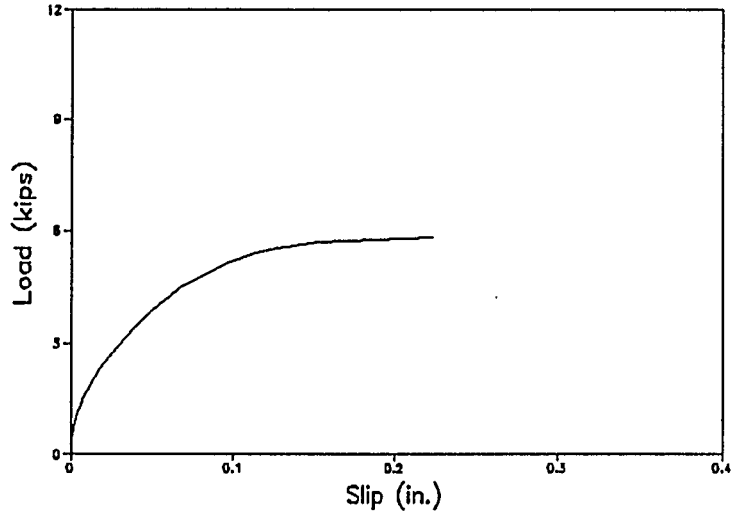

FIGURE 68, Load-slip relationship of specimen 43H3204

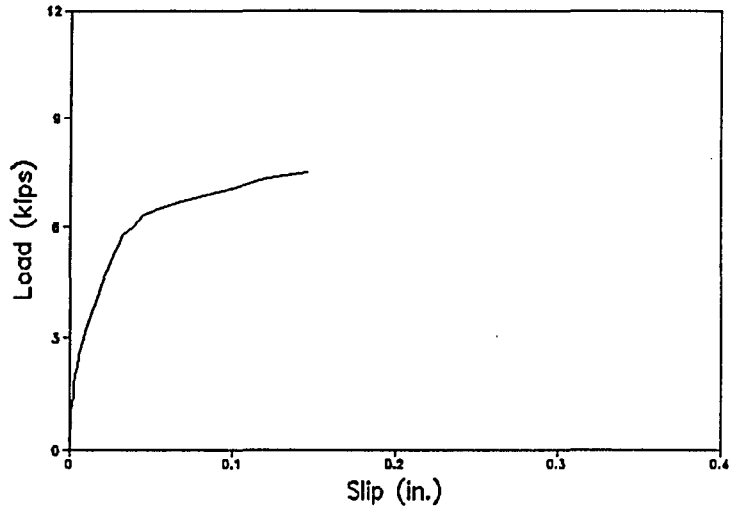

FIGURE 69, Load-slip relationship of specimen 43H3127

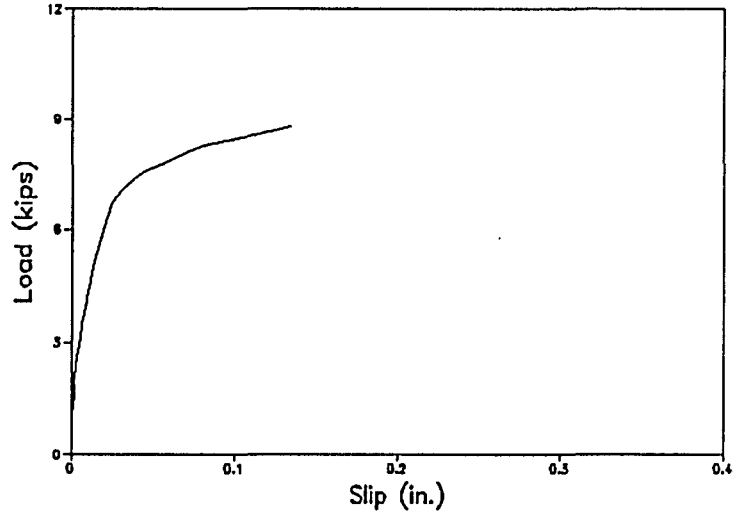

FIGURE 70, Load-slip relationship of specimen 43H31210

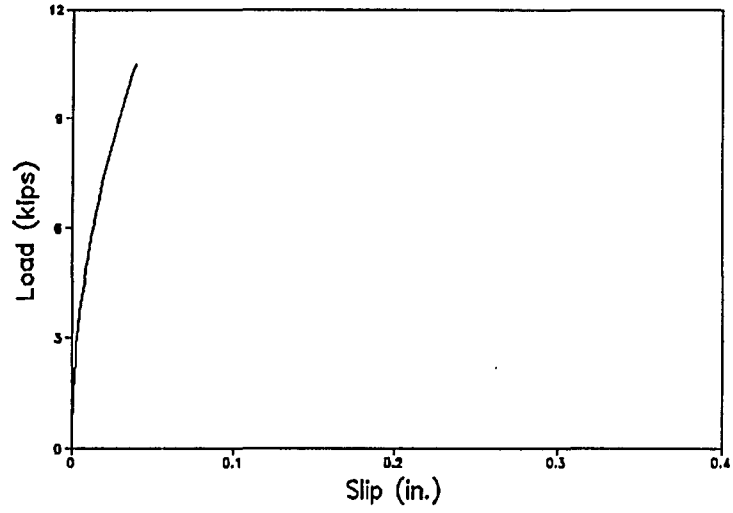

FIGURE 71, Load-slip relationship of specimen 43H31213

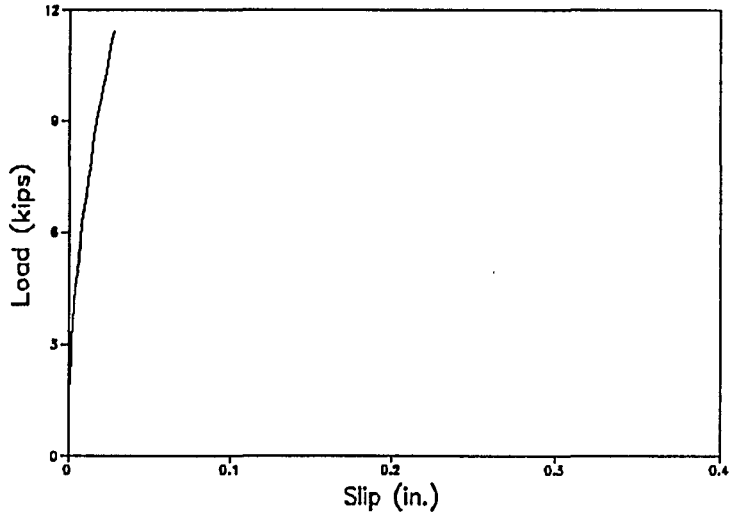

FIGURE 72, Load-slip relationship of specimen 43H31216

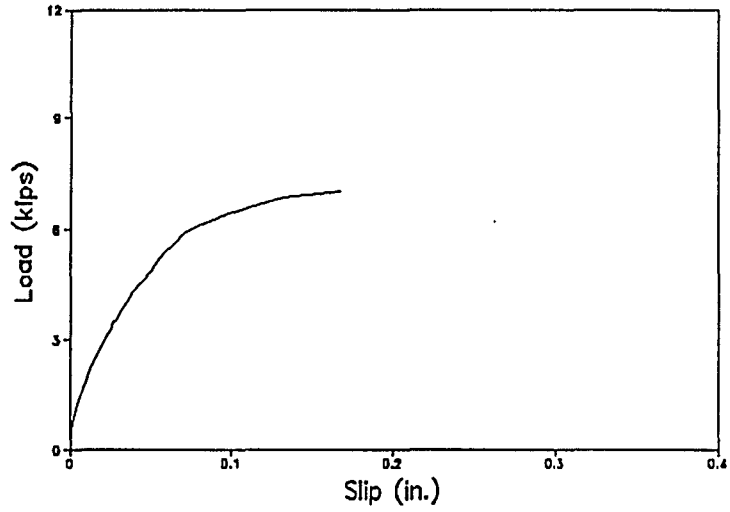

FIGURE 73, Load-slip relationship of specimen 83H3124

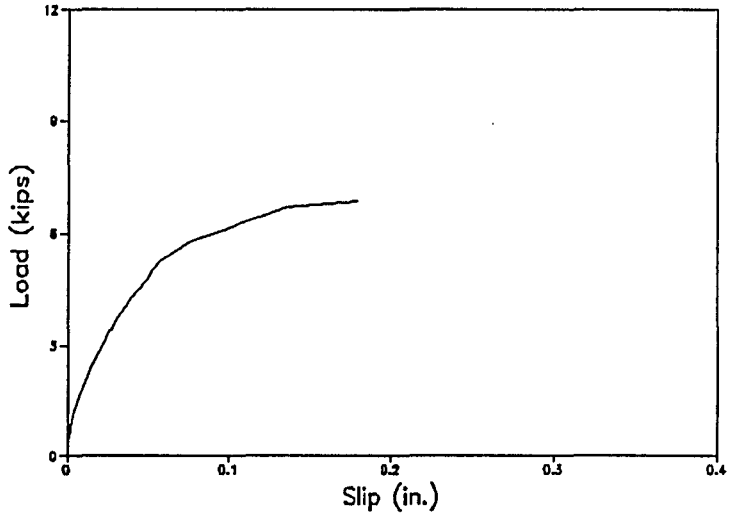

FIGURE 74, Load-slip relationship of specimen 83H3204

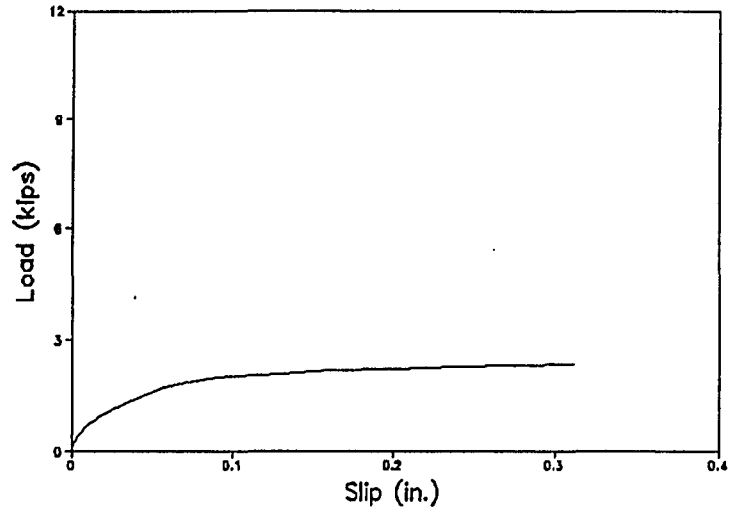

FIGURE 75, Load-slip relationship of specimen 43H0121

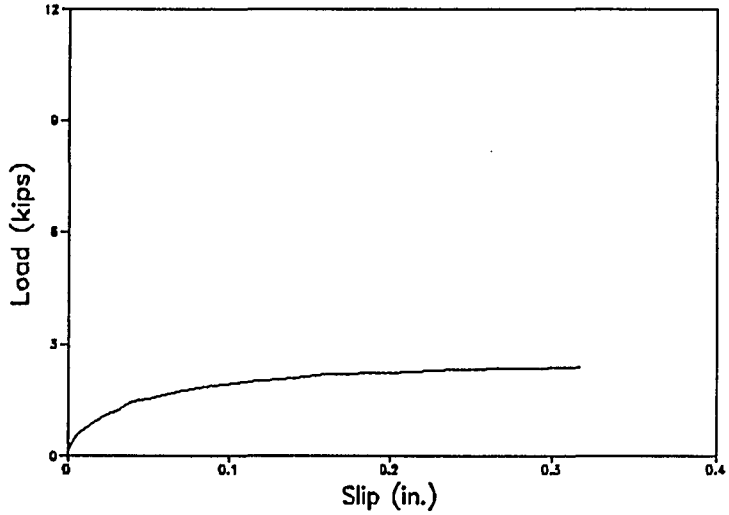

FIGURE 76, Load-slip relationship of specimen 43H0201

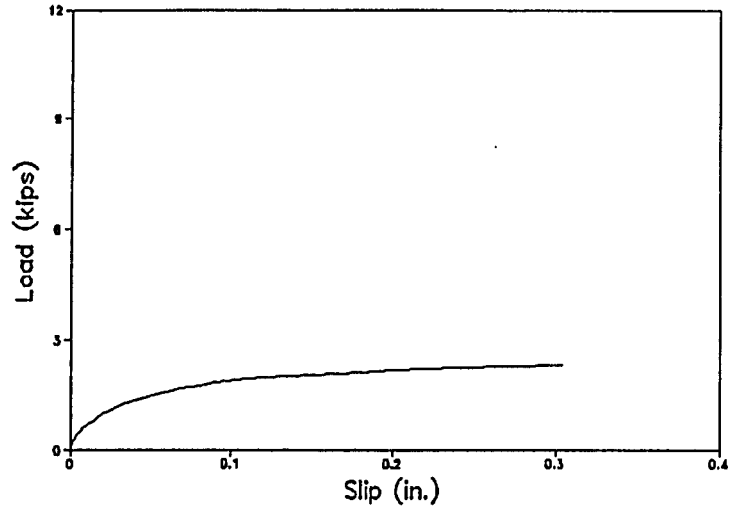

FIGURE 77, Load-slip relationship of specimen 83H0121

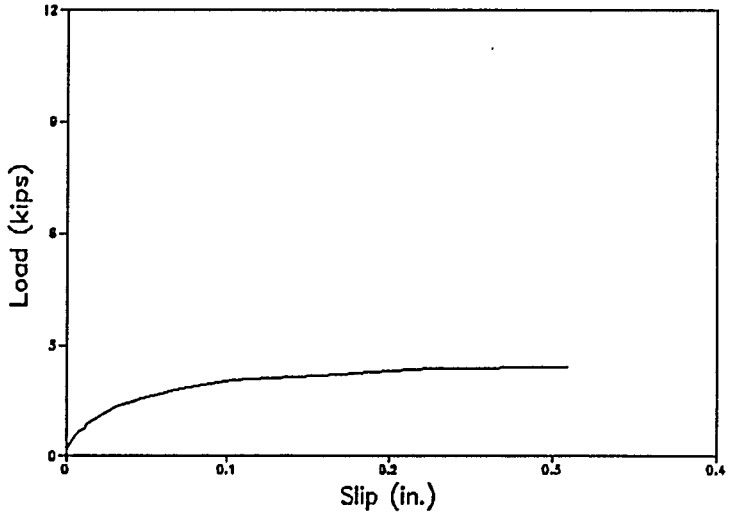

FIGURE 78, Load-slip relationship of specimen 83H0201

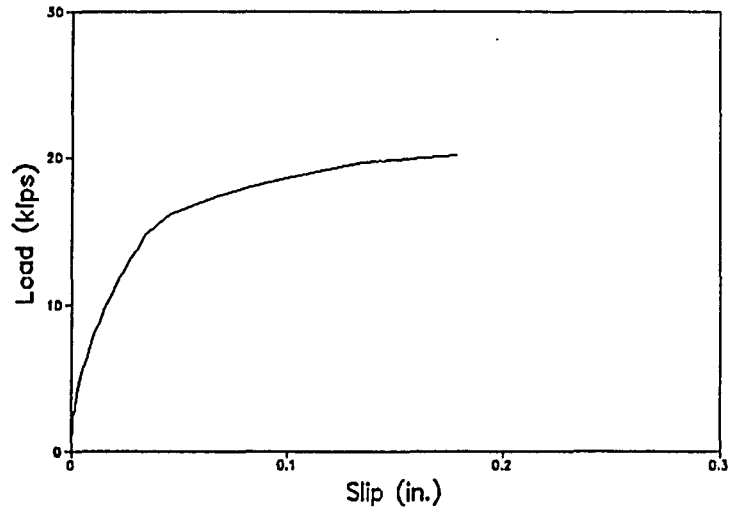

FIGURE 79, Load-slip relationship of specimen 46H3124

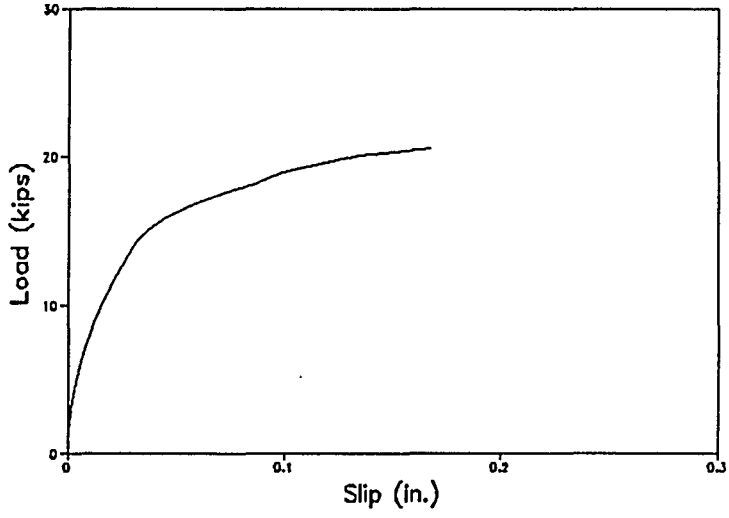

FIGURE 80, Load-slip relationship of specimen 46H3204

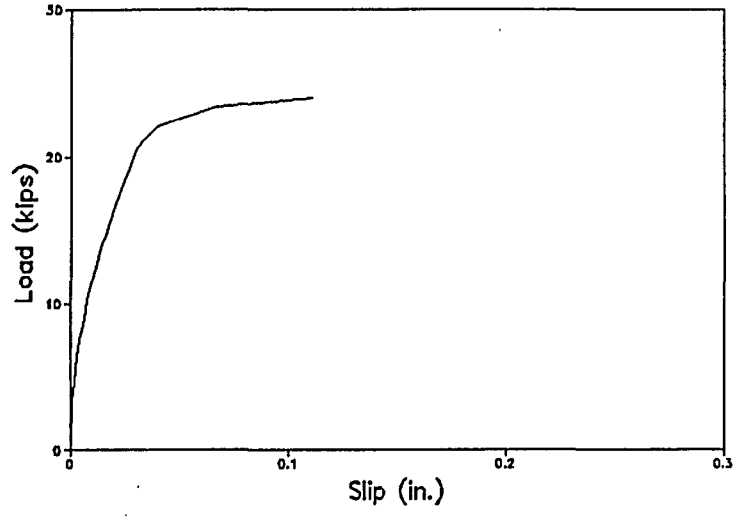

FIGURE 81, Load-slip relationship of specimen 46H3127

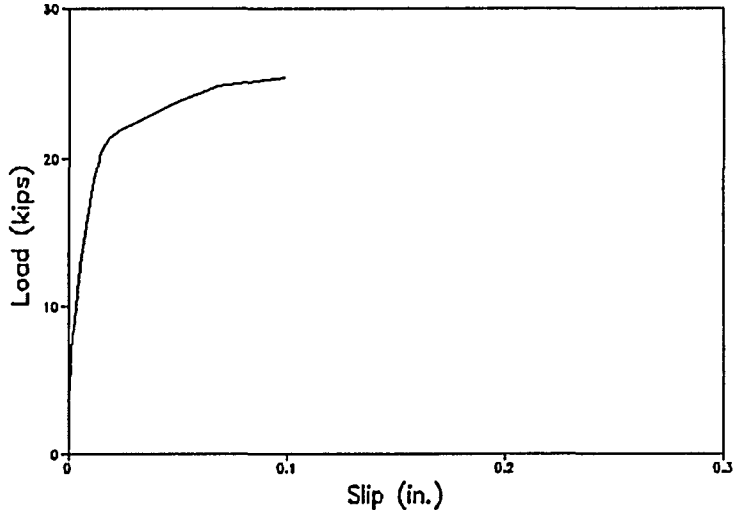

FIGURE 82, Load-slip relationship of specimen 46H31210

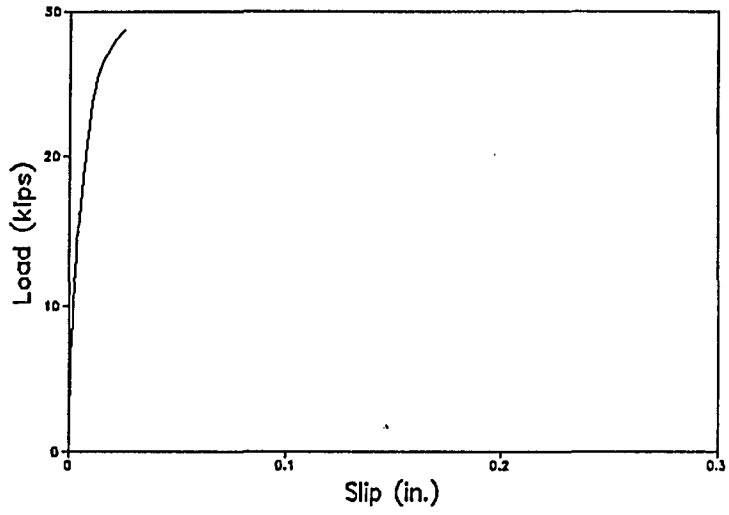

FIGURE 83, Load-slip relationship of specimen 46H31213

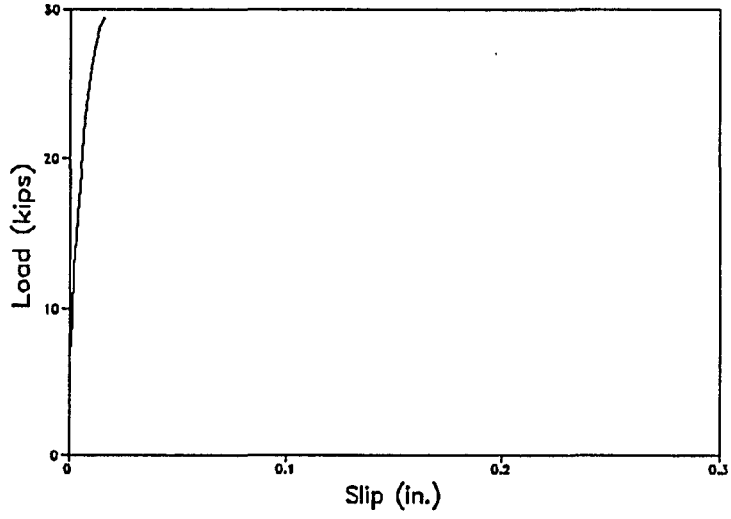

FIGURE 84, Load-slip relationship of specimen 46H31216

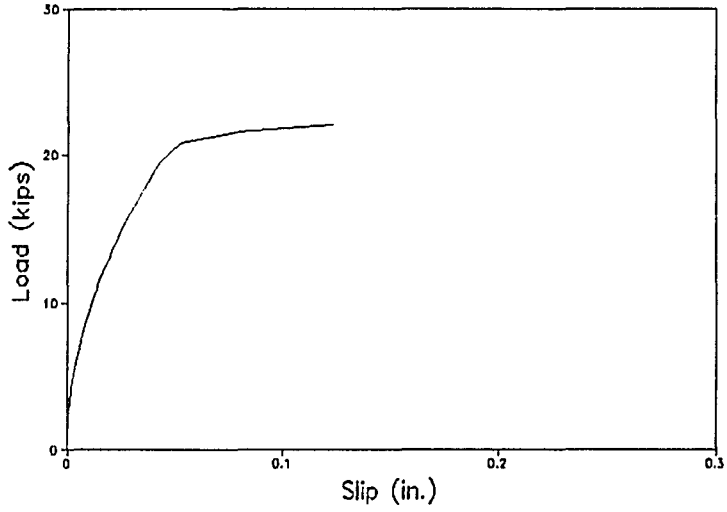

FIGURE 85, Load-slip relationship of specimen 86H3124

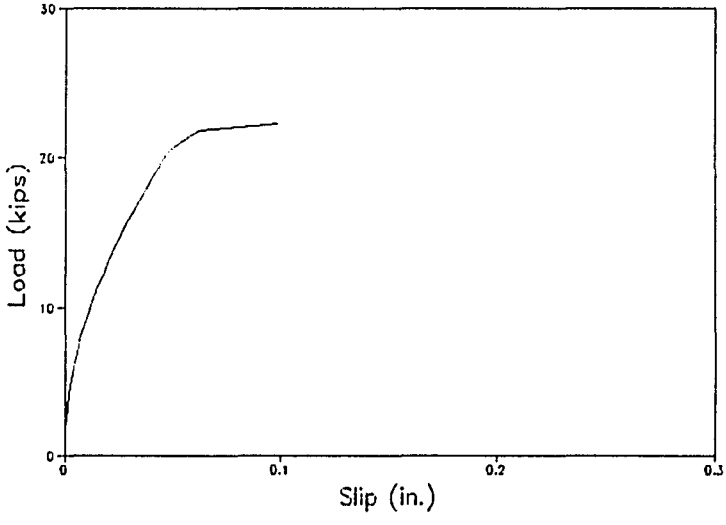

FIGURE 86, Load-slip relationship of specimen 86H3204

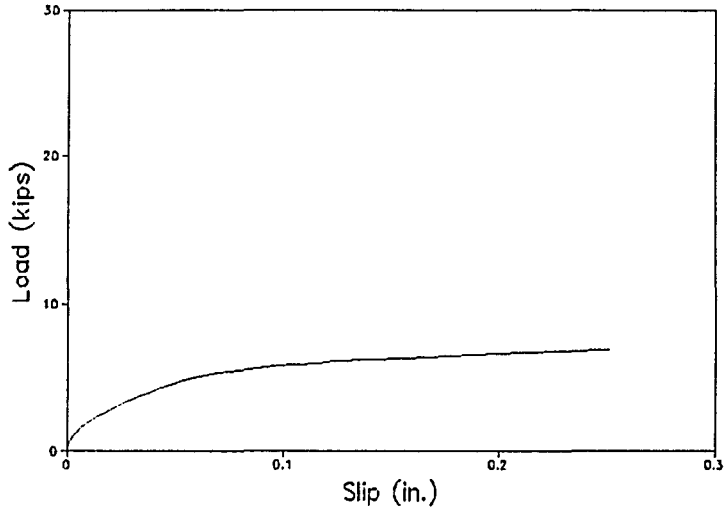

FIGURE 87, Load-slip relationship of specimen 46H0121

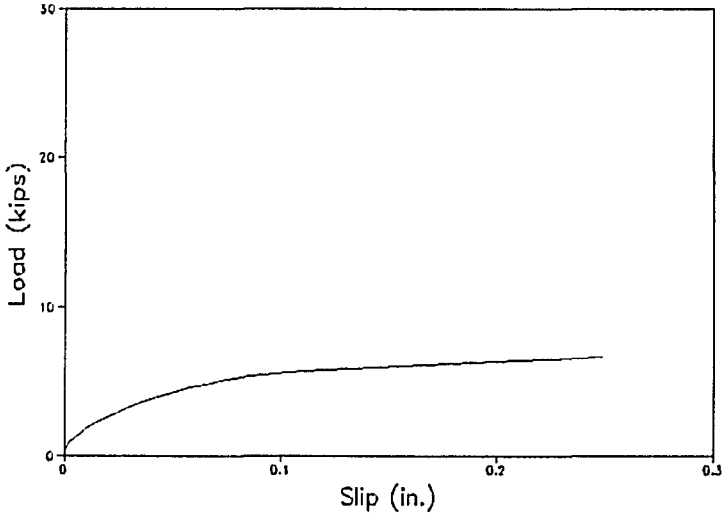

FIGURE 88, Load-slip relationship of specimen 46H0201

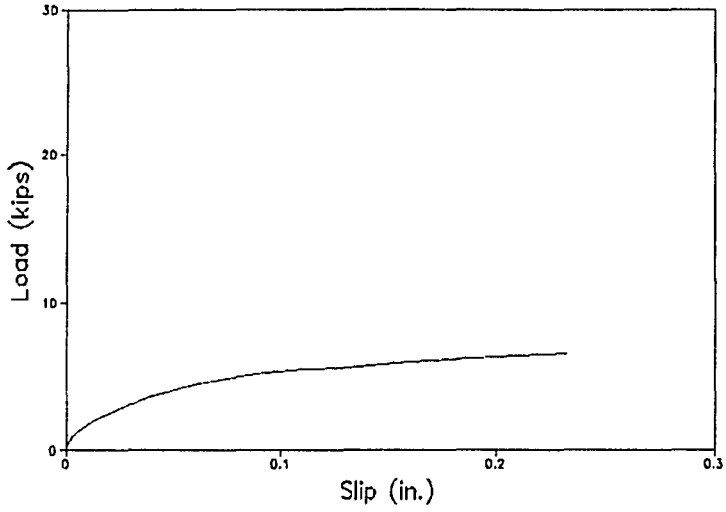

FIGURE 89, Load-slip relationship of specimen 86H0121

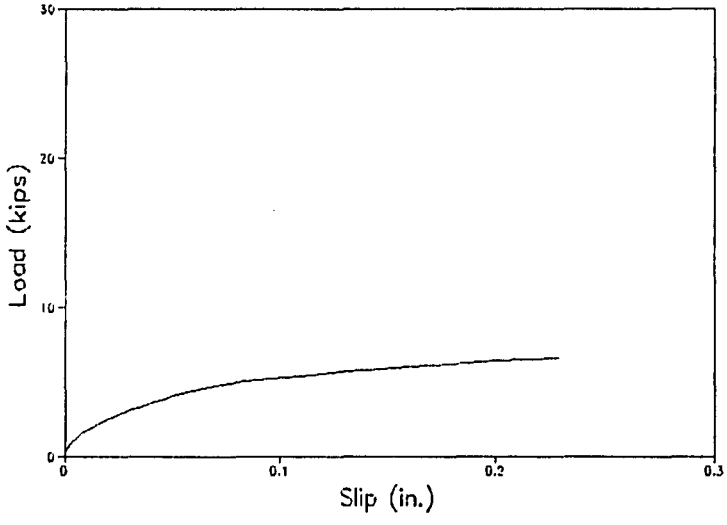

FIGURE 90, Load-slip relationship of specimen 86H0201

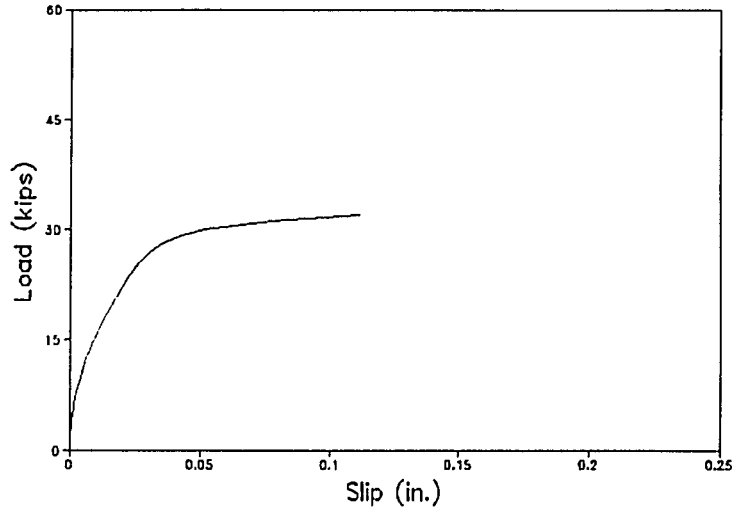

FIGURE 91, Load-slip relationship of specimen 49H3124

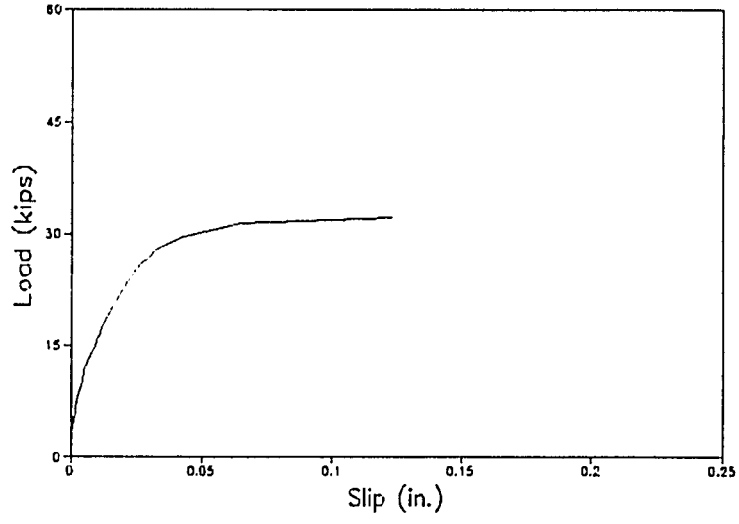

FIGURE 92, Load-slip relationship of specimen 49H3204

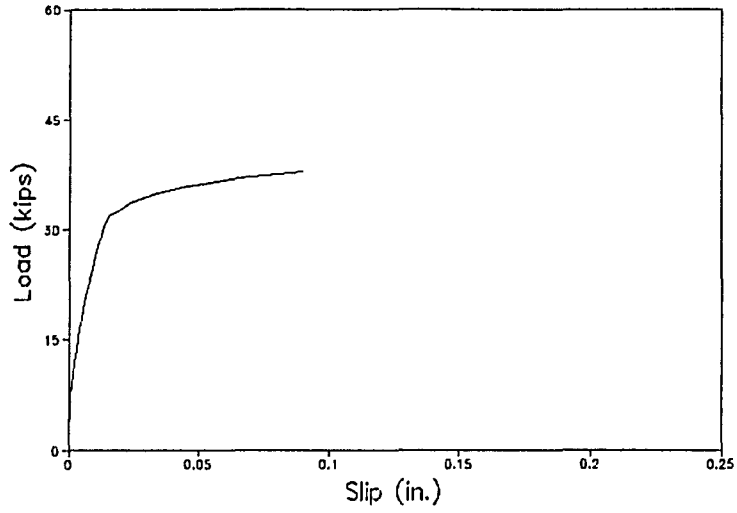

FIGURE 93, Load-slip relationship of specimen 49H3127

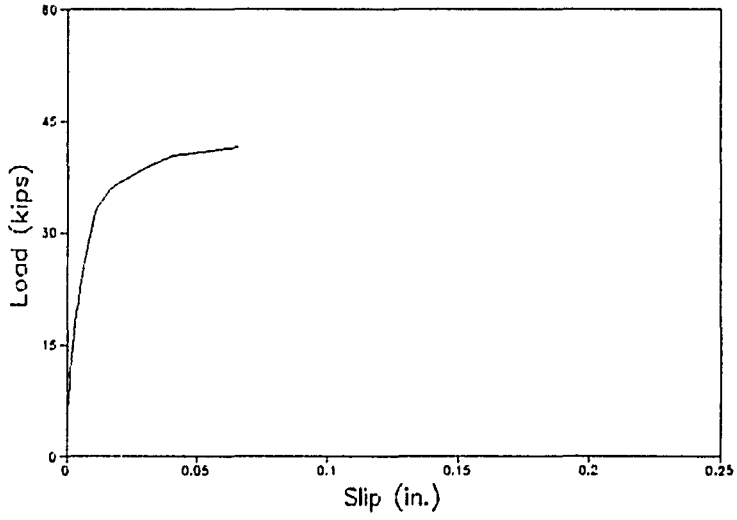

FIGURE 94, Load-slip relationship of specimen 49H31210

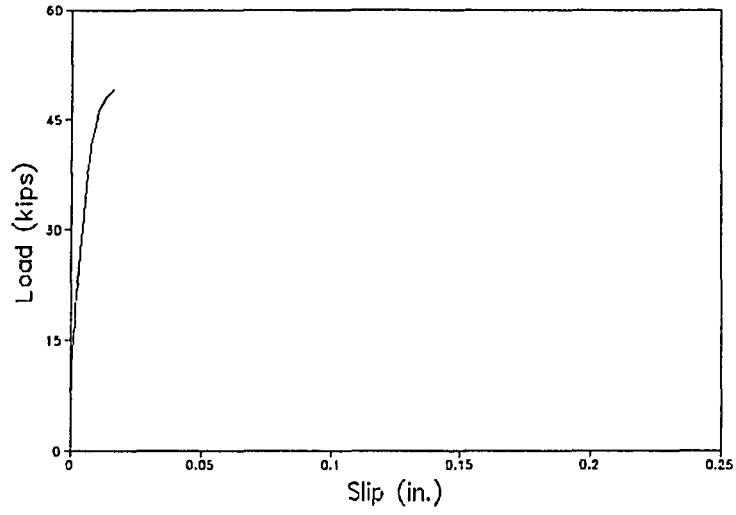

FIGURE 95, Load-slip relationship of specimen 49H31213

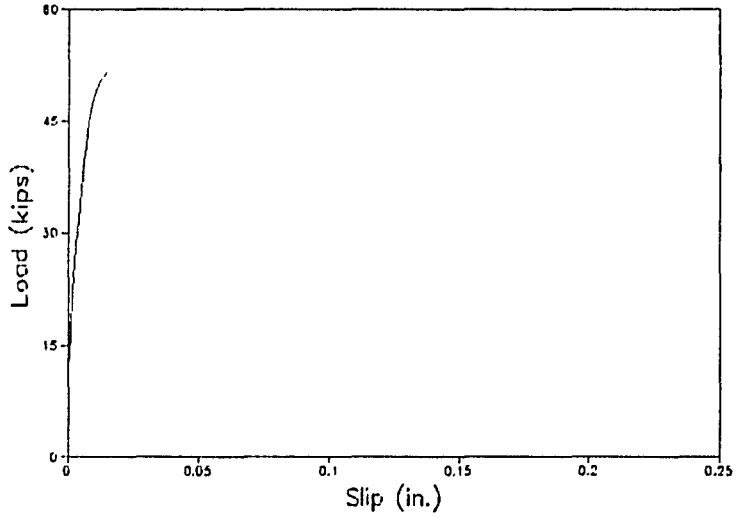

FIGURE 96, Load-slip relationship of specimen 49H31216

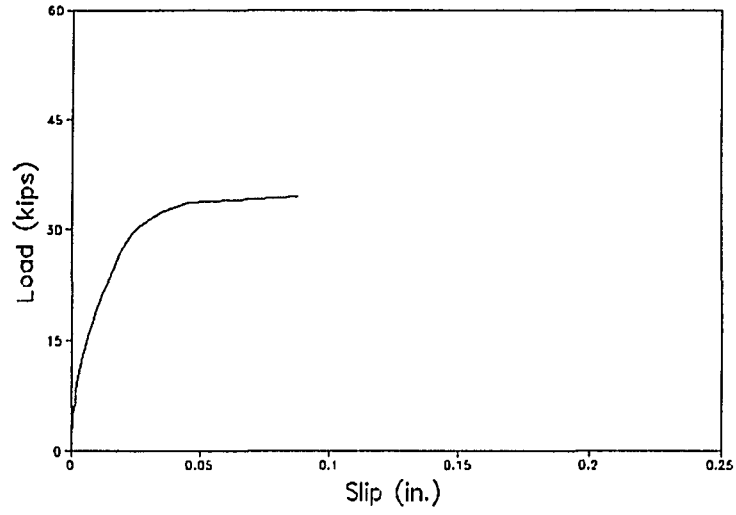

FIGURE 97, Load-slip relationship of specimen 89H3124

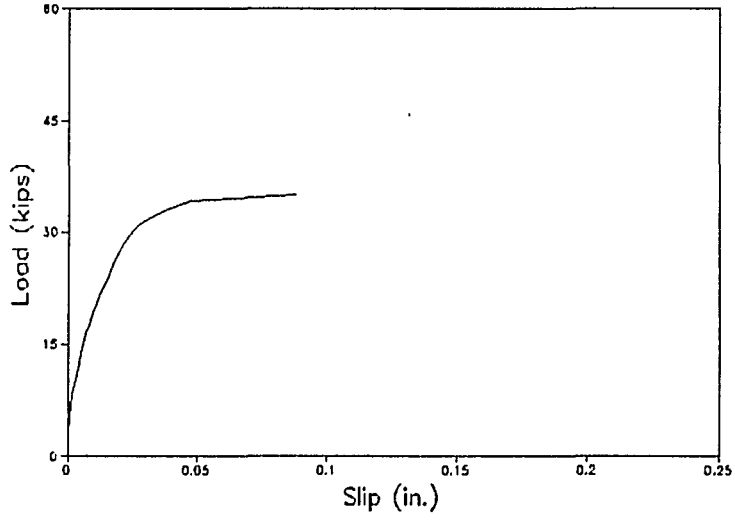

FIGURE 98, Load-slip relationship of specimen 89H3204

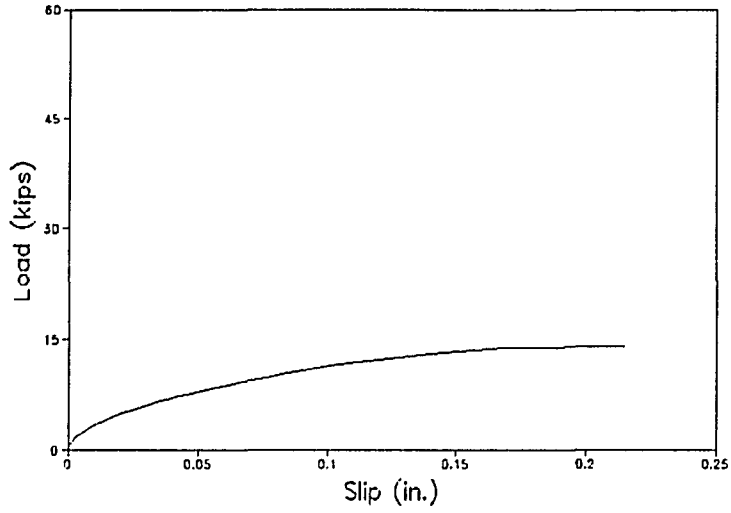

FIGURE 99, Load-slip relationship of specimen 49H0121

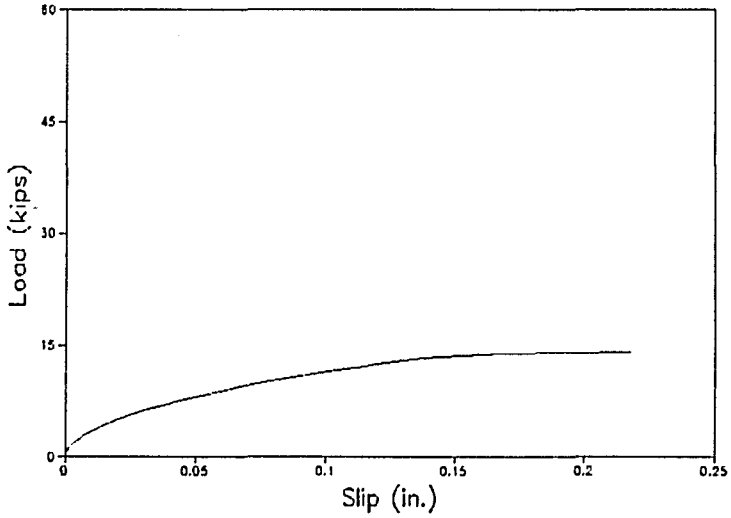

FIGURE 100, Load-slip relationship of specimen 49H0201

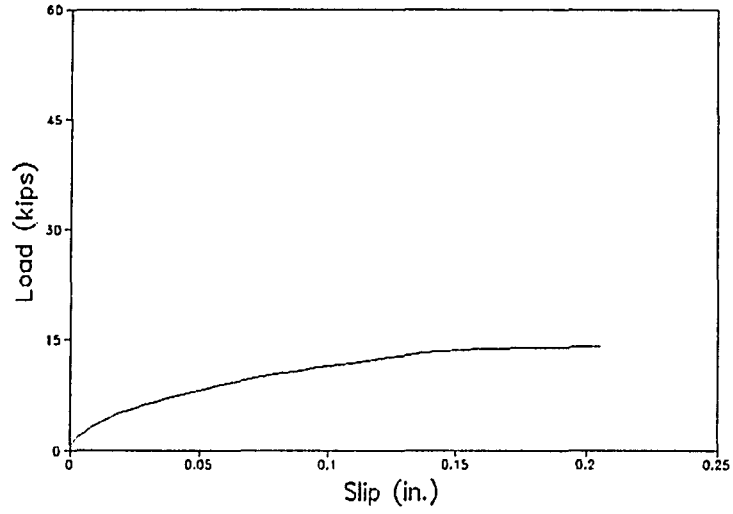

FIGURE 101, Load-slip relationship of specimen 89H0121

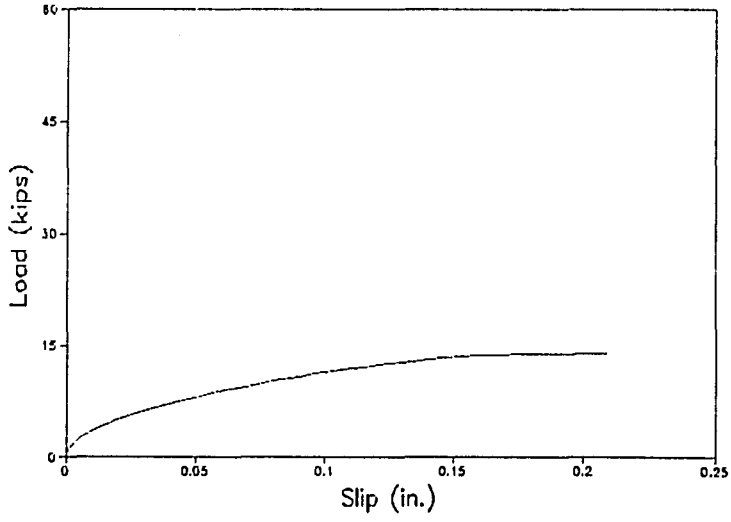

FIGURE 102, Load-slip relationship of specimen 89H0201

APPENDIX E: TABLES

TABLE 1, Experimental data of beam specimens with No. 3 GFRP rebars

Specimen	f_c', psi	T_m^*, kips	U_m^*, psi	T_m^*/T_u	S_{fmax}, in.	S_{lmax}, in.	E_i, k/in.	MOF
43B1.5T1	4010	5.6	3169	0.50	0.0186	0.0602	312	S
43B1.5T2	4010	7.0	3961	0.63	0.0134	0.0443	646	P
43B3T2	4010	7.6	2150	0.68	0.0245	0.0769	654	P
43B4B2	4330	8.1	1719	0.73	0.0036	0.0198	587	R
43B4T2	4330	8.8	1867	0.79	0.0039	0.0208	508	R
43B6B4	5080	9.7	1372	0.87	0.0039	0.0211	605	R
43B6T4	5080	8.7	1231	0.78	0.0043	0.0221	510	R
43B8B6	5080	10.2	1082	0.92	0.0038	0.0243	641	R
43B8T6	5080	8.6	912	0.77	0.0041	0.0251	549	R
83B4B2	7100	8.2	1740	0.74	0.0057	0.0248	530	R
83B4T2	7100	8.8	1867	0.79	0.0064	0.0259	464	R
83B6B4	7100	9.5	1344	0.86	0.0041	0.0204	610	R
83B6T4	7100	8.3	1174	0.75	0.0043	0.0220	546	R
83B8B6	7100	8.4	891	0.76	0.0031	0.0203	843	R
83B8T6	7100	9.5	1008	0.86	0.0033	0.0211	634	R

TABLE 2, Experimental data of beam specimens with No. 6 GFRP rebars

Specimen	f_c', psi	T_m^*, kips	U_m^*, psi	T_m^*/T_u	S_{fmax}, in.	S_{lmax}, in.	E_i, k/in.	MOF
46B3B1	4010	15.0	2122	0.51	0.0523	0.1998	907	S
46B3T1	4010	12.0	1698	0.41	0.0639	0.1987	643	S
46B3B2	4010	19.2	2716	0.65	0.0453	0.0893	1250	P
46B3T2	4010	16.0	2264	0.54	0.0492	0.1895	1023	P
46B6B2	4010	20.8	1471	0.71	0.0261	0.0956	1208	P
46B6T2	4010	17.0	1203	0.58	0.0478	0.1406	944	P
46B12B2	5680	21.2	750	0.72	0.0345	0.1343	1242	P
46B12T2	5680	19.8	700	0.67	0.0602	0.1111	1080	P
46B16B4	5680	27.4	727	0.93	0.0599	0.1789	1141	P
46B16T4	5680	25.8	684	0.88	0.0695	0.2111	854	P
46B18B6	5680	28.9	681	0.98	0.0347	0.1436	851	R
46B18T6	5680	29.4	693	1.00	0.0386	0.1607	818	R
86B12B2	6920	23.1	817	0.78	0.0678	0.1871	1444	P
86B12T2	6920	22.4	792	0.76	0.0879	0.1998	1232	P
86B16B4	6920	28.2	748	0.96	0.0564	0.1786	1175	P
86B16T4	6920	27.0	716	0.92	0.0625	0.1733	906	P
86B18B6	6920	30.1	710	1.02	0.0294	0.1556	1286	R
86B18T6	6920	29.4	693	1.00	0.0327	0.1701	1012	R

TABLE 3, Experimental data of beam specimens with No. 9 GFRP rebars

Specimen	f_c', psi	T_m^*, kips	U_m^*, psi	T_m^*/T_u	S_{fmax}, in.	S_{lmax}, in.	E_i, k/in.	MOF
49B4B1	4010	24.6	1740	0.47	0.0456	0.2131	1891	S
49B4B2	4010	35.0	2476	0.67	0.0567	0.2312	3980	P
49B8B2	4010	39.0	1379	0.75	0.0567	0.1982	2469	P
49B22B2	5760	44.1	567	0.84	0.0421	0.1655	3021	P
49B22T2	5760	43.2	556	0.83	0.1028	0.1479	1982	P
49B26B4	5760	48.1	523	0.92	0.0564	0.2111	3435	P
49B26T4	5760	46.1	502	0.88	0.0876	0.2782	2376	P
49B30B6	5760	51.2	483	0.98	0.0469	0.1248	2960	R
49B30T6	5760	51.8	489	0.99	0.0577	0.1414	1862	R
89B22B2	6490	46.0	592	0.88	0.0458	0.1761	2950	P
89B22T2	6490	44.1	567	0.84	0.0811	0.1986	1916	P
89B26B4	6490	49.7	541	0.95	0.0675	0.2023	3311	P
89B26T4	6490	47.9	521	0.92	0.0539	0.2493	2445	P
89B30B6	6490	51.9	489	0.99	0.0371	0.1189	2851	R
89B30T6	6490	54.0	509	1.03	0.0402	0.1212	2044	R

TABLE 4, Experimental data of pull-out specimens

Specimen	f_c', psi	T_m^*, kips	U_m^*, psi	T_m^*/T_u	S_{fmax}, in.	S_{lmax}, in.	E_i, k/in.	MOF
43PB1.5	4670	7.5	4244	0.68	0.0081	0.0512	534	P
43PM1.5	4670	7.2	4074	0.65	0.0146	0.0624	422	P
43PT1.5	4670	7.1	4018	0.64	0.0153	0.0667	405	P
83PB6	6640	10.9	1542	0.98	0.0029	0.0241	688	R
83PM6	6640	9.6	1358	0.86	0.0031	0.0251	560	R
83PT6	6640	9.1	1287	0.82	0.0032	0.0253	548	R
46PB6	4670	23.8	1684	0.81	0.0391	0.1711	1103	P
46PM6	4670	20.0	1415	0.68	0.0493	0.1988	878	P
46PT6	4670	19.3	1365	0.65	0.0467	0.1999	876	P
86PB12	6640	27.1	958	0.92	0.0456	0.2114	1366	P
86PM12	6640	24.9	881	0.84	0.0889	0.2675	1268	P
86PT12	6640	23.9	845	0.81	0.0998	0.2781	1258	P
49PB8	4670	47.9	1694	0.92	0.0653	0.2876	1748	P
49PM8	4670	42.2	1493	0.81	0.0785	0.2988	1172	P
49PT8	4670	41.8	1478	0.80	0.0789	0.3307	1162	P
89PB22	6640	49.3	634	0.94	0.0596	0.2112	2967	P
89PM22	6640	45.8	589	0.88	0.0873	0.3216	1617	P
89PT22	6640	45.0	579	0.86	0.0856	0.3118	1613	P

TABLE 5, Experimental data of hooked specimens with No. 3 GFRP rebars

Specimen	f_c', psi	T_m^*, kips	T_m^*/T_u	f_s^*, ksi	S_{lmax}, in.	E_i, k/in.	MOF
43H3124	5080	6.1	0.55	56	0.2234	88	S
43H3204	5080	5.8	0.53	53	0.2231	96	S
43H3127	4280	7.5	0.68	68	0.1453	268	S
43H31210	4280	8.8	0.79	80	0.1342	414	S
43H31213	4280	10.5	0.94	95	0.0388	523	R
43H31216	4280	11.4	1.03	103	0.0282	776	R
83H3124	6640	7.0	0.63	63	0.1672	128	S
83H3204	6640	6.9	0.62	62	0.1786	129	S
43H0121	5080	2.4	0.21	21	0.3114	43	R
43H0201	5080	2.4	0.21	21	0.3165	43	R
83H0121	6640	2.3	0.21	21	0.3044	45	R
83H0201	6640	2.4	0.22	22	0.3089	46	R

TABLE 6, Experimental data of hooked specimens with No. 6 GFRP rebars

Specimen	f_c', psi	T_m^*, kips	T_m^*/T_u	f_s^*, ksi	S_{lmax}, in.	E_i, k/in.	MOF
46H3124	5680	20.2	0.68	46	0.1786	604	S
46H3204	5680	20.6	0.70	47	0.1678	620	S
46H3127	4280	24.0	0.81	54	0.1111	1111	S
46H31210	4280	25.4	0.86	58	0.0989	2192	S
46H31213	4280	28.7	0.97	65	0.0256	3629	R
46H31216	4280	29.4	1.00	67	0.0155	4592	R
86H3124	6920	22.1	0.75	50	0.1231	788	S
86H3204	6920	22.3	0.76	50	0.0988	748	S
46H0121	5680	6.9	0.23	16	0.2514	110	R
46H0201	5680	6.6	0.23	15	0.2487	109	R
86H0121	6920	6.5	0.22	15	0.2322	115	R
86H0201	6920	6.5	0.22	15	0.2291	116	R

TABLE 7, Experimental data of hooked specimens with No. 9 GFRP rebars

Specimen	f_c', psi	T_m^*, kips	T_m^*/T_u	f_s^*, ksi	S_{lmax}, in.	E_i, k/in.	MOF
49H3124	5760	31.9	0.61	32	0.1111	1525	S
49H3204	5760	32.2	0.62	32	0.1231	1548	S
49H3127	4280	37.9	0.73	38	0.0897	3508	S
49H31210	4280	41.4	0.79	42	0.0655	4704	S
49H31213	4280	49.1	0.94	49	0.0161	8467	R
49H31216	4280	51.6	0.99	52	0.0152	9554	R
89H3124	6860	34.3	0.66	35	0.0876	2174	S
89H3204	6860	35.0	0.67	35	0.0879	2082	S
49H0121	5760	14.2	0.27	14	0.2148	177	R
49H0201	5760	14.2	0.27	14	0.2177	177	R
89H0121	6860	14.1	0.27	14	0.2054	185	R
89H0201	6860	14.0	0.27	14	0.2089	184	R

APPENDIX F: GRIP MECHANISM

In earlier studies, the design and development of suitable grips to transfer loads to GFRP rebars embedded in concrete have presented some difficulties. Because glass fiber based composites are very weak for loads applied transverse to the fiber direction, the region of the GFRP rebar in the grip must be protected against crushing. The grip must grasp the rebars in a manner as to avoid failure of the rebar at the grips, allowing the failure to take place in the rebar away from the grip region. A specially constructed set of sand-coated grips similar to those used in testing of GFRP rebars at West Virginia University were employed. The sketch and dimensions of grip system are shown in Fig. 1 and Table 1, respectively. The applied loads are transmitted from the jack to the GFRP rebars through these grips. The tests were successful in avoiding excessive slippage and rebar failure in the grips. The sand-coated grips have proven effective for all rebar sizes.

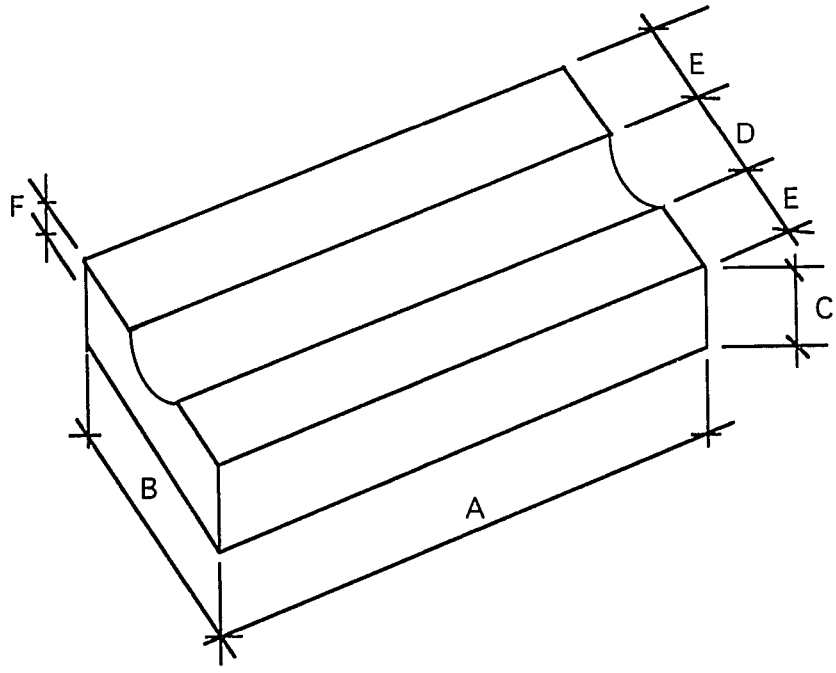

Fig. 1. - Sketch of the Grip System

Table 1. - Dimensions of the Grip System

Bar Size	A (in.)	B (in.)	C (in.)	D (in.)	E (in.)	F (in.)
#3	7-1/2	3-1/4	1/2	1/2	1-3/8	1/4
#6	7-1/2	3-1/2	1	7/8	1-5/16	7/16
#9	7-1/2	3-1/2	1	1-1/4	1-1/8	5/8

REFERENCES

ACI Committee 208. (1945). "Proposed Test Procedure to Determine Relative Bond Value of Reinforcing Bars." ACI J., 41(4), 273-292.

ACI Committee 318. (1963). "Building Code Requirements for Reinforced Concrete.", (ACI 318-63), American Concrete Institute, Detroit.

ACI Committee 318. (1971). "Building Code Requirements for Reinforced Concrete.", (ACI 318-71), American Concrete Institute, Detroit.

ACI Committee 318. (1977). "Building Code Requirements for Reinforced Concrete.", (ACI 318-77), American Concrete Institute, Detroit.

ACI Committee 318. (1989). "Building Code Requirements for Reinforced Concrete." (ACI 318-89), American Concrete Institute, Detroit, Mich. 181-211

ACI Committee 408. (1966). "Bond Stress-The State of the Art." ACI J., 63(11), 1161-1188.

ACI Committee 408. (1970). "Opportunities in Bond Research." ACI J., 67(11), 857-867.

ACI Committee 408. (1990). "Development and Splice Length Changes for Deformed Bars in Tension." American Concrete Institute, Detroit.

ACI Committee 408. (1992). "State-of-the-art Report on Bond Under Cyclic Loads." American Concrete Institute, Detroit, 3-7.

Azizinamini, A., Stark, M., Roller, J. J., and Ghosh, S. K. (1993). "Bond Performance of Reinforcing Bars Embedded in High-Strength Concrete." ACI S. J., 90(5), 554-561.

Chaallal, O., Benmokrane, B., and Masmoudi, R. (1992). "An Innovative Glass-Fiber Composite Rebar for Concrete Structures." Advanced Composite Materials in Bridges and Structures, Canadian Society for Civil Engineering, 169-177.

Chana, P. S. (1990). "A test Method to establish realistic bond stresses." Magazine of Concrete Research, 42(151), 83-90.

Chapman, R. A., and Shah, S. P. (1987). "Early-Age Bond Strength in Reinforced Concrete." ACI M. J., 84(6), 501-510.

Clark, A. P. (1946). "Comparative Bond Efficiency of Deformed Concrete Reinforcing Bars." ACI J., 43(4), 381-400.

Clark, A. P. (1948). "Highlights of the Development of Reinforced Concrete and the Study of Bond." ACI J., 19(6), 437-440.

Clark, C. R., and Johnston, D. W. (1983). "Early Loading Effects on Bond Strength." ACI J., 80(6), 532-539.

Clifton, J. R., and Mathey, R. G. (1983). "Bond and Creep Characteristics of Coated Reinforcing Bars in Concrete." ACI J., 80(4), 288-293.

Collier, S. T. (1947). "Bond Characteristics of Commercial and Prepared Reinforcing Bars." ACI J., 43(10), 1125-1133.

Daniali, S. (1992). "Development Length for Fiber-Reinforced Plastic Bars." Advanced Composite Materials in Bridges and Structures, Canadian Society for Civil Engineering, 179-188.

Darwin, D., and Graham, E. K. (1993). "Effect of Deformation Height and Spacing on Bond Strength of Reinforcing Bars." ACI S. J., 90(6), 646-657.

Darwin, D., McCabe, S. L., Idun, E. K., and Schoenekase, S. P. (1992). "Development Length Criteria:: Bars without Transverse Reinforcement." SL Report 92-1, Structural Engineering and Engineering Materials, The University of Kansas, Lawrence, Kansas 66045.

Edwards, A. D., and Yannopoulos, P. J. (1979). "Local Bond-Stress to Slip Relationships for Hot Rolled Deformed Bars and Mild Steel Plain Bars." ACI J., 76(3). 405-413.

Ehsani, M. R. (1993). "Glass-fiber reinforcing bars." in J.L. Clarke, ed., Alternative Materials for the Reinforcement and Pressing of Concrete, Blackie Academic & Professional, London.

Ehsani, M. R., Saadatmanesh, H., and Tao, S. (1993). "Bond of GFRP Rebars to Ordinary-Strength Concrete." ACI International Symposium on Non-Metallic Continuous Reinforcement, Vancouver, Canada, ACI SP-138, A. Nanni and C. W. Dolan, ed., 333-345.

Erki, M. A., and Rizkalla, S. H. (1993). "FRP Reinforcement for Concrete Strengths." Concrete Int.: Design and Constr., 15(6), 48-53.

Faza, S.S., and GangaRao, H.V.S. (1990). "Bending and Bond Behavior of Concrete Beams Reinforced with Plastic Rebars." Transportation Research Record 1290, 185-193.

Ferguson, P. M. (1977). "Small Bar Spacing or Cover-A Bond Problem for the Designer." ACI J., 74(9), 435-439.

Ferguson, P. M., Breen, J. E., and Thompson, J. N. (1965). "Pullout Tests on High-Strength Reinforcing Bars." ACI J., 62(8), 933-949.

Ferguson, P. M., and Thompson, J. N. (1962). "Development Length of High- Strength Reinforcing Bars in Bond." ACI J., 59(7), 887-921.

Ferguson, P. M., and Thompson, J. N. (1965). "Development Length for Large High-Strength Reinforcing Bars." ACI J., 62(1), 71-91.

GangaRao, H. V. S., and Faza, S. S. (1991). "Bending and Bond Behavior and Design of Concrete Beams Reinforced with Fiber Reinforced Plastic Rebars." Final Report, Constructed Facilities Center, West Virginia University, Morgantown, WV 26506-6101.

Hadje-Ghaffari, H., Choi, O. C., Darwin, D., and McCabe, S. L. (1992). "Bond of Epoxy-Coated Reinforcements to Concrete: Cover, Casting Position, Slump, and Consolidation." Structural Engineering and Engineering Materials, SL Report 92-3, The University of Kansas, Lawrence, Kansas 66045

Hamad, B. S., Jirsa, J. O., and Paulo, N. I. d'Abreu d. (1990). "Effect of Epoxy Coating on Bond and Anchorage of Reinforcement in Concrete Structures." Research Report 1181-1f, Center for Transportation Research, Bureau of Engineering Research, The University of Texas at Austin, 153-193.

Hamad, B. S., Jirsa, J. O., and Paulo, N. I. d'Abreu d. (1993). "Anchorse Strength of Epoxy-Coated Hooked Bars." ACI S. J., 90(2), 210-217.

Jeanty, P. R., Mitchell, D., and Mirza, M. S. (1988). "Investigation of "Top Bar" Effects in Beams." ACI S. J., 251-257.

Jiang, D. H., Shah, S. P., and Andonian, A. T. (1984). "Study of the Transfer of Tensile Forces by Bond." ACI J., 81(3), 251-259.

Jirsa, J. O., Lutz, L. A., and Gergely, P. (1979). "Rational for Suggested Development, Splices, and Standard Hook Provisions for Deformed Bars in Tension." Concrete Int.: Design and Constr., 47-61.

Kanakubo, T., Yonemaru, K., Fukugama, H., Fujisawa, M., and Sonobe, Y. (1993). "Bond Performance of Concrete Members Reinforced with FRP Bars." ACI International Symposium on Non-Metallic Continuous Reinforcement, Vancouver, Canada, ACI SP-138, A. Nanni and C. W. Dolan, ed., 767-788.

Keesler, R. J., and Powers, R. G. (1988). "Corrosion of epoxy coated rebars-Keys Segmental Bridge-Monroe County." Report No. 88-8A, Florida Department of Transportation, Materials Office, Corrosion Research Laboratory, Gainesville.

Kemp, E.L., and Wilhelm, W. J. (1979). "Investigation of the Parameters Influencing Bond Cracking." ACI J., 76(1),47-71.

Kemp, E.L. (1986). "Bond in Reinforced Concrete: Behavior and Design Criteria." ACI J., 83(1), 50-57.

Lahnert, B. J., Houde, J., and Gerstle, K. H. (1986). "Direct Measurement of Slip Between Steel and Concrete." ACI J., 83(6), 974-982.

Larralde, J., Burdette, J., Harris, B. (1993). "Bond Stress Distribution of RP Bars in Concrete." 38th International SAMPE Symposium and Exhibition, Vol. 38, Book 2 of 2 Books, V. Bailey, et al., ed., Anaheim Convention Center, Analseim, CA, 1775-1788.

Larralde, J., and Silva, R. (1990). "Bond Stress-Slip Relationships of FRP Rebars in Concrete." Proc. First Mat. Engrg. Congr., Vol. II, B. A. Suprenant, ed., ASCE, New York, NY, 1134-1141.

Larralde, J., and Silva, R. (1993). "Bond and Slip of FRP Rebars in Concrete." J. of Mat. in Civil Engrg., ASCE, 5(1), 30-40.

Lutz, L. A. (1970). "Analysis of Stresses in Concrete Near a Reinforcing Bar Due to Bond and Transverse Cracking." ACI J., 67(10), 778-787.

Lutz, L. A., and Gergely, P. (1967). "Mechanics of Bond and Slip of Deformed Bars in Concrete." ACI J., 64(11), 711-721.

Lutz, L. A., Mirza, S. A., and Gosain, N. K. (1993). "Changes to and Applications of Development and Lap Splice Length Provisions for Bars in Tension (ACI 318-89)." ACI S. J., 90(4), 393-406.

Mains, R. M. (1951). "Measurement of the Distribution of Tensile and Bond Stresses Along Reinforcing Bars." ACI J., 23(3), 225-252.

Marques, J. L. G., and Jirsa, J. O. (1975). "A Study of Hooked Bar Anchorages in Beam-Column Joints." ACI J., 198-209.

Maruyama, T., Honma, M., and Okkamura, H. (1993). "Experimental Study on Tensile Strength of Bent Portion of FRP Rods." ACI International Symposium on Non-Metallic Continuous Reinforcement, Vancouver, Canada, ACI SP-138, A. Nanni and C. W. Dolan, ed., 163-176.

Mashima, M., and Iwamoto, K. (1993). "Bond Characteristics of FRP Rod and Concrete after Freezing and Thawing Deterioration." ACI International Symposium on Non-Metallic Continuous Reinforcement, Vancouver, Canada, ACI SP-138, A. Nanni and C. W. Dolan, ed., 51-69.

Mathey, R. G., and Clifton, J. R. (1976). "Bond of Coated Reinforcing Bars in Concrete." ASCE, 102(ST1), 215-229.

Mathey, R. G., and Watstein, D. (1961). "Investigation of Bond in Beam and Pull-Out Specimens with High-Yield-Strength Deformed Bars." ACI J., 32(9), 1071-1089.

Minor, J., and Jirsa, J. O. (1971). "A Study of Bent Bar Anchorages." Report No. 9, Department of Civil Engineering, Rice University, Houston, Texas.

Minor, J., and Jirsa, J. O. (1975). "Behavior of Bent Bar Anchorages." ACI J., 72(4), 141-149.

Moehle, J. P., Wallace, J. W., and Hwang, S.-J. (1991). "Anchorage Lengths for Straight Bars in Tension." ACI S. J., 88(10), 531-537.

Mylrea, T. D. (1948). "Bond and Anchorage." ACI J., 19(7), 521-552.

Orangun, C. O., Jirsa, J. O., and Breen, J. E. (1977). "A Reevaluation of Test Data on Development Length and Splices." ACI J., 74(3), 114-122.

Park, R., and Paulay, T. (1975). "Reinforced Concrete Structures." John Wiley & Sons, New York, 401-404.

Perry, E. S., and Thompson, J. N. (1966). "Bond Stress Distribution on Reinforcing Steel in Beams and Pullout Specimens." ACI J., 63(8), 865-874.

Pinc, R. L., Watkins, M. D., and Jirsa, J. O. (1977). "Strength of Hooked Bar Anchorages in Beam-Column Joints." CESRL Report No. 77-3, Department of Civil Engineering/Structures Research Laboratory, The University of Texas, Austin, Texas, 49-65.

Pleimann, L. G. (1987). "Tension and Bond Pull-Out Tests of Deformed Fiberglass Rods." Final Report for Marshall-Vega Corporation, Marshall, Arkansas, Civil Engineering Department, University of Arkansas, Fayetteville, Arkansas, 5-11.

Pleimann, L. G. (1991). "Strength, Modulus of Elasticity, and Bond of Deformed FRP Rods." Advanced Composites Materials in Civil Engineering Structures, Proceedings of the Specialty Conference, Materials Engineering Division, ASCE, 99-110.

Saadatmanesh, H., and Ehsani, M. R. (1991). "Fiber Composite Bar for Reinforced Concrete Construction." J. of Composite Material, 188-203.

Somayaji, S., Shah, S. P. (1981). "Bond Stress Versus Slip Relationship and Cracking Response of Tension Members." ACI J., 78(3). 217-225.

Soroushian, P., Obaseki, K., Nagi, M., and Rojas, M. C. (1988). "Pullout Behavior of Hooked Bras in Exterior Beam-Column Connections." ACI S. J., 85(6), 269-276.

Sozen, M. A., and Moehle, J. P. (1990). "Development and Lap-Splice Lengths for Deformed Reinforcing Bars in Concrete." Report, The S & M Partnership, P. O. Box 663, Urbana, IL.

Treece, R. A., and Jirsa, J. O. (1989). "Bond Strength of Epoxy-Coated Reinforcing Bars." ACI M. J., 86(2), 167-174.

Ueda, T., Lin, I., and Hawkins, N. M. (1986). "Beam Bar Anchorage in Exterior Column-Beam Connections." ACI J., 83(3), 412-422.

Watstein, D. (1941). "Bond Stress in Concrete Pullout Specimens." ACI J., 38(1), 37-50.

Watstein, D. (1947). "Distribution of Bond Stress in Concrete Pullout Specimens." ACI J., 43(9), 1041-1052.

Wu, V. P., GangaRao H., and Prucz, J. C. (1991). "Mechanical Properties of Fiber Reinforced Plastics." Research Report, Constructed Facilities Center, College of Engineering, West Virginia University.

Yang, S., and Chen, J. (1988). "Bond Slip and Crack Width Calculations of Tension Members." ACI S. J., 85(4), 414-422.